VIBRATION ISOLATION SYSTEM FOR SPACE LAUNCH VEHICLES

A THESIS SUBMITTED TO
THE GRADUATE SCHOOL OF NATURAL AND APPLIED SCIENCES
OF
MIDDLE EAST TECHNICAL UNIVERSITY

BY

BURAK KARAMAN

IN PARTIAL FULFILLMENT OF THE REQUIREMENTS
FOR
THE DEGREE OF MASTER OF SCIENCE
IN
MECHANICAL ENGINEERING

DECEMBER 2018

Approval of the thesis:

VIBRATION ISOLATION SYSTEM FOR SPACE LAUNCH VEHICLES

submitted by **BURAK KARAMAN** in partial fulfillment of the requirements for the degree of **Master of Science in Mechanical Engineering Department, Middle East Technical University** by,

Prof. Dr. Halil Kalıpçılar
Dean, Graduate School of **Natural and Applied Sciences** _____

Prof. Dr. M. A. Sahir Arıkan
Head of Department, **Mechanical Engineering** _____

Assist. Prof. Dr. Gökhan O. Özgen
Supervisor, **Mechanical Engineering, METU** _____

Examining Committee Members:

Assoc. Prof. Dr. Yiğit Yazıcıoğlu
Mechanical Engineering Dept., METU _____

Assist. Prof. Dr. Gökhan O. Özgen
Mechanical Engineering, METU _____

Assoc. Prof. Dr. M. Bülent Özer
Mechanical Engineering Dept., METU _____

Assist. Prof. Dr. Orkun Özşahin
Mechanical Engineering Dept., METU _____

Assist. Prof. Dr. Kutluk Bilge Arıkan
Mechanical Engineering Dept., TEDU _____

Date: 27.12.2018

I hereby declare that all information in this document has been obtained and presented in accordance with academic rules and ethical conduct. I also declare that, as required by these rules and conduct, I have fully cited and referenced all material and results that are not original to this work.

Name, Surname: Burak Karaman

Signature:

ABSTRACT

VIBRATION ISOLATION SYSTEM FOR SPACE LAUNCH VEHICLES

Karaman, Burak
Master of Science , Mechanical Engineering
Supervisor: Assist. Prof. Dr. Gökhan O. Özgen

December 2018, 173 pages

In the frame of this thesis, novel vibration isolation systems for spaces launch vehicles are designed and verified by vibration tests in laboratory environment. Payloads, satellites or spacecraft, are exposed high level of vibration loads during launch. These vibration loads are transmitted from launch vehicle to the payload and may have a detrimental effect on the payload. Vibration isolation systems can be used at the payload-launch vehicle interface in order to reduce vibration environment of a payload.

In this thesis, Dnepr launch vehicle and Sentinel-2 satellite are chosen as a case study, and system-level technical requirements for vibration isolation system are determined. The vibration isolator properties, which are stiffness, loss factor and number of isolators, are derived to meet system-level technical requirements by performing random response and harmonic response analyses using mathematical model. Then, six different vibration isolator concept are achieved utilizing topology optimization, compliant mechanisms and similar systems. The detailed design of three different vibration isolator alternatives are performed to achieve required stiffness and loss factor values. Stiffness and loss factor of vibration isolators are obtained by finite element analyses. Finally, the designed vibration isolation systems are verified by finite element analyses and vibration tests in laboratory environment.

Keywords: Vibration isolation, launch vehicle, payload, finite element method, topology optimization

ÖZ

FIRLATMA ARAÇLARI İÇİN TİTREŞİM İZOLASYON SİSTEMİ

Karaman, Burak
Yüksek Lisans, Makina Mühendisliği
Tez Danışmanı: Dr. Öğr. Üyesi Gökhan O. Özgen

Aralık 2018, 173 sayfa

Bu tez çerçevesinde, fırlatma araçları için özgün titreşim izolasyon sistemleri tasarlanmış ve laboratuvar ortamında gerçekleştirilen titreşim testleri ile doğrulanmıştır. Uydu ve uzay araçları gibi faydalı yükler fırlatma sırasında yüksek seviyede titreşim yüküne maruz kalmaktadır. Bu titreşim yükleri, fırlatma aracından faydalı yüke aktarılmaktadır ve faydalı yük için zararlı etkileri bulunmaktadır. Faydalı yüke aktarılan titreşim seviyesini düşürmek için uydu-fırlatma aracı arayüzünde titreşim izolasyon sistemi kullanılmaktadır.

Bu tez çalışmasında, Dnepr fırlatma aracı ve Sentinel-2 uydusu vaka çalışması için seçilmiş ve titreşim izolasyon sistemi için sistem seviyesi teknik gereksinimler belirlenmiştir. Matematiksel model kullanılarak yapılan rassal titreşim ve harmonik titreşim analizleri sonucunda titreşim izolatörlerinin direngenlik, kayıp faktör ve adet bilgileri gibi özellikleri türetilmiştir. Topoloji optimizasyonu, esnek mekanizmalar konsepti ve benzer sistemlerden yararlanarak altı farklı titreşim izolatörü konsepti elde edilmiştir. Gerekli direngenlik ve kayıp faktör değerini sağlamak amacıyla üç farklı tasarım alternatifi için detay tasarım çalışması gerçekleştirilmiştir. Titreşim izolatörlerinin direngenlik ve kayıp faktör değerleri sonlu elemanlar analizleri ile elde edilmiştir. Tasarlanan titreşim izolasyon sistemleri sonlu elemanlar analizleri ve laboratuvar ortamında gerçekleştirilen titreşim testleri ile doğrulanmıştır.

Anahtar Kelimeler: Titreşim izolasyonu, fırlatma aracı, faydalı yük, sonlu elemanlar yöntemi, topoloji optimizasyonu

To My Family

ACKNOWLEDGMENTS

Firstly, I would like to thank my thesis supervisor Asst. Prof. Gökhan O. Özgen for his guidance and technical support throughout this thesis work.

I would like to acknowledge ROKETSAN for funding this study and SSB for accepting this thesis study as SAYP project. I am grateful to Dr. Ezgi Civek Coşkun, who is industry advisor for this SAYP project, for her understanding, advice and encouragement.

I would like to thank Sami Samet Özkan for introducing me to the field of payload vibration isolation. I am also thankful to Buğra Şimşek for data acquisition and Kemal Gürson for helping me to prepare the test setup in vibration tests. In addition, I would like to present thanks to Berkay Kılıç for helping me in various aspect of this thesis study.

I am grateful to my parents and brother for their endless support throughout my education life and my sweetheart, Eda Öney, for her patience and support not only in this thesis work but also in every aspect of my life.

TABLE OF CONTENTS

LIST OF TABLES

TABLES

LIST OF FIGURES

FIGURES

LIST OF ABBREVIATIONS

ABBREVIATIONS

CAD Computer aided design

CG Center of gravity

FEA Finite element analysis

FFT Fast Fourier transform

PSD Power spectral density

SSD Steady-state dynamics

TR Technical requirement

TRL Technology readiness level

VEM Viscoelastic material

VIS Vibration isolation system

CHAPTER 1

INTRODUCTION

Payloads, which can be satellite, spacecraft or an astronaut, are placed into Earth orbits using space launch vehicles. Payloads are exposed dynamic loads during their lifecycle, i.e. transportation, launch, in-space operations and, in some cases, landing [1]. Dynamic environments of spacecraft is summarized and categorized based on type of excitation as in Table 1-1.

Table 1-1 Dynamic environments of spacecraft [1]

Type of Excitation	**Dynamic Environments**
Low frequency transient excitations	Transportation, seismic events, rocket motor ignition overpressure, liftoff release, engine/motor thrust transients, maneuvers, stage/fairing separations, in-flight operations, and surface penetration
Low frequency random excitations	Transportation, wind and turbulence, and fluid slosh in tanks
Quasi-periodic excitations	Transportation, engine chugging, pogo, solid motor pressure oscillations, and onboard equipment
Exterior acoustic noise excitations	Engine/motor generated acoustic noise
Exterior aerodynamic noise excitations	Aerodynamic sources, and planetary descent and entry
Interior acoustic noise excitations	Engine/motor generated acoustic noise, aerodynamic sources, and planetary descent and entry
Structure-borne vibration excitations	Engine/motor generated vibration and onboard equipment
High frequency transient excitations	Pyrotechnic events and meteoroid impact

The launch environment is the most severe environment of a payload during its lifetime and it may cause failure of payloads. The structure-borne vibrations are produced by excitations from engines of the launch vehicles, aerodynamics of flight and pyrotechnic separation systems. These vibration loads are transmitted from launch vehicle to payload through payload adapter whose function is attaching the payload to the launch vehicle. Since the conventional payload adapters are very rigid structures, they directly transmit vibration loads to the payload.

Dynamic loads, which come from the launch vehicle to the payload, differ for every launch vehicle due to different type of rocket engine, number of stages and unique structural design of each launch vehicle. Some examples of dynamic environment for different launch vehicles are presented in this section.

The sinusoidal vibration levels at the payload interface of Antares launch vehicle is given in Figure 1-1. The random vibration loads at the payload interface of Antares is encompassed by acoustics loads which are presented in Figure 1-2.

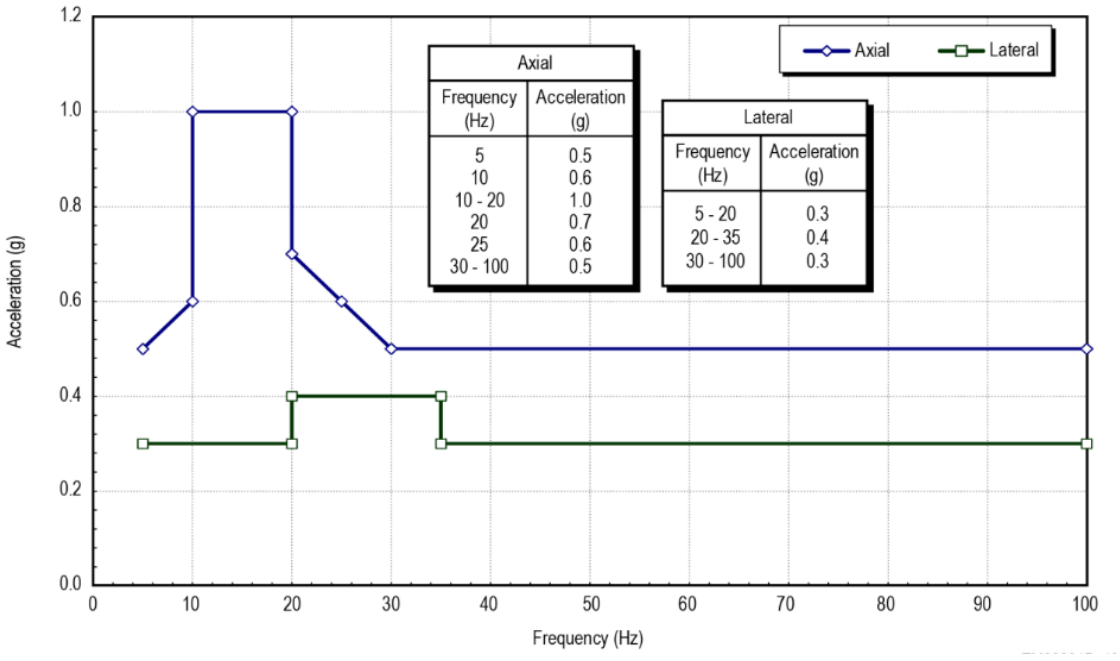

Figure 1-1 Antares - Payload Interface Sine Vibration Levels [2]

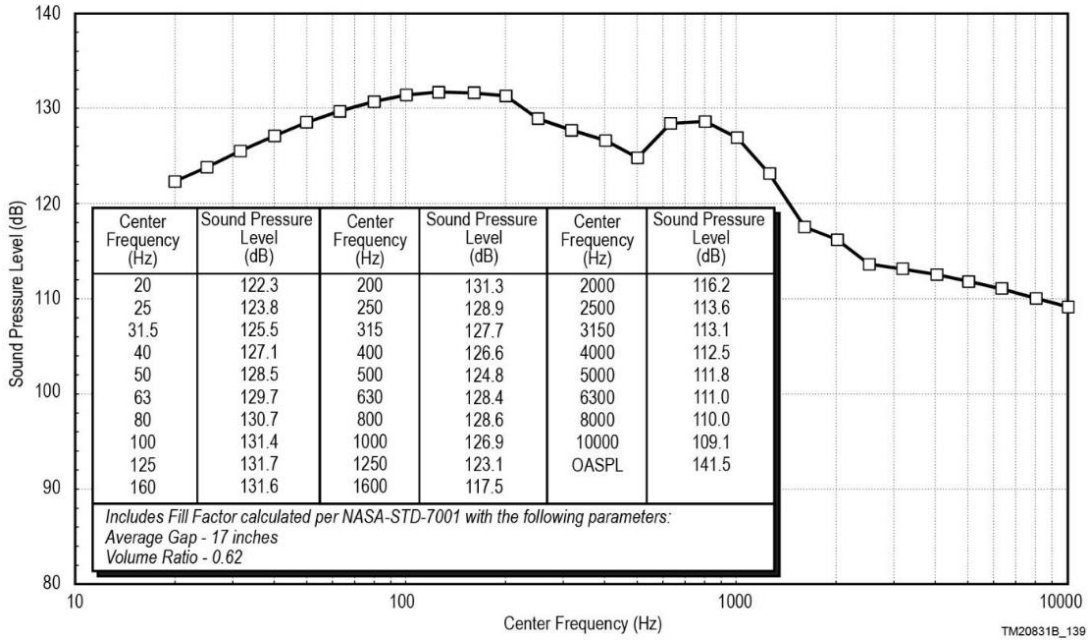

Center Frequency (Hz)	Sound Pressure Level (dB)	Center Frequency (Hz)	Sound Pressure Level (dB)	Center Frequency (Hz)	Sound Pressure Level (dB)
20	122.3	200	131.3	2000	116.2
25	123.8	250	128.9	2500	113.6
31.5	125.5	315	127.7	3150	113.1
40	127.1	400	126.6	4000	112.5
50	128.5	500	124.8	5000	111.8
63	129.7	630	128.4	6300	111.0
80	130.7	800	128.6	8000	110.0
100	131.4	1000	126.9	10000	109.1
125	131.7	1250	123.1	OASPL	141.5
160	131.6	1600	117.5		

Includes Fill Factor calculated per NASA-STD-7001 with the following parameters:
Average Gap - 17 inches
Volume Ratio - 0.62

Figure 1-2 Antares - Payload fairing internal acoustics levels [2]

The sinusoidal vibration level at the payload interface of the Ariane 5 launch vehicle is given in Figure 1-3. The random vibration environment is covered by the sine environment for frequencies under 100 Hz and by the acoustic environment for frequencies above 100 Hz.

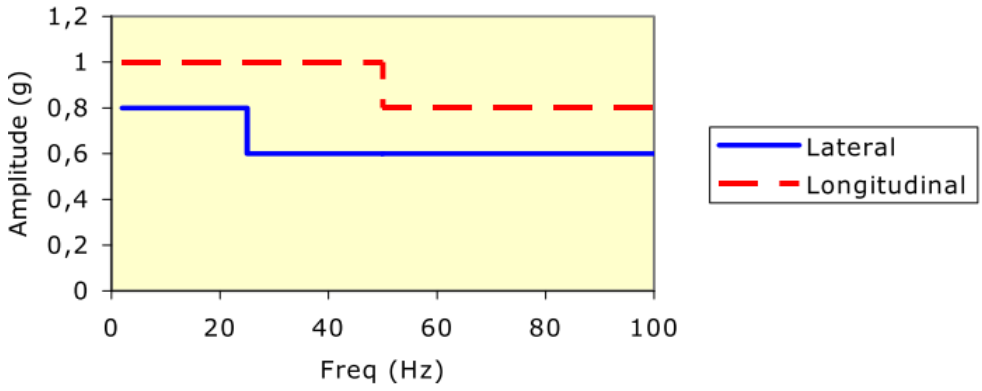

Figure 1-3 Ariane 5 - Sine excitation at spacecraft base [3]

The in-flight random vibration curve, which encompasses all flight vibration environments, of Minotaur launch vehicle is given in Figure 1-4.

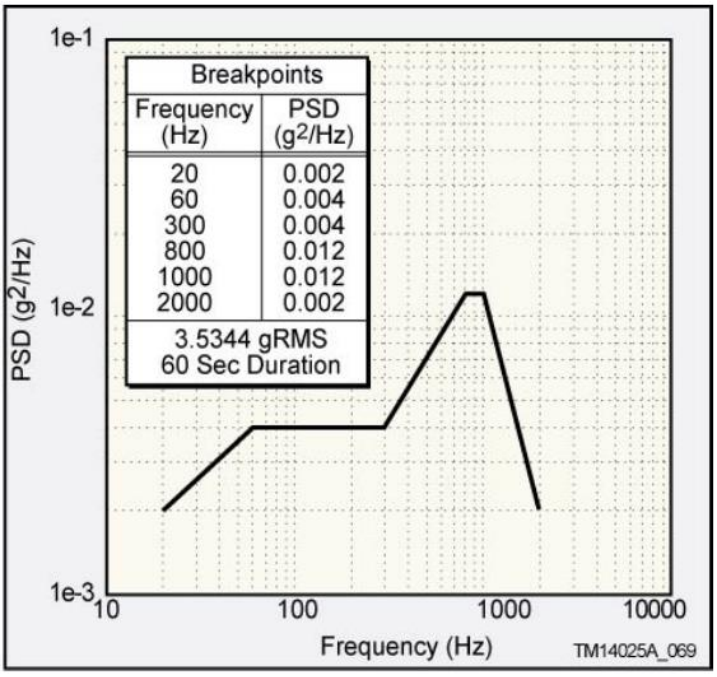

Figure 1-4 Minotaur - Payload random vibration environment during launch [4]

The random vibration levels at the payload interface of Pegasus launch vehicle is presented in Figure 1-5.

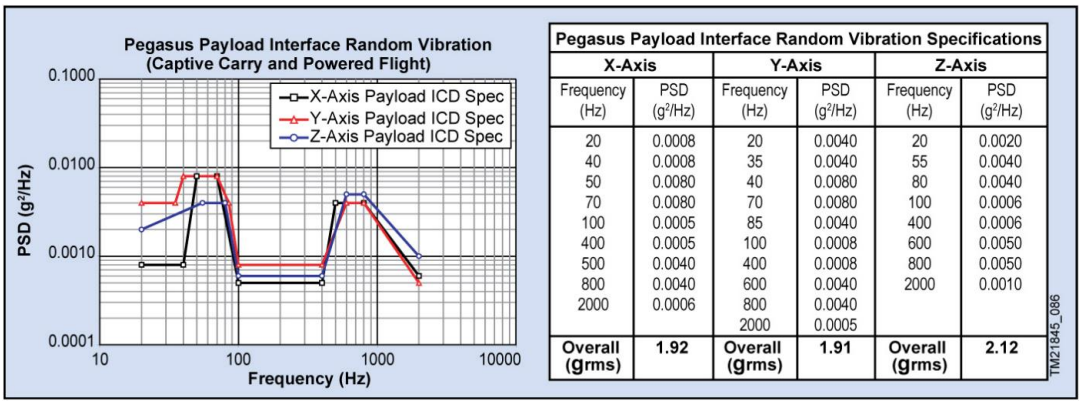

Pegasus Payload Interface Random Vibration Specifications					
X-Axis		Y-Axis		Z-Axis	
Frequency (Hz)	PSD (g^2/Hz)	Frequency (Hz)	PSD (g^2/Hz)	Frequency (Hz)	PSD (g^2/Hz)
20	0.0008	20	0.0040	20	0.0020
40	0.0008	35	0.0040	55	0.0040
50	0.0080	40	0.0080	80	0.0040
70	0.0080	70	0.0080	100	0.0006
100	0.0005	85	0.0040	400	0.0006
400	0.0005	100	0.0008	600	0.0050
500	0.0040	400	0.0008	800	0.0050
800	0.0040	600	0.0040	2000	0.0010
2000	0.0006	800	0.0040		
		2000	0.0005		
Overall (grms)	1.92	Overall (grms)	1.91	Overall (grms)	2.12

Figure 1-5 Pegasus - Payload Interface Random Vibration Specification [5]

Maximum quasi-static and dynamic accelerations, amplitudes of harmonic oscillations in longitudinal and lateral directions, and spectral density of vibro-accelerations at payload-launch vehicle interface of Dnepr launch vehicle is given in Table 1-2 to Table 1-5.

Table 1-2 Dnepr - Maximum Quasi-static and Dynamic Accelerations [6]

Load Source	Acceleration	
	Longitudinal (X)	Lateral (y, z)
LV movement inside TLC	2.5±0.7	±0.3
After LV exit from TLC	±1.0	±0.8
1st stage burn:		
Maximum dynamic head	3.0±0.5	0.5±0.5
Maximum longitudinal acceleration	7.5±0.5	0.1±0.5
2nd stage burn – maximum longitudinal acceleration	7.8±0.5	0.2
3rd stage burn	-0.3...-0.5	0.25

Table 1-3 Dnepr - Amplitude of Harmonic Oscillations – Longitudinal Axis [6]

Frequency sub-band, Hz	5-10	10-15	15-20
Amplitude, g	0.5	0.6	0.5
Duration, sec.	10	30	60

Table 1-4 Dnepr - Amplitude of Harmonic Oscillations – Lateral Axes [6]

Frequency sub-band, Hz	2-5	5-10	10-15
Amplitude, g	0.2-0.5	0.5	0.5-1.0
Duration, sec.	100	100	100

Table 1-5 Dnepr - Spectral Density of Vibro-accelerations [6]

Frequency sub-band, Hz	Load Source	
	Liftoff, LV flight segment where M=1, q_{max}	1st stage burn (except for LV flight segment where M=1, q_{max}), 2nd stage burn, 3rd stage burn
	Spectral Density, g^2/Hz	
20-40	0.007	0.007
40-80	0.007	0.007
80-160	0.007-0.022	0.007
160-320	0.022-0.035	0.007-0.009
320-640	0.035	0.009
640-1280	0.035-0.017	0.009-0.0045
1280-2000	0.017-0.005	0.0045
Root Mean Square Value, σ, g	6.5	3.6
Duration, sec.	35	831

There are numerous studies in the literature in order to reduce the vibration environment of a payload. There are patented vibration isolation systems for launch vehicles and some of them are used in many launch missions with success. Vibration isolation system can be used at the interface of payload and launch vehicle as shown in Figure 1-6.

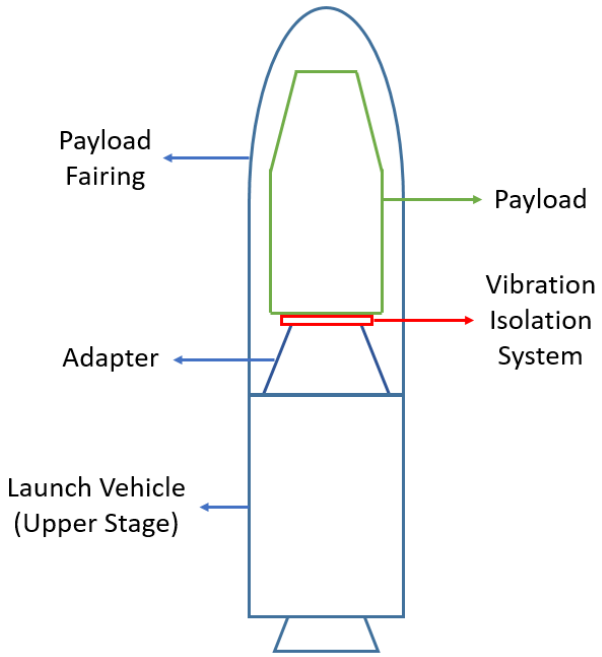

Figure 1-6 Vibration Isolation System at Payload-Launch Vehicle Interface

1.1. Motivation

By using vibration isolation system at the interface of payload and launch vehicle, the weight and cost of the payload can be reduced. Moreover, increased life and reliability of a payload can be achieved. Therefore, it is very advantageous to use vibration isolation system for space launch vehicle. Since the proven vibration isolation systems in literature are patented, there is a need to develop novel vibration isolation system for space launch vehicles.

1.2. Objective

The objective of this thesis is to design novel vibration isolation system which can be adaptable to different kinds of launch vehicles and payloads. The aim is to achieve Technology Readiness Level (TRL) – 4 for this technology.

1.3. Thesis Outline

Chapter 1 is the introduction to the thesis topic and presents the dynamic load environment of payloads. Chapter 2 gives literature survey related with vibration isolation systems and compliant mechanisms which have the potential for designing a vibration isolator. Chapter 3 describes the case study which is chosen to determine the technical requirements of vibration isolation system to be developed in this thesis work. Furthermore, vibration isolator properties are derived and related theoretical background is presented. In Chapter 4, conceptual design of vibration isolators is performed utilizing topology optimization, compliant mechanisms and similar systems. Detailed design of a vibration isolation systems is explained in Chapter 5. Verification plan and verification work for the designed vibration isolation systems are presented in Chapter 6.

CHAPTER 2

LITERATURE SURVEY

2.1. Vibration Isolation Systems for Space Launch Vehicles

Payloads, satellites or spacecraft, are exposed high level of vibration loads during launch. These loads are transmitted through payload adapters which are conventionally very rigid structures. Since these vibration loads may have detrimental effect on payload during launch, payload vibration isolation system can be used in order to reduce vibration environment which comes from the launch vehicle. There are three different kinds of vibration isolation system for whole spacecraft isolation: replacing the adapter with an isolator, installing an isolator at the interface of the adapter, adding damping to the existing adapter [7]. The first two approaches are called soft ride whereas the third approach is expressed as hard ride. Hard ride is a way of vibration attenuation and is used when there is restriction on the usable volume for payload inside fairing.

There are numerous studies in the literature related with vibration isolation of payload. Winthrop and Cobb presented a broad survey of the literature for vibration isolation technology for space applications [8]. They defined the terminology for vibration control and discussed the vibration isolation problem. Some current space specific applications and vibration control elements is also discussed. They emphasized the importance of smart materials which make semi-active control concepts physically viable.

Zheng has performed parametric studies of the whole spacecraft vibration isolation to show the influences of design parameters on the isolation performance [7]. The transmissibility is obtained by modelling the isolation spacecraft system as a two-

degree-of-freedom system. It is concluded that transmissibility can be reduced by the soft ride isolation system and damping is essential to reduce the vibration amplitudes at resonance frequencies.

Miao and Zheng have performed analytical study on whole flexible spacecraft vibration isolation since both launch vehicle and spacecraft are flexible structures [9]. The vibration isolation of flexible structure is different from that of the rigid structure. They stated that the isolation frequency must not be too low to avoid any interference with the launch vehicle's GNC system and to avoid collision between the spacecraft and the fairing. An explicit expression for the relation between the transmissibility and the isolation parameters is obtained and some numerical results are presented for a case study. It is claimed that the vibration transmissibility can be reduced by decreasing the stiffness of the isolator and/or increasing the damping. Moreover, it is emphasized that a coupling analysis is essential in the design of an isolation system because vibration isolators weakens the coupling between the spacecraft and the launch vehicle.

Jun, Hongxing and Zhiyi have presented an experimental evaluation of the whole-spacecraft passive vibration isolation system with a demonstration unit [10]. A series of vibration isolators are inserted in the joint between the adapter and the launch vehicle, and constrained layer damping treatment is applied on the outer surface of the adapter to increase its damping. Based on the experimental results, vertical and lateral dynamic responses is decreased by the whole-spacecraft isolation system.

Liu and Zheng have performed parameter analysis to obtain whole-spacecraft vibration isolation by modification of the existing payload adapter which is conventionally very stiff structure and transmits dynamic loads directly [11]. They obtained the simplified and condensed model based on Craig-Bampton component modal synthesis and theory about modal effective mass. It is shown that decreasing the stiffness of the payload adapter improves the vibration isolation performance, and increasing the damping of the adapter reduces the peak transmissibility.

Thomas, Fadick and Fram have designed a launch vehicle payload adapter with emphasis on its vibration isolation characteristics [12]. It is stated that the low axial mode frequency requirement conflicts with the relatively high pitch frequency requirement. They solved this problem by designing a composite adapter which utilize highly directional composite fiber laminates.

Zhang, Fang, Ding and Wang established the multistage rocket coupled system dynamics model with the whole-spacecraft vibration isolation system [13]. They discussed the other vibration isolation technological approaches by using the analytical expression. It is concluded that whole-rocket vibration isolation technology can reduce the dynamic environment of spacecraft during launch. Decreasing the stiffness of the interstage and increasing the damping of the vibration isolation system is proposed to reduce the vibration transferred to the spacecraft.

Liu, Liang, Zheng and Huang have studied the method of analysis and dynamic design of an octostrut platform for vibration isolation of whole-spacecraft [14]. A typical octostrut vibration isolation platform, which has eight flexible struts, is shown in Figure 2-1. It is indicated that octostrut vibration isolation platform is an effective method for improving the dynamic environment of a spacecraft during launch. Moreover, usage of a constraint mechanism along with the platform is recommended to prevent large lateral displacement of the upper end of the spacecraft.

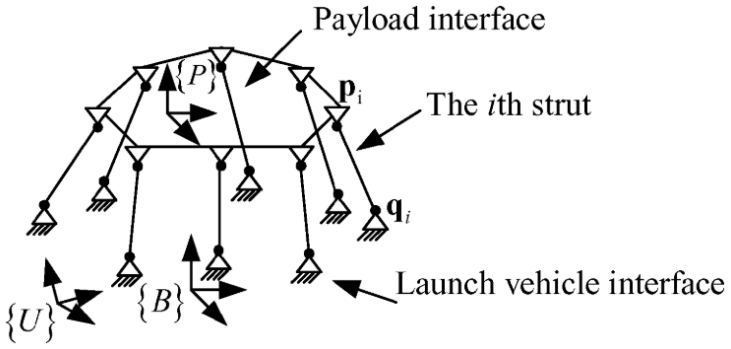

Figure 2-1 Typical octostrut vibration isolation platform

Zhang, Fang and Zang introduced the non-probabilistic reliability theory to investigate dynamic features of whole-spacecraft vibration isolation [15]. They established the non-probabilistic reliable model and index which reflect dynamic features of vibration isolation system. The effectiveness of non-probabilistic reliability design principle is shown with numerical results.

Edberg, Bartos, Goodding, Wilke and Davis have developed launch vibration isolation system (LVIS) which reduces the vibration loads transmitted to the payload during launch [16]. An axial isolation frequency is determined based on a number of simulations and hardware, which is shown in Figure 2-2, is designed to meet the requirements. Low axial stiffness, high damping for axial motion and high rocking stiffness can be achieved by a unique hydraulic cross-linking system. A pneumatic support can be adapted to payloads of varying mass by adjusting its internal pressure.

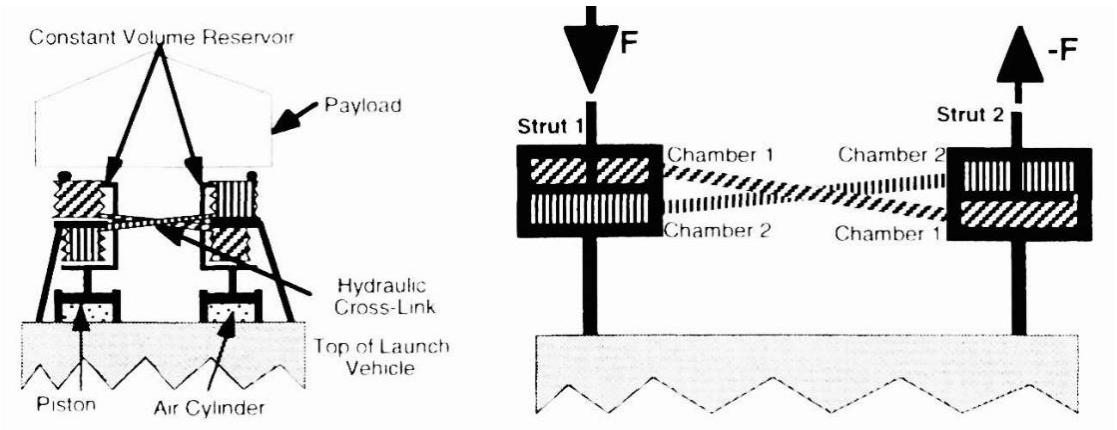

Figure 2-2 Vibration isolation concept in the LVIS program [16]

Fang, Li and Huang presented a new structure of whole-spacecraft vibration isolation system which uses viscoelastic material for damping [17]. They indicated the effectiveness of vibration isolation system in both vertical and horizontal direction with experimental results. Effect of area and geometry of the viscoelastic material on damping is also shown.

Zhang, Fang, Chen and Wang have presented a new type of discrete whole-spacecraft vibration isolation platform [18]. They obtained the natural frequencies and modal damping ratios by the complex modal analysis of the vibration isolation system. They evaluated the performance of the discrete whole-spacecraft vibration isolation platform by the transmissibility at some key points of the flexible spacecraft. Analysis and simulation results are verified with test results, and effectiveness of discrete vibration isolation platform is shown.

Liu, Witarto, Nie, Shi and Mo proposed periodic material-based vibration isolators for satellites [19]. The periodic isolators have frequency band gaps in which vibration isolation is achieved. The frequency band gaps are determined based on the elastodynamics and the Bloch-Floquet theorem. A parametric study for the design of periodic isolators and the finite element analysis of a satellite with designed periodic isolators are performed. Schematic view of a satellite with 3-layer periodic isolators is shown in Figure 2-3. It is concluded that periodic isolator provides vibration isolation in all directions when the excitation frequency falls in its frequency band gaps.

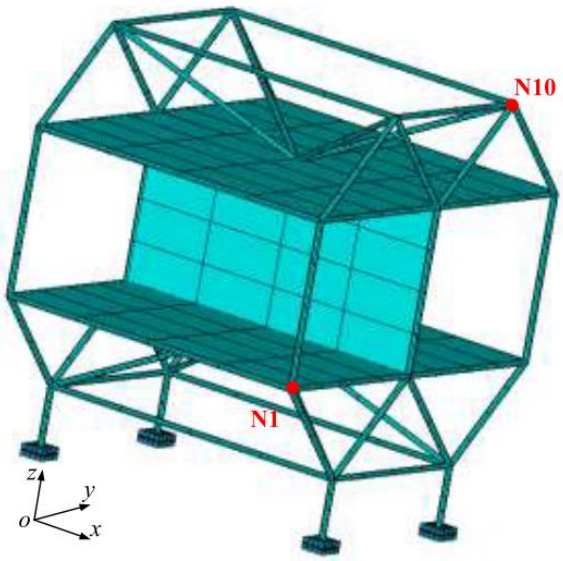

Figure 2-3 A satellite with 3-layer periodic isolators [19]

Yang, Bo, Tianzhi and Wenhu have studied a method for whole-spacecraft vibration isolation system, and discussed the response problems and stiffness problem of isolation system [20]. They placed the vibration isolation system between payload adapter and launch vehicle. Stiffness and damping of vibration isolator is provided by ribs which is indicated in Figure 2-4. The shear of the viscoelastic materials between the ribs provide damping. The natural frequency of the system can be controlled by adjusting the number of ribs. They computed the reliability and reliability sensitivity for a simplified model with two degree-of-freedoms. They performed experiments to prove the correctness of numerical results and analyzed the experimental data to identify the parameters of the vibration isolation system.

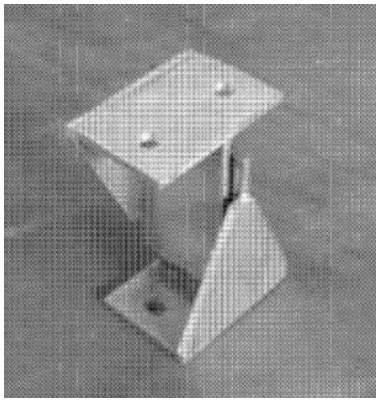

Figure 2-4 Ribs of vibration isolator [20]

Khorrami, Rastegar and Erwin have presented a novel three degrees-of-freedom vibration isolation system for payloads in launch vehicles [21]. The vibration isolation system consists of a mechanical constraining mechanism which prevents rocking motion and rotation about the longitudinal axis of the launch vehicle. It also consists of isolation units which reduce the vibration in the axial and lateral directions. Moreover, it has adaptive-passive adjustment mechanism for varying quasi-static

acceleration. They have fabricated small-scale version of the designed vibration isolation system for proof of concept demonstration.

Lee-Glauser and Ahmadi studied the effectiveness of various base-vibration-control systems for the payload and its subsystem [22]. They suggested two modified designs for trunnions which are rubber-bearing and resilient-friction as shown in Figure 2-5. The dynamic response of the payload is analyzed by using the normal-modes expansion technique. Based on the analysis results, usage of rubber-bearing and/or resilient-friction trunnion systems is suggested for effective protection of the payloads and payload subsystems.

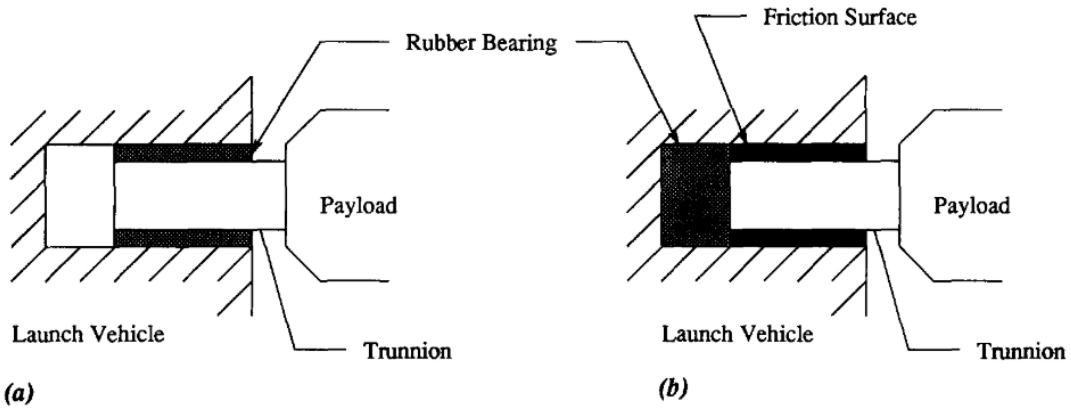

Figure 2-5 Schematic views of trunnion systems: (a) rubber-bearing, (b) resilient-friction [22]

McDonnell Douglas Corporation have two patented designs: passive axial vibration isolation system [23] and passive lateral vibration isolation system [24] for a spacecraft launch vehicle. The axial vibration isolation system, which includes upper and lower interface rings for attachment of payload and launch vehicle, is shown in Figure 2-6. The flexure feature in the upper portion of the isolation system provides flexibility in the axial direction while restricting lateral and rocking motion. The degree of compliance is determined by the so-called clocking angle α, which is also

shown in Figure 2-6. Axial flexure of the upper beam provides damping. The circular beam can be fabricated as a lamination of concentric beams separated by high damping material to obtain additional damping. The passive lateral vibration isolation system includes upper and lower mounting plates and a circular array of flexures which are placed between upper and lower interface as shown in Figure 2-7. It provides excellent lateral vibration isolation for payload when replaced with conventional, rigid payload attachment fittings.

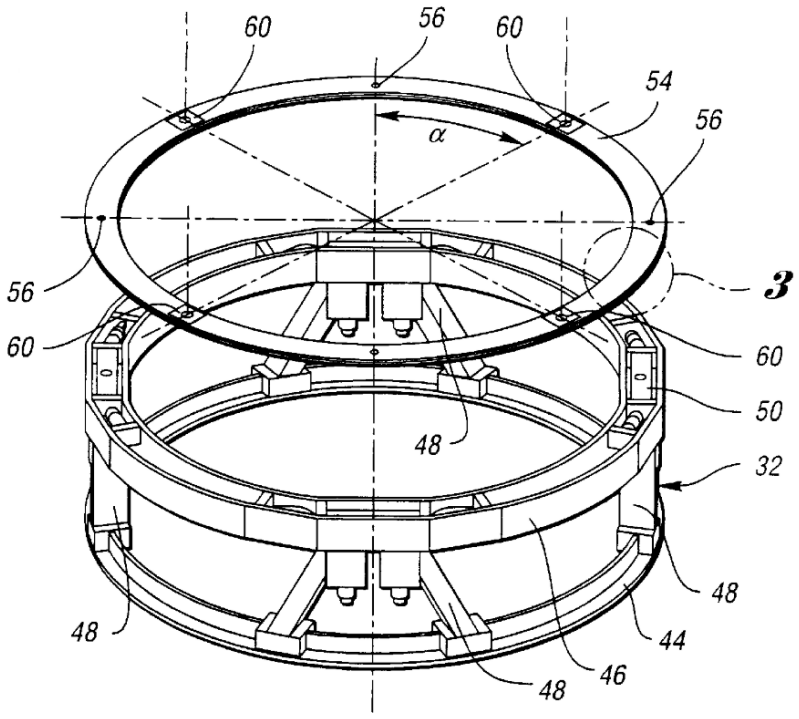

Figure 2-6 Passive axial vibration isolation system [23]

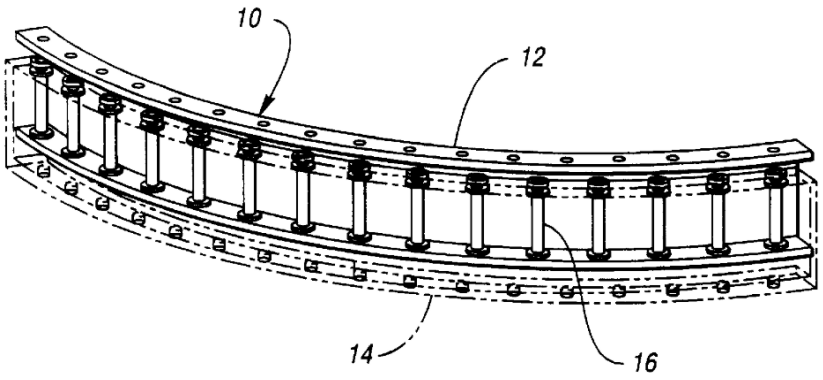

Figure 2-7 Passive lateral vibration isolation system [24]

There are 3 vibration isolation systems which are developed and patented by CSA Engineering, Inc.: SoftRide UniFlex [25], SoftRide MultiFlex [26] and SoftRide OmniFlex [27]. SoftRide vibration isolation systems were used with success in many launch mission, which are presented in Table 2-1 [28].

Table 2-1 SoftRide Programs [28]

	Launch Vehicle	**Spacecraft**
1	Taurus	GFO (Navy)
2	Taurus	STEX (NRO)
3	Taurus	MTI (DOE)
4	Taurus	QuikTOMS (NASA)
5	Minotaur 1	Jawsat (Air Force)
6	Minotaur 1	MightySat (Air Force)
7	Minotaur 1	XSS-11 (Air Force)
8	Minotaur 1	Cosmic (Air Force)
9	Minotaur 1	TacSat-2 (Air Force)
10	Pegasus	AIM (NASA)
11	Terrier / Orion	Valpe 1 (Air Force)

	Launch Vehicle	Spacecraft
12	Terrier / Orion	Valpe 2 (Air Force)
13	Atlas V	STP1 – FalconSat 3
14	Delta II	OSTM (NASA)
15	Pegasus	IBEX (NASA)
16	Delta IV Heavy	NROL-26 (NRO)
17	Taurus	OCO (NASA)
18	Minotaur 1	TacSat-3 (Air Force)

SoftRide UniFlex is an axial vibration isolation device for implementing a whole-spacecraft passive isolation system [25]. These devices consist of damped metallic flexures, as shown in Figure 2-8, which provide relative flexibility in the desired direction. UniFlex introduce compliance in the axial direction, but are relatively stiff in the lateral directions. The geometry of the dual-beam flexure (length, thickness, width) may be sized to properly tune the isolation frequency as needed. These flexures must have high strength because they carry very large static and dynamic loads. Titanium is typically the optimum material for these beams because it has a very high strength to weight ratio. Damping is required in the resilient mounts to reduce the amplitude of response of the payload at the isolation frequency. The required damping of the isolation device is gained by applying a VEM layer. The constrained layer damping treatment consists of layer of VEM attached to the inner surface of each beam. The VEM is constrained by attaching a thin metallic layer to its exposed surface as shown in Figure 2-9.

Figure 2-8 SoftRide UniFlex isolator [29]

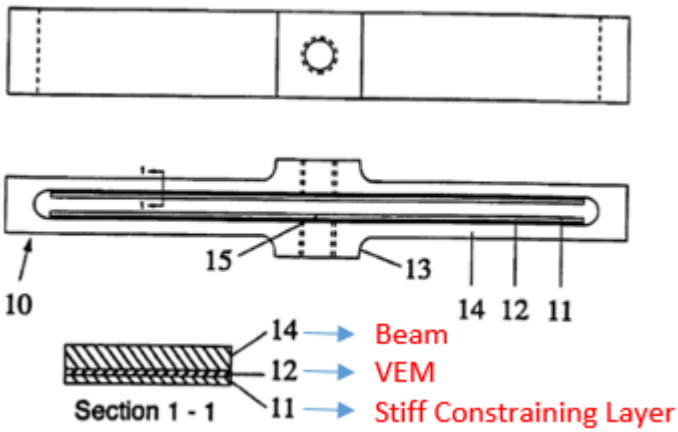

Figure 2-9 Damping treatment of UniFlex [25]

Whole-spacecraft vibration isolation system is the only mechanical connection between the launch vehicle and spacecraft. UniFlex vibration isolators are located at aft of the spacecraft separation system as shown in Figure 2-10.

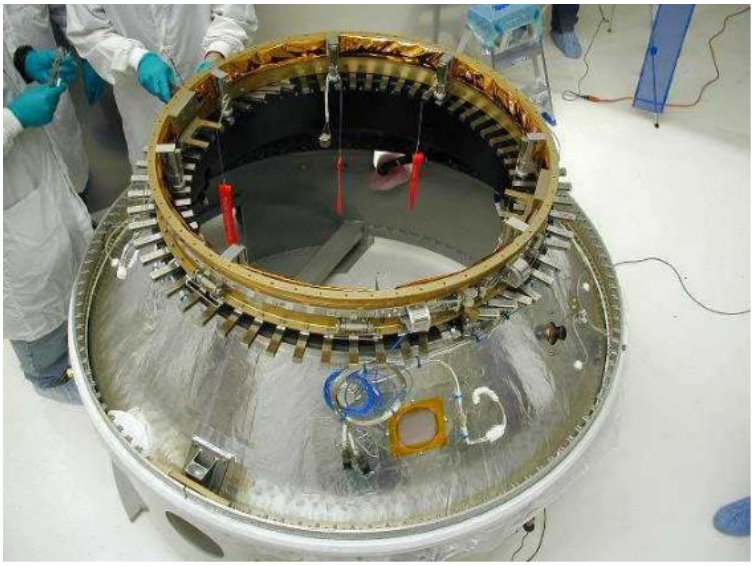

Figure 2-10 SoftRide UniFlex installation [29]

Gibbs, Francis, Spicer and Schaeffer performed vibration tests for NASA's Orbiting Carbon Observatory (OCO) spacecraft with SoftRide UniFlex vibration isolation system [30]. The test configuration is indicated in Figure 2-11. They stated the differences of the execution and control methodology of the test of an isolated system compare to non-isolated system. Results of OCO vibration tests showed that entire spacecraft acted as a single degree-of-freedom system and it has axial mode around 28 Hz. Therefore, input vibration profile is modified by applying a simple input notch local to the 28 Hz mode as shown in Figure 2-12.

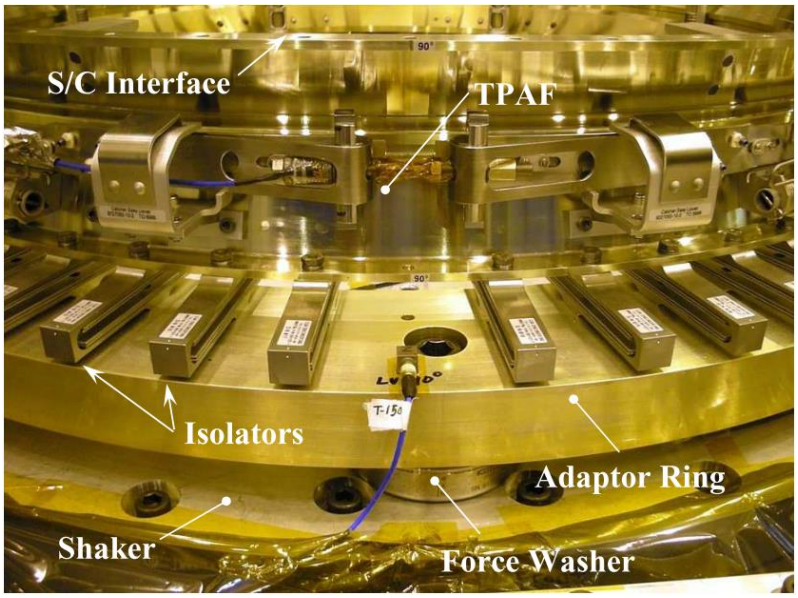

Figure 2-11 SoftRide UniFlex Isolators in OCO Test Configuration [30]

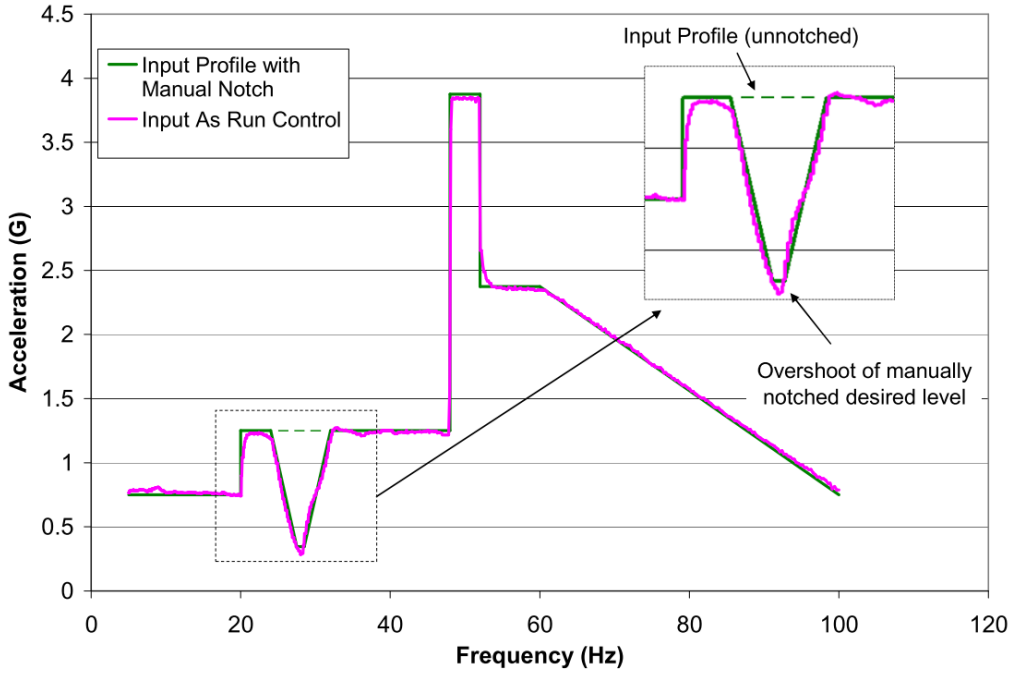

Figure 2-12 Target input force vs measured input response of OCO vibration test [30]

SoftRide MultiFlex provides vibration isolation in all three axes of any orthogonal coordinate system [26]. MultiFlex consists of a pair of UniFlex isolators which are connected to one another by way of the stand-off post as indicated in Figure 2-13. The axial stiffness of MultiFlex is governed by the two axial devices connected serially. The lateral stiffness of the MultiFlex is determined by the torsional stiffness of the flexure beams and the local moment bending stiffness of the flexure beams. Predictable and linear lateral compliance is achieved because the two axial devices are moment connected to one another by the stand-off post of high strength, linear-elastic material. Constrained layer damping treatment present in the axial devices provide damping for both axial and lateral motions. MultiFlex vibration isolators are located between the launch vehicle and payload adapter as shown in Figure 2-14.

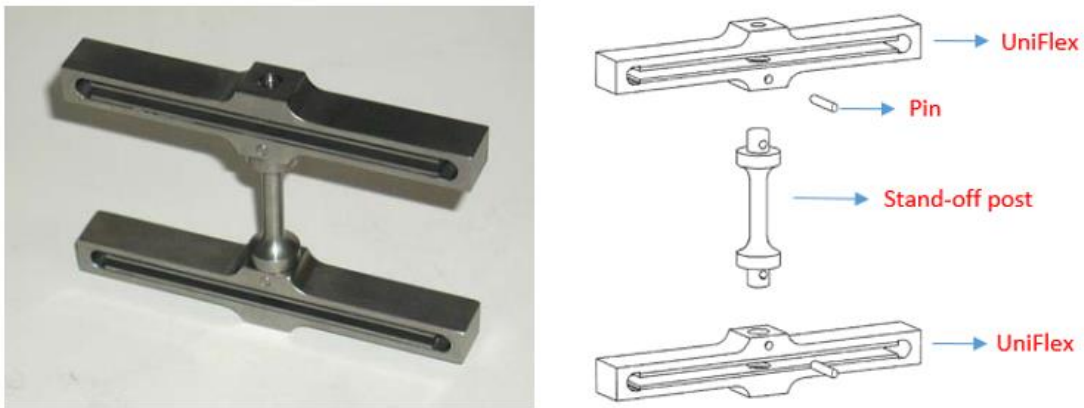

Figure 2-13 SoftRide MultiFlex isolator [26]

Figure 2-14 SoftRide MultiFlex installation [29]

Flight data from the Minotaur/JAWSAT mission, in which SoftRide vibration isolation system is used, is presented in Figure 2-15. Accelerometers are placed on both the hard side (launch vehicle side) and soft side (spacecraft side) of the isolation system. It is observed that excellent vibration isolation is achieved in both lateral and axial directions.

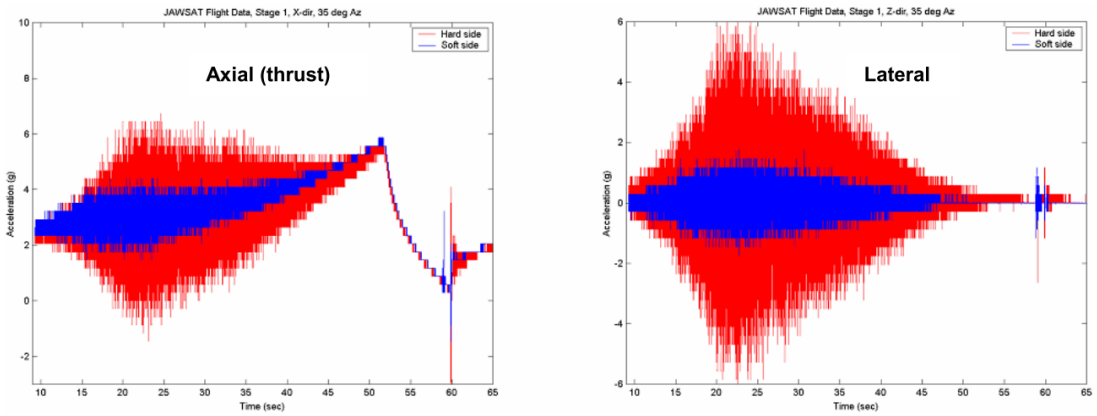

Figure 2-15 SoftRide flight data from the Minotaur/JAWSAT mission [31]

SoftRide OmniFlex is a low profile, multi-axis, highly passively damped, vibration isolation mount [27]. OmniFlex provides independently determinable compliance in all directions of vibration. Lateral compliance is provided by the flexure loop section within the flexure element between the lower and upper flexure sections. Size, shape and cross section of the flexures governs the axial and lateral stiffness. One of the most important advantages of OmniFlex is its high passive damping. VEM layer is attached to both the lower and upper flexure sections, and a relatively stiff constraining layer is attached to the opposite face of the VEM layer as shown in Figure 2-16. Significant shear is induced into the constrained VEM layer by the relative translational motion between the upper and lower flexure sections. OmniFlex vibration isolators are located between the spacecraft and payload adapter as shown in Figure 2-17.

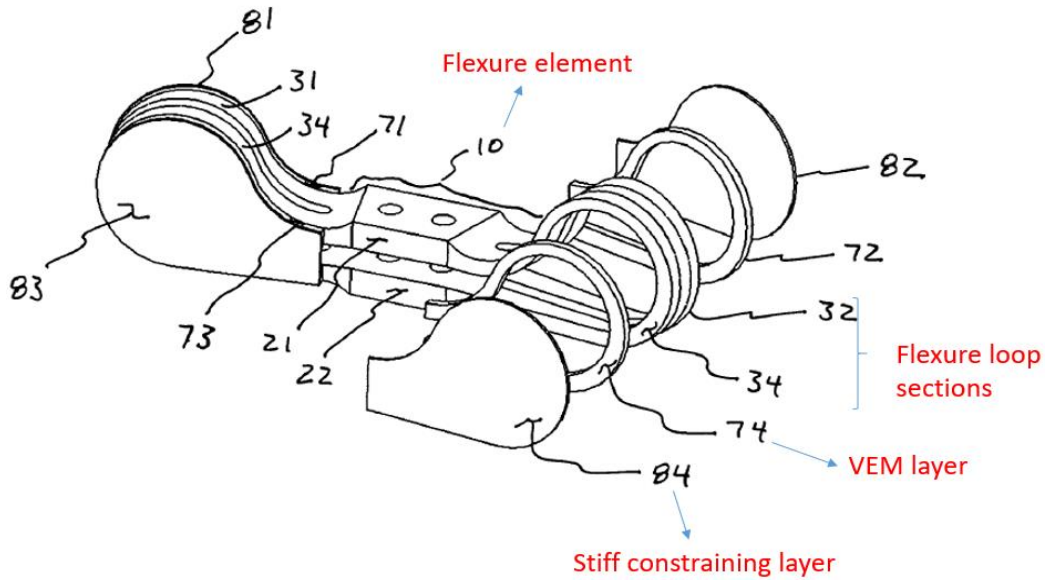

Figure 2-16 SoftRide OmniFlex isolator [27]

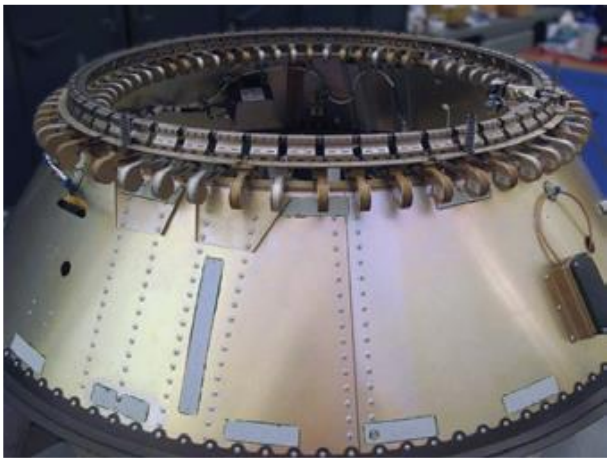

Figure 2-17 SoftRide OmniFlex installation [32]

Whole-spacecraft hybrid isolation system is developed and patented to improve the performance of passive isolation system [33]. It is an improvement on the SoftRide UniFlex vibration isolator by attaching the piezoceramic wafers to the high strain areas of the flexures as shown in Figure 2-18. An out-of-phase signal is applied to the piezoceramics by using a low-pass filter feed-forward controller to cancel out disturbances. A transmissibility comparison between the passive and hybrid isolation systems is given in Figure 2-19. It is seen from the transmissibility curve that the isolator mode is attenuated by a factor of 32 in case of hybrid isolation system.

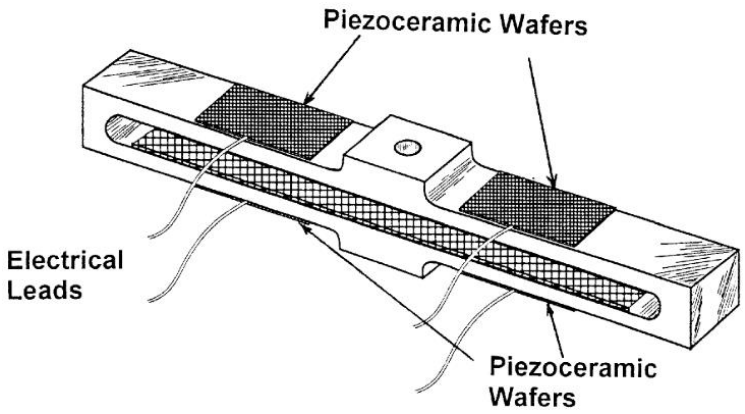

Figure 2-18 Hybrid vibration isolator [33]

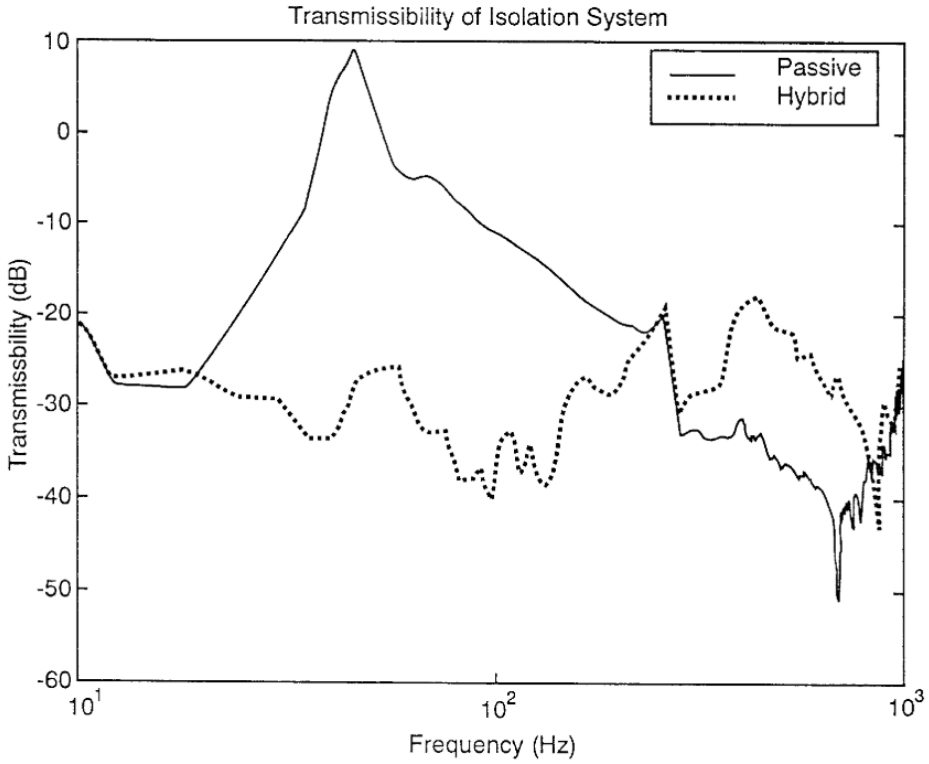

Figure 2-19 Transmissibility of hybrid and passive vibration isolation systems [33]

There are a lot of studies in the literature related with active and semi-active vibration isolation systems for whole-spacecraft vibration isolation. Evert, Janzen, Anderson,

Gerhart and Henderson described the design and development of the isolation systems, actuation and isolation architectures and control strategies [34]. Jarosh, Agnes and Karahalis investigated potential hybrid vibration isolation using adaptive control with a passive isolator [35]. Jha, Bailey and Ahmadi presented passive, active and hybrid control systems to reduce payload vibrations during space shuttle launch [36]. They stated that combining the passive isolators and active controller into a hybrid control system can provide vibration isolation for most types of base excitation. Chi, Cao and Huang explored the possibility of active damping of whole-spacecraft vibration isolation by using the voice-coil based actuator [37]. It is concluded that vibration isolation can be achieved by active and hybrid damping at the resonant frequency with Linear Quadratic Regulator (LQR) controller. Collette, Souleille, Lampert and Rodrigues presented a novel concept of active vibration isolator which is composed of a compliant metallic structure, a sensor and a piezoelectric actuator as shown in Figure 2-20 [38]. Vibration tests are performed with three different test set-ups for proof of concept of active vibration isolator. Fei, Song, Ma and Jiang studied active vibration isolation technology based on predictive control for whole-spacecraft vibration isolation [39]. Jean, Ohayon and Bihan studied semi-active vibration isolation of a spacecraft using Magneto-Rheological (MR) dampers [40].

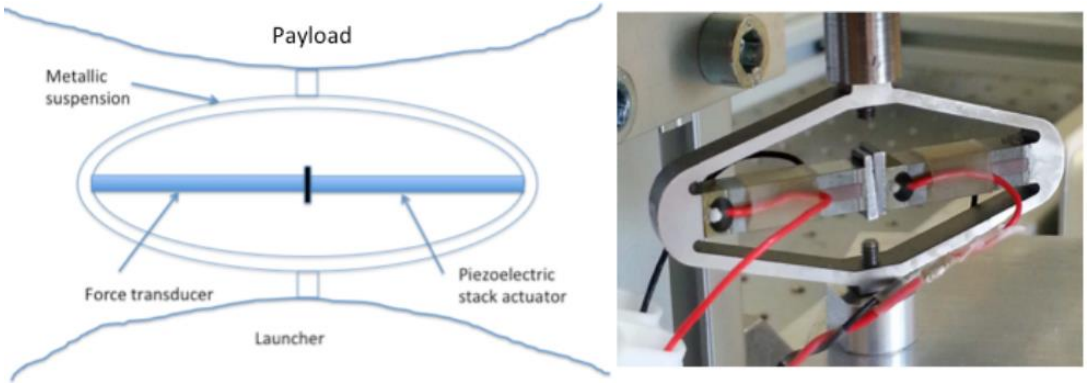

Figure 2-20 Concept of active vibration isolator [38]

2.2. Compliant Mechanism

Compliant mechanisms can be utilized in order to design vibration isolator. A compliant mechanism is a mechanism that gains some of their mobility from the deflection of flexible members [41]. On the other hand, a traditional rigid-body mechanisms commonly use very stiff or rigid parts that are connected with movable joints (Figure 2-21). Since compliant mechanisms require fewer parts, they may have advantage of simplified manufacturing process and lower cost. Another advantage of compliant mechanisms is increased performance due to reduced wear and backlash [42]. In addition, maintenance of compliant mechanisms is low since there is no need for lubrication at joints. Moreover, they are applicable for microelectromechanical systems since it is possible to miniaturize compliant mechanisms. There are also some disadvantages of compliant mechanisms such as difficulty of analysis, fatigue life, limited motion, storage of strain energy and stress relaxation [42].

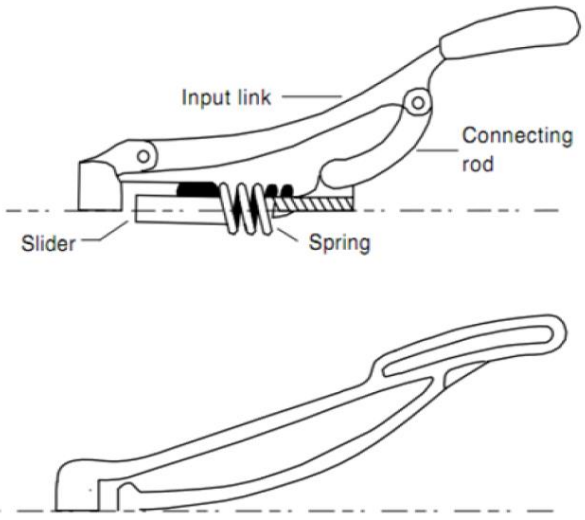

Figure 2-21 Rigid-body mechanism and compliant mechanism comparison [43]

Compliant mechanisms have potential for use in variety of disciplines such as micro systems [44], space applications [45], vehicle suspension systems [46], precision engineering [47] and vibration isolation systems [43]

2.2.1. Modeling of Compliant Mechanisms

A concept must be modeled to determine acceptable values for design parameters or confirm the performance of a given design [42]. The modeling approaches can be classified as closed form and approximate techniques or according to amount of relative deflection. These modeling approaches are [42],[48]:

- Closed-form modeling approaches (applicable for smaller and precision movements)
- The pseudo-rigid-body model approach (for larger deflections and more complex mechanisms)
- Finite element analysis

2.2.2. Synthesis of Compliant Mechanisms

There are three main synthesis techniques for synthesizing new compliant mechanisms [42],[48]:

- Modifying a concept found in the library
- Replacing an existing rigid-body mechanism
- Starting from functional requirements
    - Freedom and constraint topologies
    - Use of building blocks
    - Topology optimization

Modifying a concept found in the handbook library is the simplest way to synthesize a compliant mechanism. There are large number of compliant mechanism elements

and devices in the handbook library [42]. Some useful mechanisms for designing vibration isolator are given in Figure 2-22 - Figure 2-26.

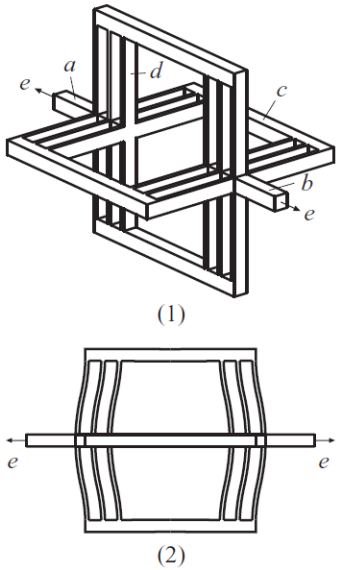

Figure 2-22 Leaf Spring Translational Joint[42]

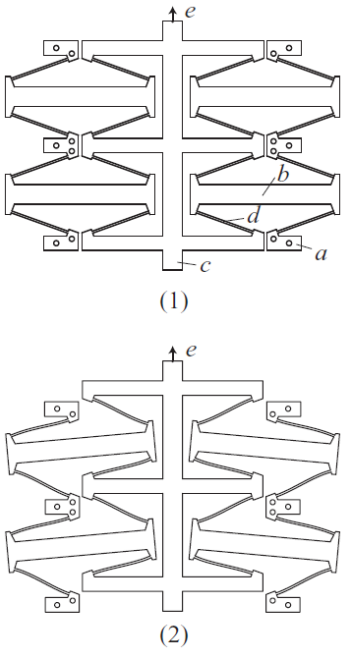

Figure 2-23 X Bob[42]

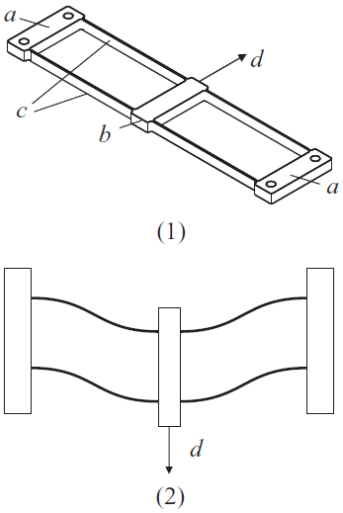

Figure 2-24 Parallel Translator[42]

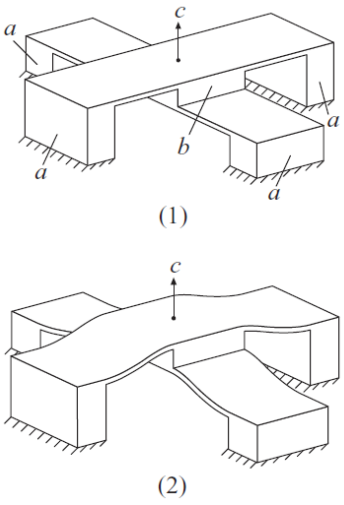

Figure 2-25 Precision Cross-Bladed Translator[42]

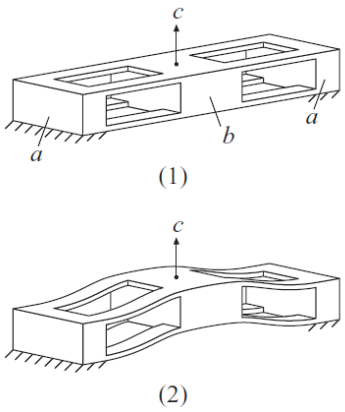

Figure 2-26 Parallel Blade Translator[42]

2.2.3. Compliant Mechanisms in Vibration Isolation Systems

Application of compliant mechanism for passive vibration isolation system have been explored by Vijayan and Karthikeyan [43],[49],[50],[51],[52]. Topology optimization is performed using ANSYS to determine the distribution path for force transmission as in Figure 2-27.

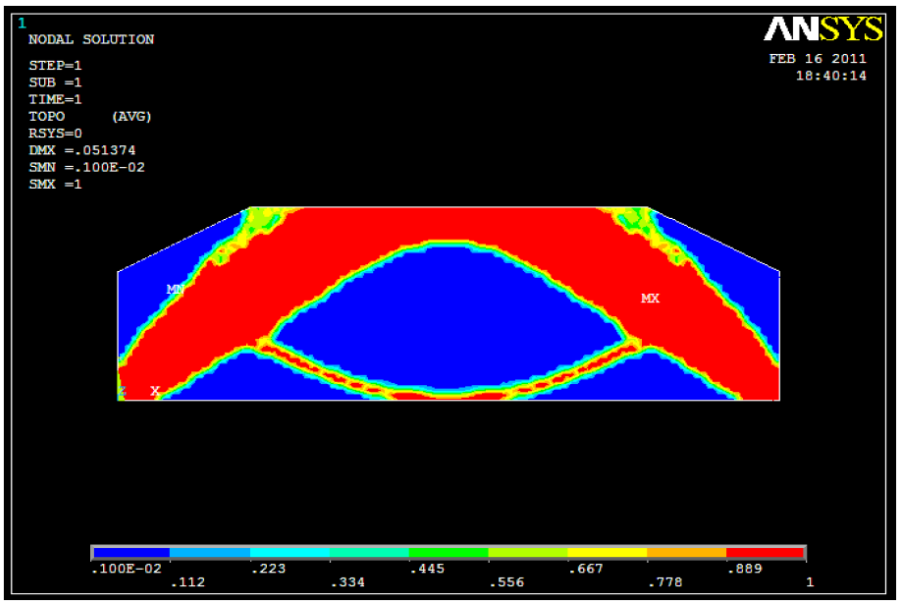

Figure 2-27 Topology optimization results for 50% volume reduction [43]

It is possible to design variety of compliant mechanism by using building blocks given in Figure 2-28.

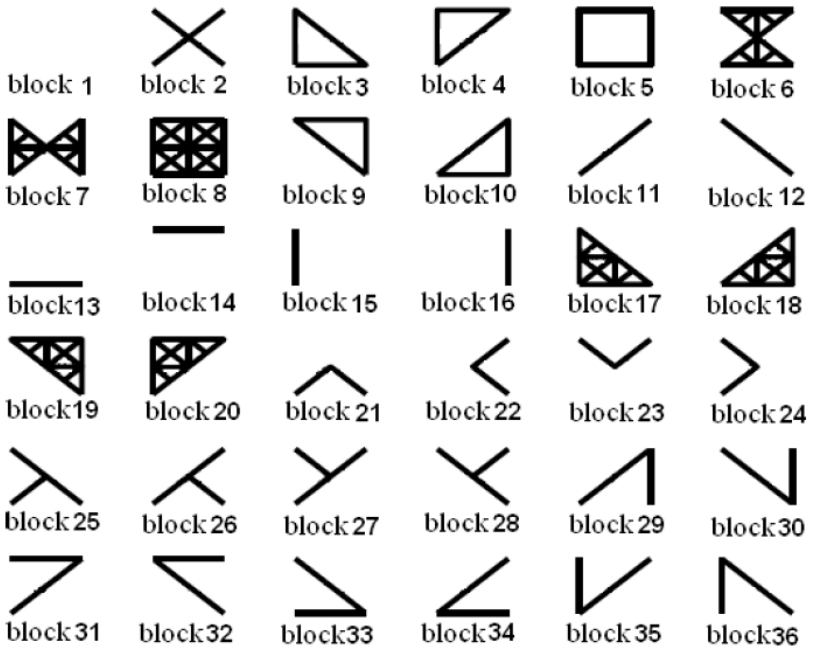

Figure 2-28 Library of building blocks [43]

Compliant mechanism is synthesized from building blocks as in Figure 2-29.

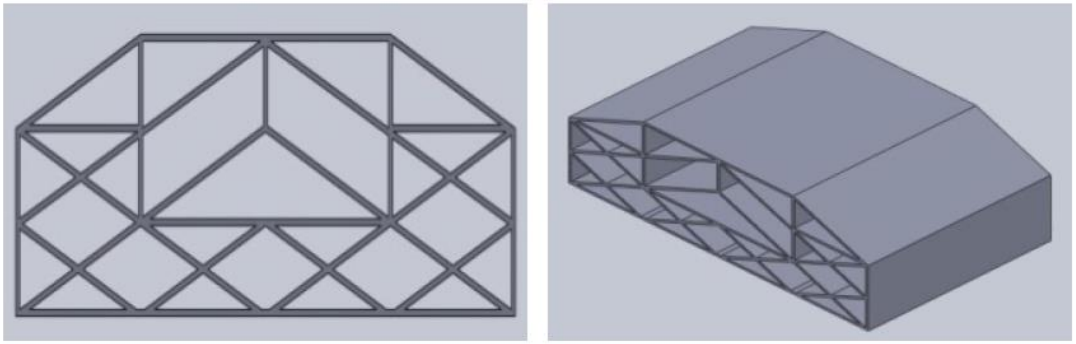

Figure 2-29 Compliant isolator design [43]

Vijayan and Karthikeyan (2009) have also conducted a study related to compliant mechanism for active vibration isolation [53]. Topology optimization is used to design compliant mechanism and feedforward control method is applied. It is shown that effective vibration isolation can be achieved by a compliant mechanism equipped with an actuator [53].

Lyon, Erickson, Evans and Howell (1999) developed a method to predict the first modal response of compliant mechanism using the pseudo-rigid-body model [54]. Yu, Howell, Lusk, Yue and He (2005) developed a dynamic model of compliant mechanisms using the pseudo-rigid-body model based on the theory of dynamic equivalence [55]. The dynamic equation and the natural frequency of compliant mechanism is obtained [55].

The frequency characteristics of compliant mechanisms are investigated by Wang and Yu [56]. Natural frequencies and mode shapes of the compliant mechanism are obtained using the dynamic model which is proposed on the basis of the finite element method. The relationship between the design parameters of compliant mechanisms and natural frequency is derived for compliant parallel-guiding mechanism. It is concluded that sensitivity of natural frequency to the thickness is relatively high whereas sensitivity to the width is very small [56].

Ling, Cao, Jiang and Lin (2016) investigated the attenuated displacement amplification of multistage compliant mechanisms, as in Figure 2-30, theoretically [57].

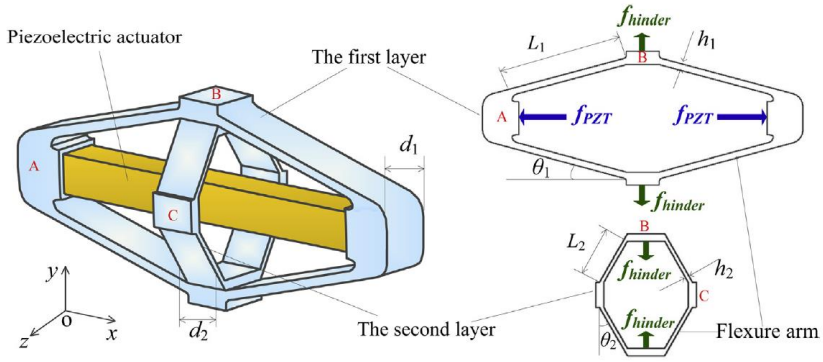

Figure 2-30 Topology of a typical multistage compliant mechanism [57]

CHAPTER 3

TECHNICAL REQUIREMENTS OF VIBRATION ISOLATION SYSTEM

3.1. Case Study

Dnepr, which is a launch vehicle evolved from intercontinental ballistic missile, and Sentinel-2 satellite, which is developed by European Space Agency, is chosen for this case study. The schematic view of Sentinel-2 and Dnepr are presented in Figure 3-1 and Figure 3-2, respectively. Vibration isolation system (VIS) is located between the payload and launch vehicle as shown in Figure 1-6. Technical requirements of VIS are determined in this case study to reduce vibration loads which is transmitted to payload, Sentinel-2, from Dnepr launch vehicle through payload adapter. One of the standard off-the-shelf payload adapters, diameter of 1194 mm, is selected in this case study and shown in Figure 3-3.

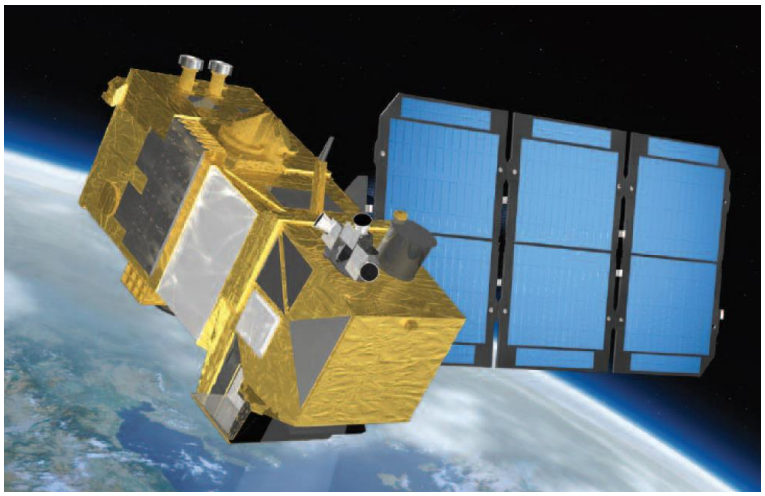

Figure 3-1 Sentinel-2 [58]

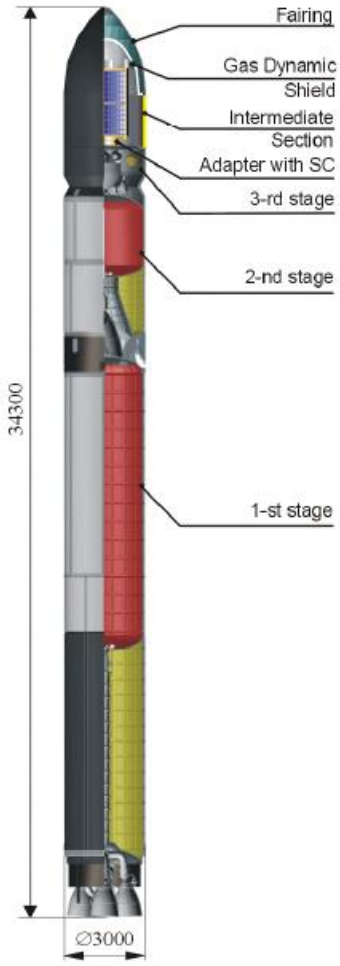

Figure 3-2 Dnepr launch vehicle [6]

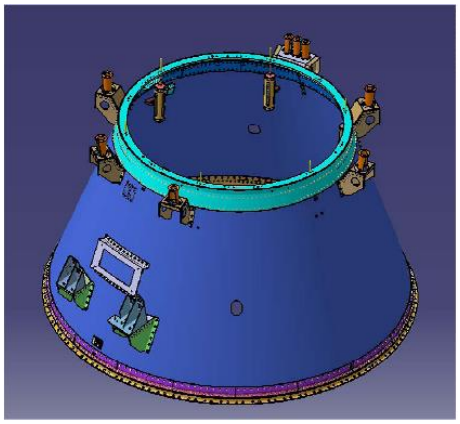

Figure 3-3 Payload adapter – PLA 1194 VG [59]

The mass of the Sentinel-2 is 1200 kg and its dimensions are 3.4 m x 1.8 m x 2.35 m [58]. The moment of inertia values, which are presented in Table 3-1, are obtained by assuming the Sentinel-2 as a homogenous cylinder with 2350mm diameter and 3400mm height.

Table 3-1 Inertial Properties of Sentinel-2

Inertial Property	**Value**	**Unit**
Mass	1200	kg
Ix	1570	kg.m^2
Iy	828	kg.m^2
Iz	1570	kg.m^2

Three types of dynamic loads are acting on the payload-launch vehicle interface, namely quasi-static accelerations, harmonic vibrations and random vibrations [6]. Maximum quasi-static and dynamic accelerations, amplitudes of harmonic oscillations in longitudinal and lateral directions, spectral density of vibro-accelerations at payload-launch vehicle interface of Dnepr launch vehicle is given in Table 1-2 to Table 1-5.

3.2. System-Level Technical Requirements

The functional requirements of vibration isolation system:

- VIS must reduce random vibration loads which are transmitted to the payload from launch vehicle during launch.
- VIS must constrain displacement of payload under harmonic vibration loads which are transmitted to the payload from launch vehicle during launch.
- VIS must provide mechanical connection between payload and launch vehicle.
- VIS must withstand static weight of payload.
- VIS must withstand quasi-static loads during launch.

- VIS must be adaptable to different launch vehicles and payloads.

The performance requirements of vibration isolation system:

- Response RMS acceleration of any point on payload must be lower than 2 gRMS under random vibration input of 6.5 gRMS in longitudinal direction which is given in Table 1-5.
- Response RMS acceleration of any point on payload must be lower than 2 gRMS under random vibration input of 6.5 gRMS in lateral direction which is given in Table 1-5.
- Harmonic displacement amplitude of any point on payload must be lower than 20 mm under harmonic vibration input in longitudinal direction which is given in Table 1-3.
- Harmonic displacement amplitude of any point on payload must be lower than 20 mm under harmonic vibration input in lateral direction which is given in Table 1-4.
- Static load capacity of VIS shall be 1200 kg.
- VIS shall withstand the quasi-static acceleration of 8.3 g in longitudinal direction.
- VIS shall withstand the quasi-static acceleration of 1 g in lateral direction.
- Static deflection of vibration isolators shall be lower than 3 mm under the quasi-static acceleration of 8.3 g in longitudinal direction.
- Static deflection of vibration isolators shall be lower than 3 mm under the quasi-static acceleration of 1 g in lateral direction.

The physical requirements of vibration isolation system:

- Total mass of VIS must be lower than 30 kg.
- Total height of VIS must be lower than 100 mm.

The mechanical interface requirements of vibration isolation system:

- VIS must have suitable mechanical interface for attachment of payload.
- VIS must have suitable mechanical interface for attachment of launch vehicle.

3.3. Determination of Vibration Isolator Properties

Based on system-level performance requirements of vibration isolation system, vibration isolator properties, which are stiffness and damping, must be determined as well as the number of vibration isolators in VIS. Firstly, 12 parameter sets with different stiffness, loss factor and number of isolators are created as in Table 3-2. Then, modal analyses and response analyses for harmonic and random vibration inputs are performed for different sets of parameters in order to examine the effect of isolator properties on system-level performance.

Table 3-2 Parameter Sets of Vibration Isolation System

Parameter Set	Number of Isolators	Loss Factor	k_x [N/mm]	k_y [N/mm]	k_z [N/mm]
Set-1	60	0.1	1000	1000	1000
Set-2	60	0.1	2000	1000	2000
Set-3	60	0.1	500	500	500
Set-4	60	0.1	500	2000	500
Set-5	60	0.1	500	5000	500
Set-6	60	0.1	1000	2000	1000
Set-7	60	0.1	500	1000	500
Set-8	30	0.1	1000	2000	1000
Set-9	120	0.1	250	500	250
Set-10	60	0.05	500	1000	500
Set-11	60	0.2	500	1000	500
Set-12	60	0.2	500	500	500

The analyses for the parameters in Table 3-2 are performed using mathematical model that is developed in MATLAB®. In these analyses, vibration isolators are modelled as massless spring elements with constant stiffness coefficients and hysteretic damping. The stiffness of a vibration isolator in the directions of the coordinate axes is expressed as [60]

$$k_{xx} = k_p\lambda_{xp}^2 + k_q\lambda_{xq}^2 + k_r\lambda_{xr}^2 \tag{3.1}$$

$$k_{yy} = k_p\lambda_{yp}^2 + k_q\lambda_{yq}^2 + k_r\lambda_{yr}^2 \tag{3.2}$$

$$k_{zz} = k_p\lambda_{zp}^2 + k_q\lambda_{zq}^2 + k_r\lambda_{zr}^2 \tag{3.3}$$

$$k_{xy} = k_p\lambda_{xp}\lambda_{yp} + k_q\lambda_{xq}\lambda_{yq} + k_r\lambda_{xr}\lambda_{yr} \tag{3.4}$$

$$k_{xz} = k_p\lambda_{xp}\lambda_{zp} + k_q\lambda_{xq}\lambda_{zq} + k_r\lambda_{xr}\lambda_{zr} \tag{3.5}$$

$$k_{yz} = k_p\lambda_{yp}\lambda_{zp} + k_q\lambda_{yq}\lambda_{zq} + k_r\lambda_{yr}\lambda_{zr} \tag{3.6}$$

where,

p, q, r : the principal elastic axes

x, y, z : the reference coordinate system axes

k_{xx}, k_{yy}, k_{zz} : proper translation stiffness constants

k_{xy}, k_{xz}, k_{yz} : cross translational stiffness constants

k_p, k_q, k_r : the translational stiffness constants

λ_{xp}, λ_{xq}, ... : the cosines of the angles between the principal elastic axes p, q, r and the reference coordinate system axes x, y, z

Vibration isolators are orthogonal and angular stiffness of the isolators are neglected. Structural damping model is used with complex spring stiffness

$$k^* = k(1 + i\eta) \tag{3.7}$$

where k is the stiffness coefficient, i is the complex number and η is the loss factor.

There are six equations of motion (EOM) which describe the six degrees-of-freedom (DOF) system [60]. Matrix form of EOM for this 6 DOF vibration isolation system is given as follows:

$$[M]\{\ddot{q}\} + [K]\{q\} = \{F\} \tag{3.8}$$

where [M] is 6x6 mass matrix, [K] is 6x6 stiffness matrix, {F} is 6x1 forcing vector and {q} is 6x1 response vector of center of gravity (CG) point.

Modal analysis is performed in order to determine the natural frequencies. The eigenvalue problem can be obtained from EOM and following equation must be solved to calculate the natural frequencies

$$\det([K] - w^2[M]) = 0 \tag{3.9}$$

Response of a system for harmonic vibration input is as follows

$$\{q\} = [\alpha]\{F\} \tag{3.10}$$

where [α] is the 6x6 receptance matrix

$$[\alpha] = ([K] - \omega^2[M])^{-1} \tag{3.11}$$

For random vibration input, matrix spectral density of the output is [61]:

$$\mathbf{S}_{XX}(\omega) = \mathbf{H}^*(\omega)\mathbf{S}_{FF}(\omega)\mathbf{H}^{\mathrm{T}}(\omega) \tag{3.12}$$

where, $\mathbf{H}(\omega)$ is the frequency response function given by

$$\mathbf{H}(\omega) = \begin{bmatrix} H_{11}(\omega) & \cdots & H_{1N}(\omega) \\ \vdots & \ddots & \vdots \\ H_{N1}(\omega) & \cdots & H_{NN}(\omega) \end{bmatrix} \tag{3.13}$$

and $\mathbf{S}_{FF}(\omega)$ is the force spectral density given by

$$\mathbf{S}_{FF}(\omega) = \begin{bmatrix} S_{F_1F_1}(\omega) & \cdots & S_{F_1F_N}(\omega) \\ \vdots & \ddots & \vdots \\ S_{F_NF_1}(\omega) & \cdots & S_{F_NF_N}(\omega) \end{bmatrix} \tag{3.14}$$

Mathematical model of vibration isolation system is verified with finite element model which is constructed in Abaqus as seen in Figure 3-4 which indicates the schematic view of VIS and points of interests. Y-direction is expressed as axial or longitudinal direction whereas x and z-directions are expressed as lateral directions. Due to symmetry of the VIS, only one of the lateral directions, x or z direction, is examined in response analyses in addition to the axial direction.

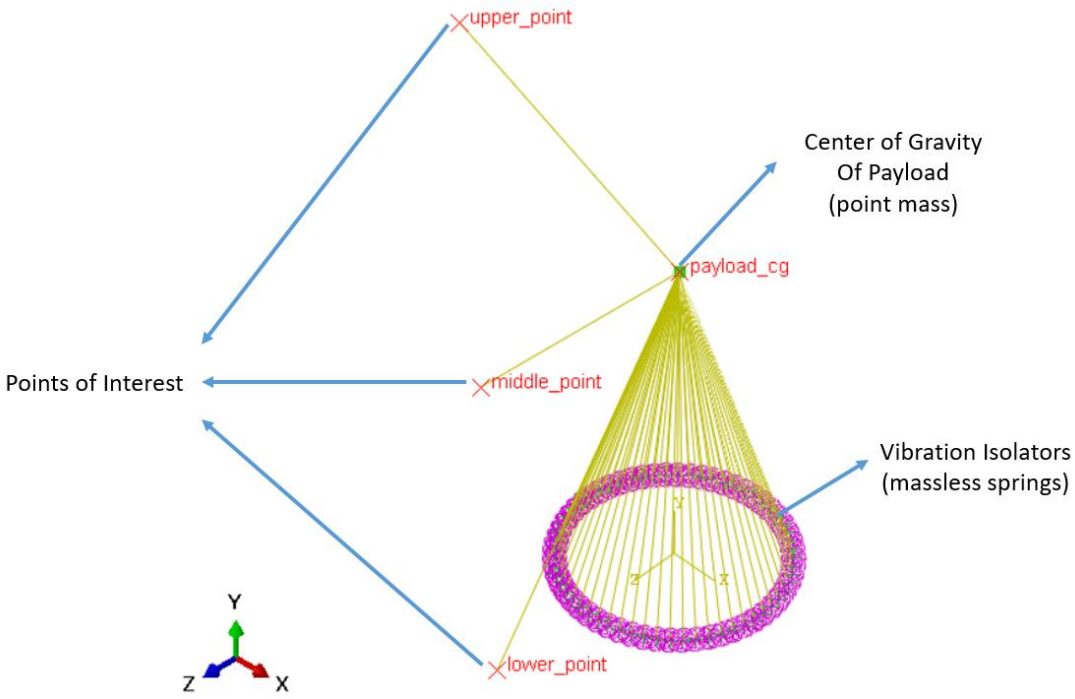

Figure 3-4 Schematic View of Vibration Isolation System

The results of random vibration analyses for the vibration input of 6.5 gRMS, which is given in Table 1-5, are given in Table 3-3 for the sets of parameters given in Table

3-2. In addition, the results of harmonic vibration analyses for the harmonic vibration inputs, which are given in Table 1-3 and Table 1-4, are presented in Table 3-4.

Table 3-3 The results of random vibration analyses for different parameter sets

	CG		Upper Point		Middle Point		Lower Point	
Parameter Set	**Axial gRMS**	**Lateral gRMS**	**Axial gRMS**	**Lateral gRMS**	**Axial gRMS**	**Lateral gRMS**	**Axial gRMS**	**Lateral gRMS**
Set-1	1.94	0.78	2.31	0.98	2.31	0.78	2.31	2.54
Set-2	1.94	1.07	2.56	1.28	2.56	1.07	2.56	3.41
Set-3	1.58	0.65	1.89	0.81	1.89	0.65	1.89	2.11
Set-4	2.33	0.55	2.54	0.87	2.54	0.55	2.54	1.96
Set-5	3.05	0.41	3.19	0.95	3.19	0.41	3.19	1.69
Set-6	2.33	0.74	2.64	1.01	2.64	0.74	2.64	2.48
Set-7	1.94	0.61	2.20	0.83	2.20	0.61	2.20	2.06
Set-8	1.94	0.61	2.20	0.83	2.20	0.61	2.20	2.06
Set-9	1.94	0.61	2.20	0.83	2.20	0.61	2.20	2.06
Set-10	2.77	0.88	3.13	1.18	3.13	0.88	3.13	2.93
Set-11	1.35	0.43	1.54	0.59	1.54	0.43	1.54	1.45
Set-12	1.07	0.46	1.30	0.57	1.30	0.46	1.30	1.48

Table 3-4 The results of harmonic vibration analyses for different parameter sets

	Upper Point		Middle Point		Lower Point	
Parameter Set	**Axial Disp. [mm]**	**Lateral Disp. [mm]**	**Axial Disp. [mm]**	**Lateral Disp. [mm]**	**Axial Disp. [mm]**	**Lateral Disp. [mm]**
Set-1	5.1	32.2	5.1	17.0	5.1	12.5
Set-2	5.1	31.7	5.1	16.4	5.1	12.5
Set-3	5.2	64.5	5.2	34.0	5.2	12.6
Set-4	5.0	17.8	5.0	12.8	5.0	12.5
Set-5	5.0	12.8	5.0	12.6	5.0	12.5
Set-6	5.0	16.8	5.0	12.8	5.0	12.5
Set-7	5.1	33.3	5.1	17.9	5.1	12.5
Set-8	5.1	33.3	5.1	17.9	5.1	12.5
Set-9	5.1	33.3	5.1	17.9	5.1	12.5
Set-10	5.1	64.2	5.1	34.4	5.1	12.5
Set-11	5.1	16.9	5.1	13.2	5.1	12.5
Set-12	5.2	32.7	5.2	18.0	5.2	12.6

The parameter sets that do not satisfy the system-level performance requirements are highlighted with red in Table 3-3 and Table 3-4. The only parameter set which meet all system-level performance requirements is Set-11. Therefore, design of vibration isolators is performed to achieve isolator properties given in Table 3-5 for VIS of 60 isolators.

Table 3-5 Vibration Isolator Properties for VIS of 60 isolators

Property	**Unit**	**Value**
k_x	[N/mm]	500
k_y	[N/mm]	1000
k_z	[N/mm]	500
Loss factor	-	0.2

For some applications, using larger or smaller number of isolators can be preferable due to practical reasons. It is possible to change number of isolators and their stiffness values by keeping the effective stiffness same. For example, if usage of 20 isolators is desired, instead of 60, in this case study, the required stiffness values of vibration isolators would be three times larger as presented in Table 3-6.

Table 3-6 Vibration Isolator Properties for VIS of 20 isolators

Property	**Unit**	**Value**
k_x	[N/mm]	1500
k_y	[N/mm]	3000
k_z	[N/mm]	1500
Loss factor	-	0.2

Moreover, the internal resonance frequencies of vibration isolators must be as high as possible in order to eliminate wave effect which is illustrated in Figure 3-5. As seen in Figure 3-5, there are numerous peaks in the high frequency range for helical spring, which is made of steel, because of its relatively high mass. Note that all isolators have mass in real life even though vibration isolators are modelled as massless springs.

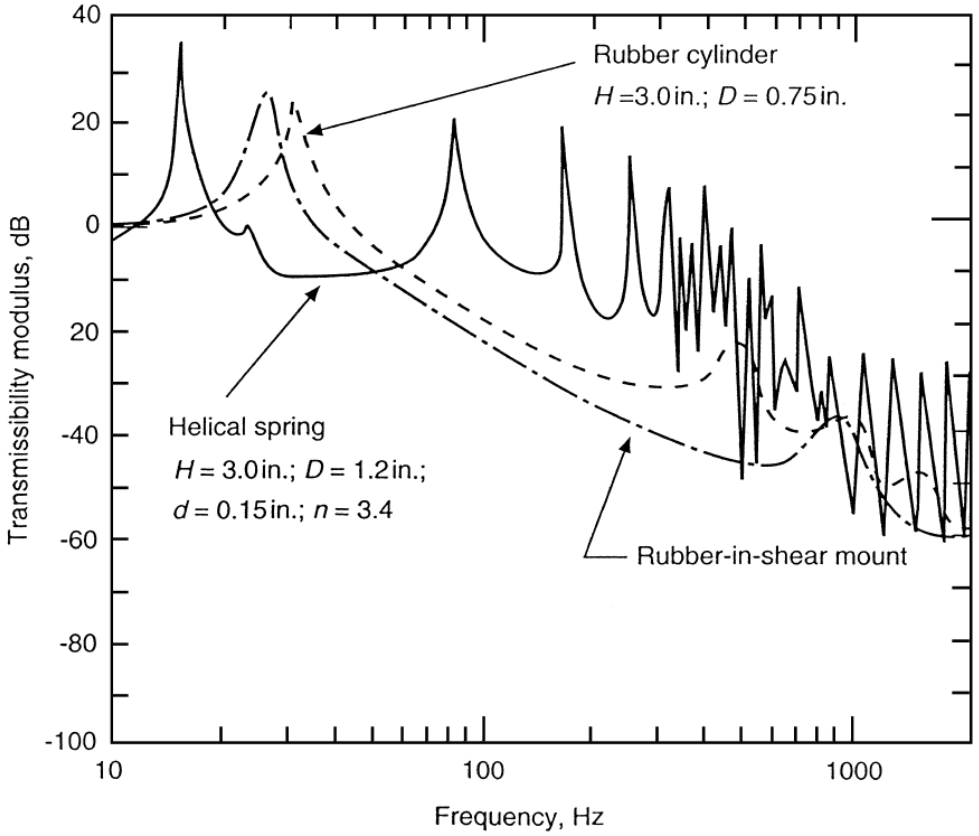

Figure 3-5 Transmissibility in a Broad Frequency Range for Three Different Types of Isolators [60]

The internal resonances of vibration isolators will be obtained for two different boundary conditions which are BC-1 and BC-2 (Figure 3-6).

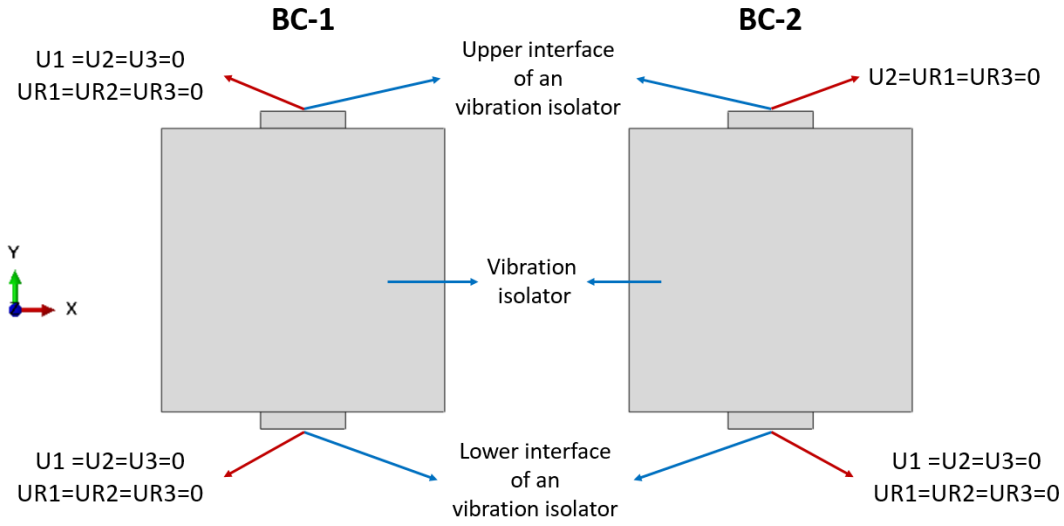

Figure 3-6 Boundary conditions for obtaining internal resonances of vibration isolators

CHAPTER 4

CONCEPTUAL DESIGN OF VIBRATION ISOLATION SYSTEM

The conceptual design of a vibration isolator, which satisfies the requirements in 3.3, is performed by three different methods: topology optimization, inspiration by existing vibration isolators and compliant mechanisms.

4.1. Conceptual Design Studies Based on Topology Optimization

The system design in which a measure of performance is to be optimized while satisfying constraints can be formulated as an optimization problem [62]. The standard design optimization model is to find a vector of design variables

$$\mathbf{x} = (x_1, x_2, \dots, x_n) \tag{4.1}$$

to minimize the objective function

$$f(\mathbf{x}) = f(x_1, x_2, \dots, x_n) \tag{4.2}$$

subject to the *p* equality constraints

$$h_j(\mathbf{x}) = h_j(x_1, x_2, \dots, x_n) = 0; \quad j=1 \text{ to } p \tag{4.3}$$

and the *m* inequality constraints

$$g_i(\mathbf{x}) = g_i(x_1, x_2, \dots, x_n) \leq 0; \quad i=1 \text{ to } m \tag{4.4}$$

If one or more constraint functions are violated, it is called infeasible design. If all the constraints are satisfied, it is expressed as feasible design. The optimum design gives the minimum possible value of the objective function and satisfies all the constraints [63].

The structural optimization problems can be divided into three classes: sizing, shape and topology optimization [64]. In sizing optimization, the goal is to find optimal structural thickness such as thickness distribution of a plate or cross-sectional properties of a beam. In shape optimization, the design variable is the form of the boundary of the structural domain. The most general form of structural optimization is the topology optimization which is concerned with material distribution. Topology optimization involves the determination of features and connectivity of the domain [65]. Three classes of structural optimization are illustrated in Figure 4-1.

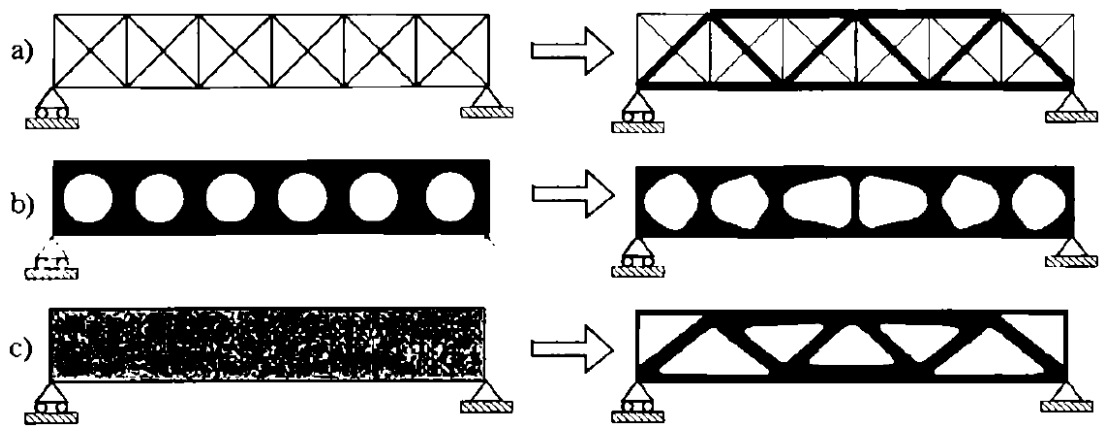

Figure 4-1 Three classes of structural optimization. a) Sizing, b) shape, c) topology. [65]

In this thesis study, student edition of OptiStruct® is used for topology optimization in order to design a vibration isolator. OptiStruct® solves topology optimization problems using the solid isotropic material with penalization (SIMP) method [63]. The solver calculates a material density for each element and these are used as the design variable. Material density of each element should be 1 or 0, which defines the element as solid or void, respectively. However, these density values vary continuously between 0 and 1. Intermediate values of density do not represent real material and the

solutions, which involve intermediate densities in the structural domain, are not meaningful. Therefore, penalization technique is used to force the density of each element to take a value of either 0 or 1. This technique can be expressed as:

$$\bar{K} = \rho^p * K \tag{4.5}$$

where, $\bar{K}$ is the penalized stiffness matrix, ρ is the density, p is the penalization factor and K is the real stiffness matrix. Note that the penalization factor is always greater than 1 and it takes higher values in case of existence of the manufacturing constraints.

Topology optimization is applied in order to design a novel vibration isolator which satisfies the requirements in Table 3-5. Student edition of OptiStruct® is used for topology optimization and HyperMesh® is used as a finite element pre-processor.

Firstly, design space and non-design space for a vibration isolator is determined as in Figure 4-2. The diameter of chosen payload adapter, number of vibration isolators, requirement related with total height of a vibration isolation system and mechanical interfaces of vibration isolators are taken into consideration by determining these spaces.

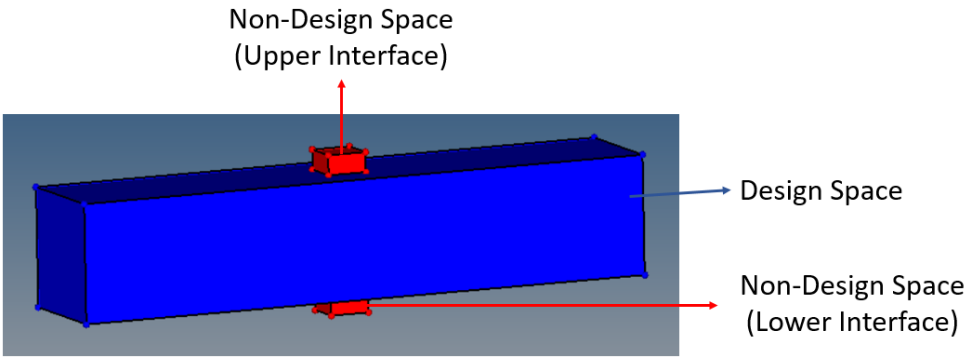

Figure 4-2 Design and non-design space for topology optimization of a vibration isolator

For a predetermined design space shown in Figure 4-2, optimization parameters are defined. Total mass is defined as objective function to be minimized. Static displacements under static load in three coordinate axes are defined as constraints. Static loads are applied at upper interface of a vibration isolator in three coordinate axes separately while applying fixed boundary condition at the lower interface. Static displacement constraints are derived from stiffness requirements of vibration isolators in Table 3-5. Since the displacement is simply the ratio of applied force to the stiffness, the static displacement constraints for a node in the upper interface for 1000 N static load are:

$$1.9\ mm \leq \Delta x \leq 2.1\ mm \tag{4.6}$$

$$0.9\ mm \leq \Delta y \leq 1.1\ mm \tag{4.7}$$

$$1.9\ mm \leq \Delta z \leq 2.1\ mm \tag{4.8}$$

Note that magnitude of a static load is chosen as 1000 N arbitrarily because actual interested parameter is stiffness rather than displacement value and stiffness values are not dependent on magnitude of static load. Moreover, volume fraction, which is the ratio of a final design volume to the initial design volume, is defined as a constraint due to strength requirement. Lower limit for volume fraction is taken as 0.05 and 0.1, and two different solutions are obtained for each of these values. If this constraint was not defined, the result of a topology optimization would be the smallest possible design due to objective function but it would not withstand the static loads. Furthermore, member size control is applied to achieve more discrete design. Member size control penalizes the intermediate density values, limits the smallest dimension to be retained in topology design and minimizes the checkerboard effect [63].

The results of topology optimization for two different volume fraction constraints are presented in Figure 4-3. Note that Aluminum 6061 is chosen as isolator material due to its widespread availability.

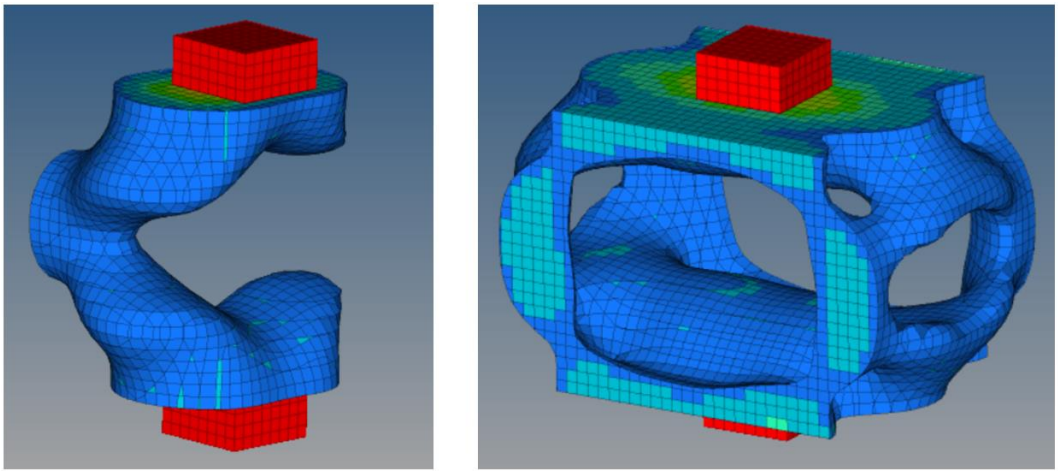

Figure 4-3 Topology optimization results

Based on topology optimization results, 3 different novel design concepts are created and they are named as T1, T1-C and T2. T1 vibration isolator concept is shown in Figure 4-4.

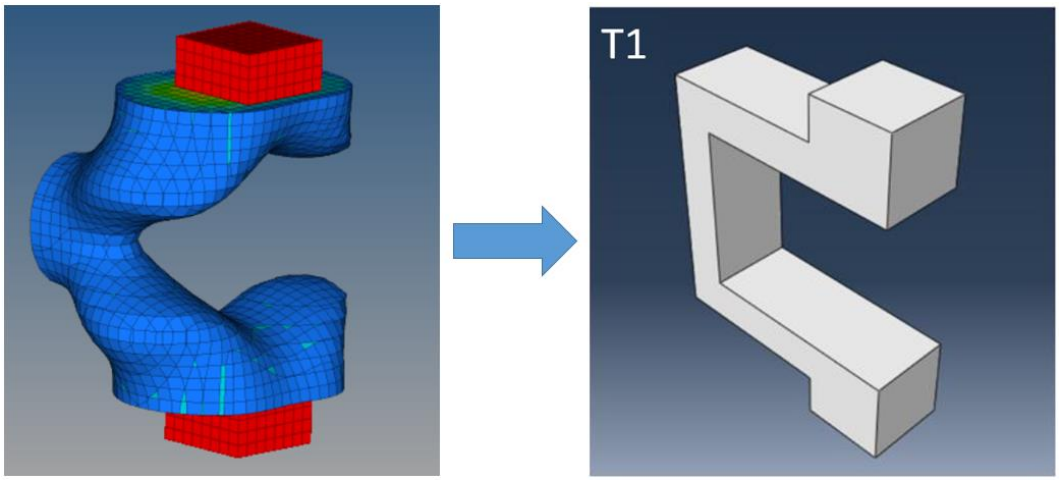

Figure 4-4 Conceptual design of T1 vibration isolator based on topology optimization result

The number of vibration isolators in vibration isolation system is 60 for the case study as stated in Table 3-5 and these vibration isolators are located at the upper interface of a payload adapter. T1-C vibration isolator concept is created considering the usage of a single large isolator instead of numerous number of discrete isolators. T1-C vibration isolator can be considered as continuous form of T1 vibration isolation system as indicated in Figure 4-5.

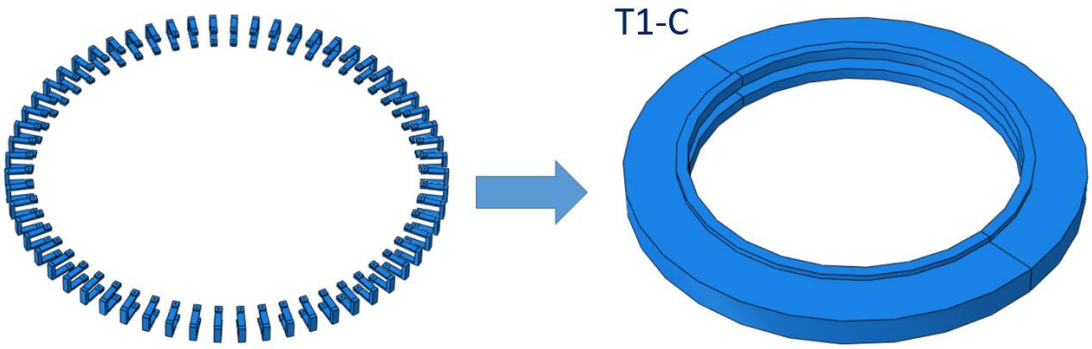

Figure 4-5 Conceptual design of T1-C vibration isolator based on T1 vibration isolation system

The another novel vibration isolator concept, which is also created based on topology optimization result, is named as T2 and shown in Figure 4-6.

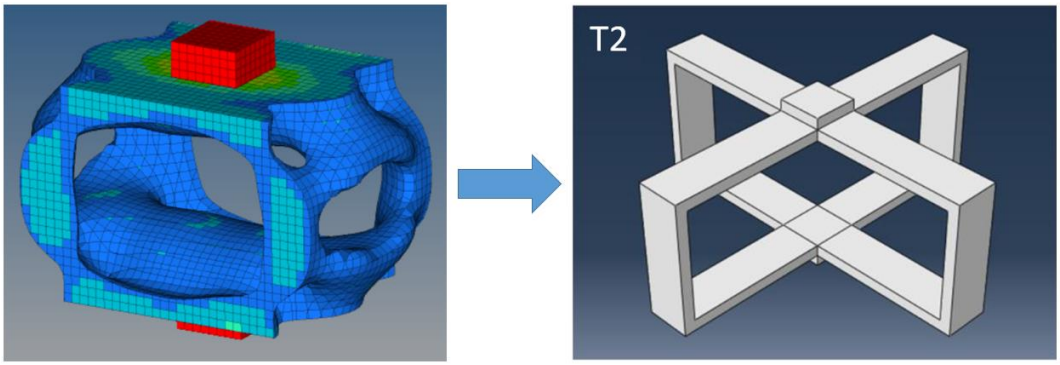

Figure 4-6 Conceptual design of T2 vibration isolator based on topology optimization result

It is important to state that T2 vibration isolator concept can be achieved by utilizing a compliant mechanism called precision cross-bladed translator (Figure 2-25). T2 is basically a couple of precision cross-bladed translators that are connected in series. Moreover, conceptual design of C1 vibration isolator, which is illustrated in Figure 4-7, is obtained by inspiring from precision cross-bladed translator mechanism.

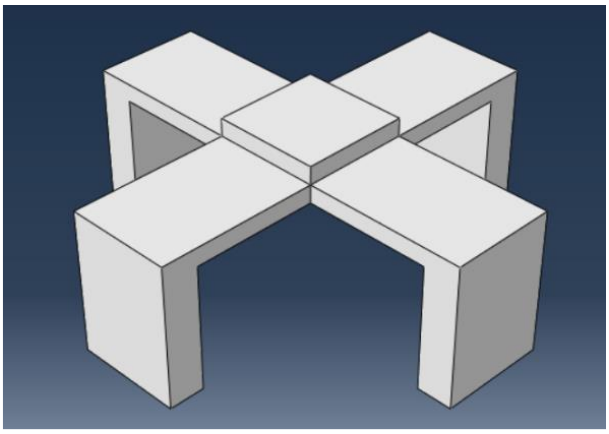

Figure 4-7 Conceptual design of C1 vibration isolator based on compliant mechanisms

It is possible to obtain desired stiffness characteristics with C1 isolator concept. But it has disadvantage related with mechanical interface. Since it has four interface points at the lower region, it requires larger interface area on payload adapter, which is non-standard for payload adapter.

4.2. Conceptual Design Studies Based on Existing Vibration Isolators

The vibration isolator concepts S1 and S2, which are presented in Figure 4-8 and Figure 4-9 respectively, are developed after examining SoftRide vibration isolators and understanding their working principle.

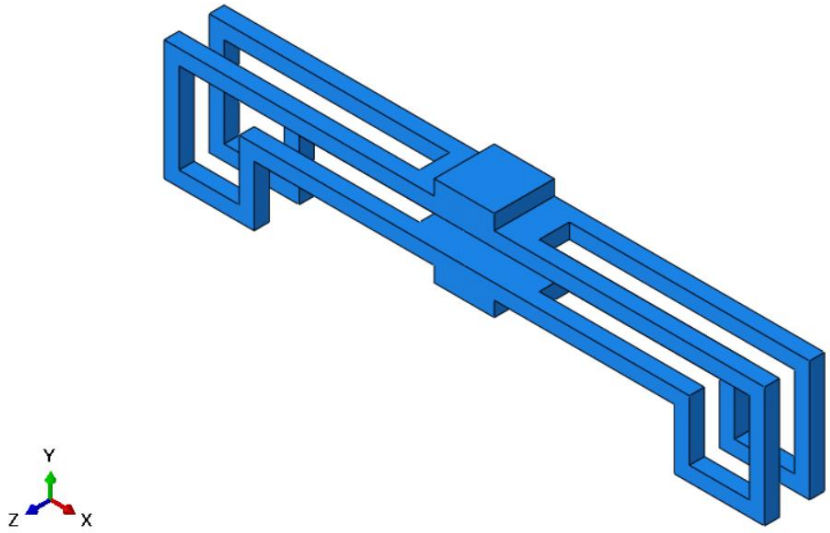

Figure 4-8 Conceptual design of S1 vibration isolator based on similar vibration isolators

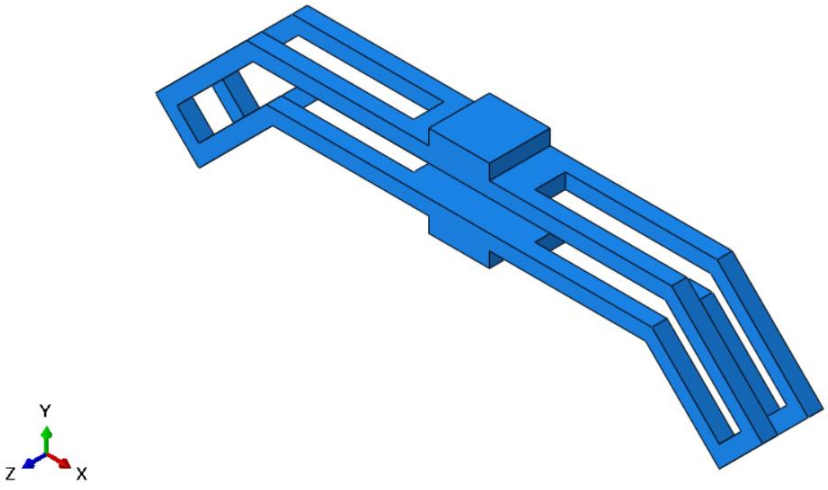

Figure 4-9 Conceptual design of S2 vibration isolator based on similar vibration isolators

CHAPTER 5

DETAILED DESIGN OF VIBRATION ISOLATION SYSTEM

Detailed design of vibration isolator concepts, which are created as explained in Chapter 4, are performed to achieve required stiffness and loss factor values. Three isolator concepts, namely T1, T2, and S1, are selected among six conceptual design alternatives and detailed design of these isolator concepts are conducted as presented in subsequent sections.

5.1. Detailed Design of T1

Firstly, design of metallic part of T1 is performed by determining the dimensions of parameters which are depicted in Figure 5-1. These parameters are determined such that T1 has compliance in three translational axes with stiffness constants given in Table 3-5.

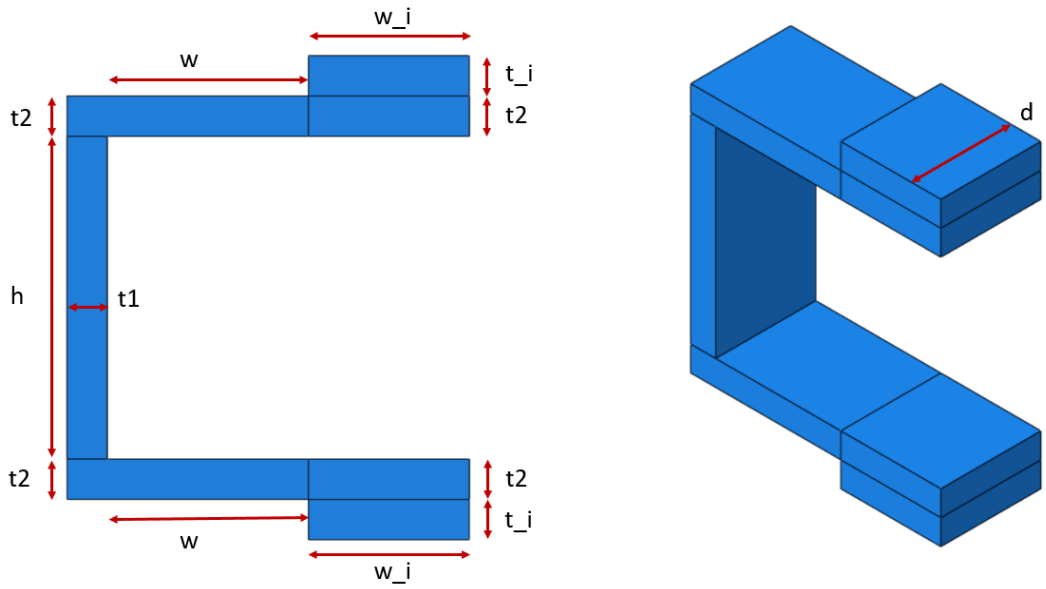

Figure 5-1 Design Parameters of T1-Vibration Isolator

Static load analyses of T1-vibration isolator with different sets of design parameters are performed in order to understand the effect of design parameters on stiffness constants. Abaqus is used in this study for stiffness measurement of a vibration isolator by finite element analysis. In these analyses, upper and lower reference points are created on the upper and lower interfaces of a vibration isolator as shown in Figure 5-2. These reference points are connected to the interface surfaces using “coupling” type of constraint in Abaqus. Boundary conditions are defined such that all six degrees of freedom are constrained at lower interface and five degrees of freedom, all DOFs other than DOF of applied static force, are constrained at upper interface. Then, static force is applied at upper reference point in one of the translational directions. “Static, General” step is used in Abaqus and displacement at upper reference point is measured in the direction of applied force. Then, the proper translation stiffness constant of a vibration isolator in the direction of applied force is obtained by dividing the applied static force to the measured displacement at the upper interface point. In order to obtain stiffness constants of a vibration isolator in all directions, three different analyses with the applied forces in x, y, and z directions must be performed separately.

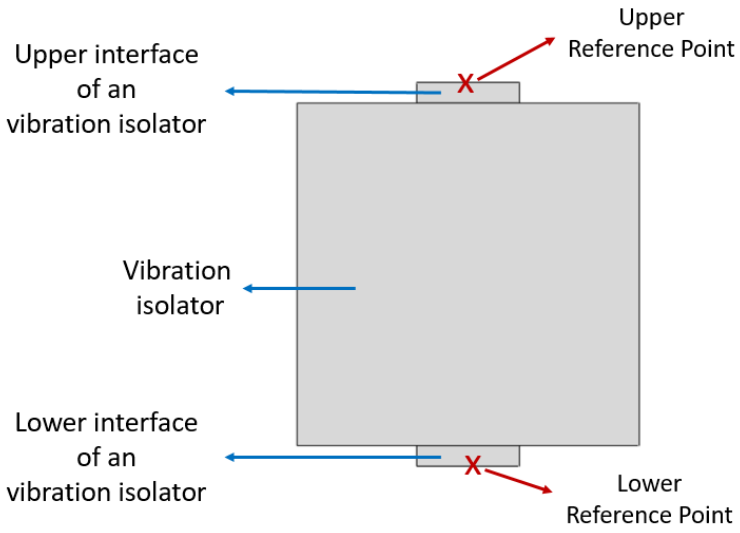

Figure 5-2 Schematic view of vibration isolator

Three proper translation stiffness constants k_{xx}, k_{yy}, k_{zz} are computed simply by dividing the applied force to the displacement in the same direction. On the other hand, three cross translational stiffness constants k_{xy}, k_{xz}, k_{yz} are determined from force-displacement relation in Eq.(5.1) by solving 3 equations for 3 unknowns. Note that the stiffness constants have reciprocity properties [60].

$$\begin{bmatrix} F_x \\ F_y \\ F_z \end{bmatrix} = \begin{bmatrix} k_{xx} & k_{xy} & k_{xz} \\ k_{xy} & k_{yy} & k_{yz} \\ k_{xz} & k_{yz} & k_{zz} \end{bmatrix} \times \begin{bmatrix} \Delta x \\ \Delta y \\ \Delta z \end{bmatrix} \tag{5.1}$$

The stiffness constants of T1 design alternatives are tabulated in Table 5-1. Design parameters related with interface region are kept constant for all design alternatives such that d = 20 mm, w_i = 20 mm, and t_i = 5 mm. Note that Aluminum 6061 is chosen as isolator material due to its widespread availability.

Table 5-1 The stiffness constants of T1 design alternatives

T1 Design Alternatives	**h** [mm]	**w** [mm]	**t1** [mm]	**t2** [mm]	**k_x** [N/mm]	**k_y** [N/mm]	**k_z** [N/mm]
T1_A1	40	50	12	6	**378**	**676**	**394**
T1_A2	40	45	12	6	**412**	**872**	**441**
T1_A3	40	50	15	6	**380**	**713**	**407**
T1_A4	40	50	12	8	**757**	**1252**	**623**
T1_A5	30	50	12	6	**613**	**698**	**569**
T1_A6	40	50	16	8	**768**	**1414**	**661**
T1_A7	40	50	12	7	**552**	**951**	**510**
T1_A8	40	50	14	7	**556**	**1007**	**525**
T1_A9	42	50	14	7	**512**	**1001**	**493**

T1_A9 design alternative of T1 type vibration isolator is selected since it meets the stiffness requirements. Then, different damping applications are investigated to achieve required loss factor which is 0.2. The viscoelastic material with stiff constraining layer is used for three different damping concepts, which are named as D1, D2 and D3, as shown in Figure 5-3, Figure 5-4 and Figure 5-5.

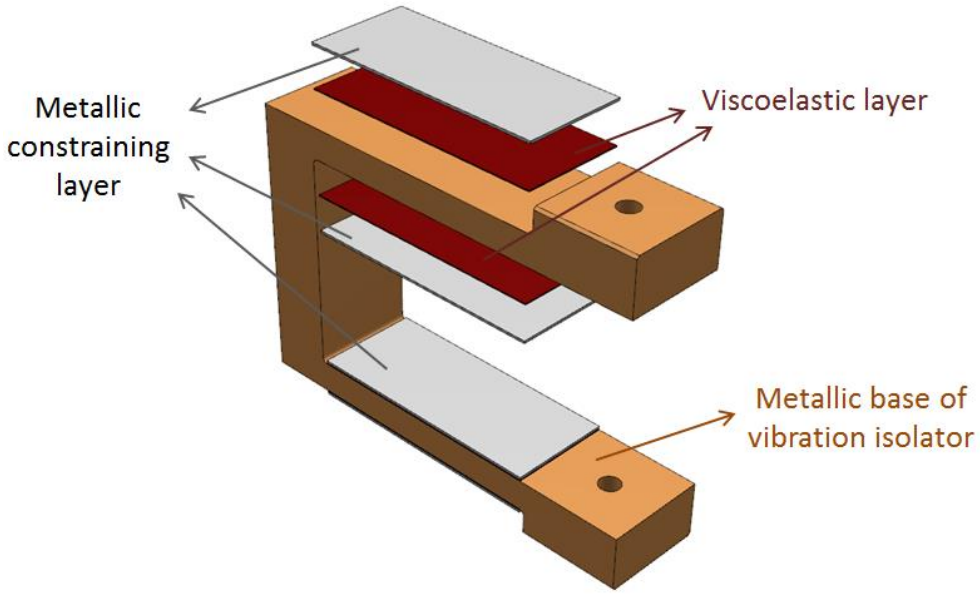

Figure 5-3 Damping concept – D1

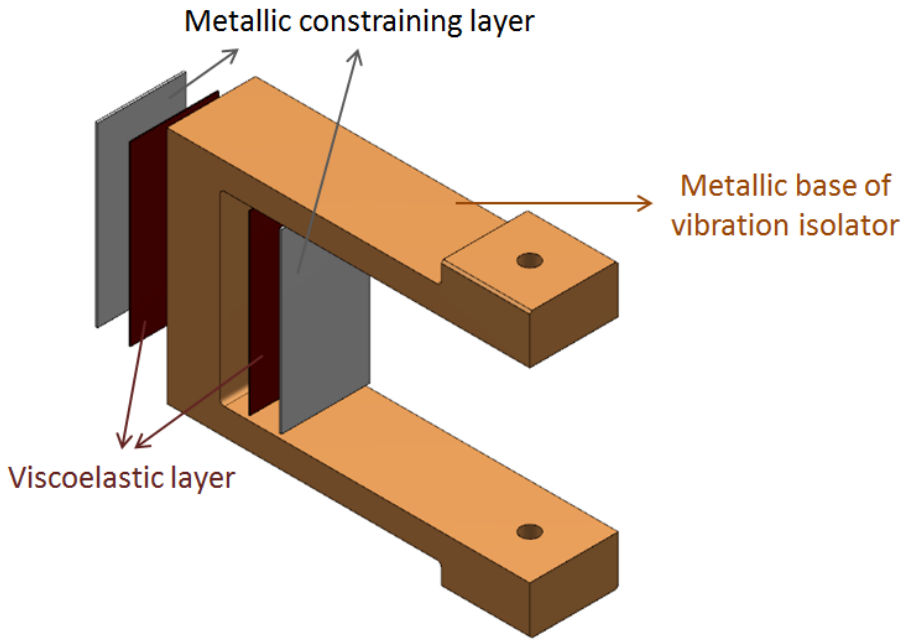

Figure 5-4 Damping concept – D2

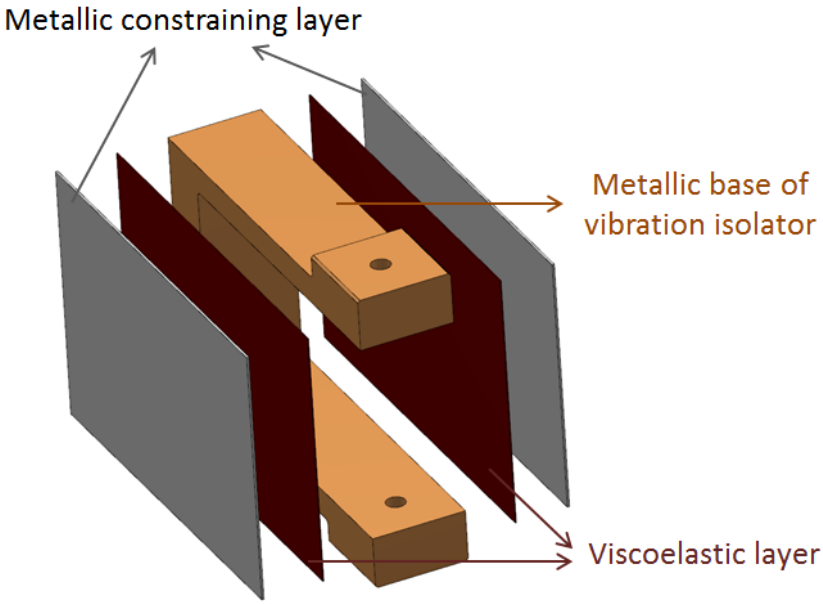

Figure 5-5 Damping concept – D3

The constrained layer damping product used in this study is 3M Damping Foil 2552. This damping foil consists of a viscoelastic polymer, ISD 112, and an aluminum foil backing. The thickness of viscoelastic material is 0.127 mm and the thickness of constraining layer is 0.254 mm. Shear modulus and loss factor nomograph of ISD 112 is provided by supplier and presented in Appendix A.

The complex stiffness and loss factor of vibration isolators are obtained by using direct method in which the input displacement and the blocking output force are measured [66]. The ratio of the harmonic output force to the harmonic input displacement in complex numbers gives the complex stiffness of the vibration isolator. Then, loss factor is obtained by dividing the imaginary part of the complex stiffness by the real part of the complex stiffness.

Abaqus is used in this study for loss factor measurement of a vibration isolator by finite element analysis. In these analyses, upper and lower reference points are created on the upper and lower interfaces of a vibration isolator as shown in Figure 5-2. These

reference points are connected to the interface surfaces using “coupling” type of constraint in Abaqus. Boundary conditions are defined such that all six degrees of freedom are constrained at lower interface and five degrees of freedom, all DOFs other than DOF of applied harmonic force, are constrained at upper interface. Then, harmonic force is applied at upper reference point for the interested frequency range. “Steady-state dynamics, Direct” step is used in Abaqus since frequency dependent viscoelastic material properties can be defined in this analysis type. Harmonic displacement at upper reference point and harmonic force at lower reference point are measured in complex numbers in the direction of applied force. Then, complex stiffness of a vibration isolator in the direction of applied force is obtained by dividing the harmonic force by the harmonic displacement in complex numbers. In order to obtain complex stiffness of a vibration isolator in all directions, three different analyses with the applied forces in x, y, and z directions must be performed separately.

The complex stiffness and loss factor values for different damping concepts are obtained by using direct method and the results are presented in Table 5-2. It is important to note that complex stiffness and loss factor values are dependent on frequency. The values presented in Table 5-2 are for constant frequency, which is 50 Hz, for comparison purposes.

Table 5-2 The complex stiffness and loss factor for different damping concepts

Damping Concept	Direction	Reaction Force [N]	Displacement [mm]	Complex Stiffness, K* [N/mm]	Loss Factor
D1	x	1010.143+0.125i	1.932+0.023i	522.78-6.16i	0.012
D1	y	1005.338+0.01i	0.999+0.002i	1006.34-2i	0.002
D1	z	1009.859+0.04i	1.966+0.008i	513.65-2.07i	0.004
D2	x	1010.127	1.958	515.9	0.000
D2	y	1005.261+0.005i	1+0.001i	1005.26-i	0.001
D2	z	1009.751+0.002i	1.974	511.53	0.000
D3	x	1006.209+1.6i	1.152+0.289i	822.06-204.84i	0.249
D3	y	1001.908+1.145i	0.366+0.225i	1988.05-1219.03i	0.613
D3	z	1011.933+0.189i	2.353+0.0318i	429.98-5.73i	0.013

As seen from Table 5-2 that it is not possible to have required amount of damping by D1 or D2 damping concepts. Furthermore, it is seen that high amount of loss factor can be achieved with D3 damping concept. Therefore, damping concept D3 is selected for further design studies. Note that this damping concept can be considered as viscoelastic link rather than constrained layer surface damping treatment.

In order to understand the effect of VEM layer thickness and constraining layer thickness on loss factor, finite element analyses are performed for different configurations and the results are given in Table 5-3.

Table 5-3 The complex stiffness and loss factor for different configurations of D3

Configuration	t_VEM [mm]	t_CONS [mm]	Direction	Complex Stiffness K* [N/mm]	Loss Factor
D3_A0	0.127	0.254	x	822.06-204.84i	0.25
D3_A0	0.127	0.254	y	1988.05-1219.03i	0.61
D3_A0	0.127	0.254	z	429.98-5.77i	0.01
D3_A1	0.254	0.254	x	666.94-154.04i	0.23
D3_A1	0.254	0.254	y	1343.42-665.8i	0.50
D3_A1	0.254	0.254	z	425.97-3.71i	0.01
D3_A2	0.127	0.508	x	832.94-221.44i	0.27
D3_A2	0.127	0.508	y	1990.03-1273.06i	0.64
D3_A2	0.127	0.508	z	431.52-6.53i	0.02
D3_A3	0.127	1.27	x	839.14-231.41i	0.28
D3_A3	0.127	1.27	y	1985.34-1287.8i	0.65
D3_A3	0.127	1.27	z	446.71-10.66i	0.02
D3_A4	0.127	2.54	x	841.05-235.12i	0.28
D3_A4	0.127	2.54	y	1993.58-1303.23i	0.65
D3_A4	0.127	2.54	z	459.19-13.85i	0.03
D3_A5	0.254	2.54	x	671.88-167.14i	0.25
D3_A5	0.254	2.54	y	1347.18-690.16i	0.51
D3_A5	0.254	2.54	z	442.82-7.94i	0.02
D3_A6	0.127	5.08	x	841.3-236.86i	0.28
D3_A6	0.127	5.08	y	2000.22-1326.38i	0.66
D3_A6	0.127	5.08	z	491.12-18i	0.04

Table 5-3 indicates that increasing thickness of VEM layer decreases the loss factor. Moreover, loss factor slightly increases when the thickness of constraining layer is increased. Since significant increase in loss factor cannot be achieved by changing thicknesses of VEM layer or constraining layer, 3M Damping Foil 2552 is used as it is provided by the supplier. In other words, D3_A0 configuration is selected for damping applications of vibration isolators.

T1_A9 design alternative with D3_A0 damping application is named as DT1_v0. The real part of complex stiffness and loss factor of DT1_v0 for 0-100 Hz frequency range are tabulated in Table 5-4. Note that the stiffness and loss factor values around natural frequencies of VIS are highlighted. Complex stiffness values for frequencies higher than 100 Hz are not examined because isolation frequencies are below 100 Hz.

Table 5-4 Complex stiffness and loss factor of DT1_v0

Direction	x		y		z	
Frequency [Hz]	Real (K*) [N/mm]	Loss Factor	Real (K*) [N/mm]	Loss Factor	Real (K*) [N/mm]	Loss Factor
0	547	0.05	1116	0.07	491	0.00
5	683	0.21	1499	0.33	494	0.01
10	718	0.23	1604	0.37	495	0.01
15	752	0.25	1711	0.41	496	0.01
20	786	0.26	1817	0.44	497	0.01
25	818	0.28	1923	0.47	498	0.01
30	849	0.28	2029	0.50	499	0.02
35	879	0.29	2135	0.52	500	0.02
40	908	0.29	2241	0.54	501	0.02
45	935	0.30	2347	0.55	502	0.02
50	961	0.30	2452	0.57	503	0.02
55	976	0.30	2515	0.57	504	0.02
60	990	0.30	2578	0.58	505	0.02
65	1003	0.30	2640	0.58	506	0.02
70	1017	0.30	2702	0.59	506	0.02
75	1029	0.30	2765	0.59	507	0.02
80	1042	0.30	2827	0.60	508	0.02

Direction	x		y		z	
Frequency [Hz]	Real (K*) [N/mm]	Loss Factor	Real (K*) [N/mm]	Loss Factor	Real (K*) [N/mm]	Loss Factor
85	1054	0.30	2889	0.60	509	0.02
90	1066	0.30	2951	0.60	510	0.02
95	1077	0.30	3013	0.60	511	0.02
100	1088	0.30	3074	0.61	512	0.02

As seen from Table 5-4, stiffness constants of damped isolator, DT1_v0, are larger than those of undamped isolator, T1_A9, which are given in Table 5-1. Therefore, dimensions of metallic part of vibration isolator must be updated after damping application to meet stiffness requirement. For this reason, thickness of vibration isolator, i.e. design parameters "t1" and "t2", is reduced. The dimensions of updated damped vibration isolator, DT1_v1, are given in Table 5-5. The real part of complex stiffness and loss factor of DT1_v1 are presented in Table 5-6.

Table 5-5 The dimensions of DT1_v1

h [mm]	w [mm]	t1 [mm]	t2 [mm]	d [mm]	w_i [mm]	t_i [mm]
42	50	12	6	20	20	5

Table 5-6 Complex stiffness and loss factor of DT1_v1

Direction	x		y		z	
Frequency [Hz]	Real (K*) [N/mm]	Loss Factor	Real (K*) [N/mm]	Loss Factor	Real (K*) [N/mm]	Loss Factor
0	372	0.06	757	0.08	360	0.00
5	496	0.26	1086	0.40	364	0.01
10	527	0.28	1177	0.43	365	0.02
15	558	0.30	1268	0.48	367	0.02
20	587	0.31	1359	0.51	368	0.02
25	616	0.32	1450	0.54	369	0.02
30	643	0.33	1542	0.56	370	0.02
35	669	0.33	1632	0.59	371	0.03

Direction	x		y		z	
Frequency [Hz]	Real (K*) [N/mm]	Loss Factor	Real (K*) [N/mm]	Loss Factor	Real (K*) [N/mm]	Loss Factor
40	694	0.33	1723	0.60	372	0.03
45	718	0.34	1814	0.62	374	0.03
50	740	0.34	1904	0.63	375	0.03
55	753	0.34	1958	0.64	375	0.03
60	765	0.34	2012	0.64	376	0.03
65	776	0.34	2065	0.64	377	0.03
70	788	0.34	2119	0.65	378	0.03
75	799	0.33	2172	0.65	379	0.03
80	809	0.33	2225	0.65	380	0.04
85	820	0.33	2278	0.66	381	0.04
90	830	0.33	2331	0.66	381	0.04
95	839	0.33	2384	0.66	382	0.04
100	849	0.33	2437	0.66	383	0.04

The detailed design of T1 type vibration isolator is done and DT1_v1 configuration is chosen. Even though it does not strictly meet the stiffness requirement, it is expected to satisfy system level performance requirements because loss factor of DT1_v1 is high enough. The verification of T1 vibration isolation system, which consist of DT1_v1 vibration isolators, is presented in section 6.2.1 and 6.3.1.

Mass of the T1 vibration isolator, DT1_v1, is 0.1 kg and total mass of the vibration isolation system, which consists of 60 T1 vibration isolator, is 6 kg. Total height of the vibration isolation system is 64 mm. Hence, T1 vibration isolation system meet system-level physical requirements which are stated in 3.2.

The internal resonances of designed T1 vibration isolator, DT1_v1, are determined for two different boundary conditions given in Figure 3-6. The first internal resonance frequency of T1 is 1479 Hz for BC-1 and 484 Hz for BC-2. The corresponding mode shapes are shown in Figure 5-6 and Figure 5-7 for BC-1 and BC-2, respectively.

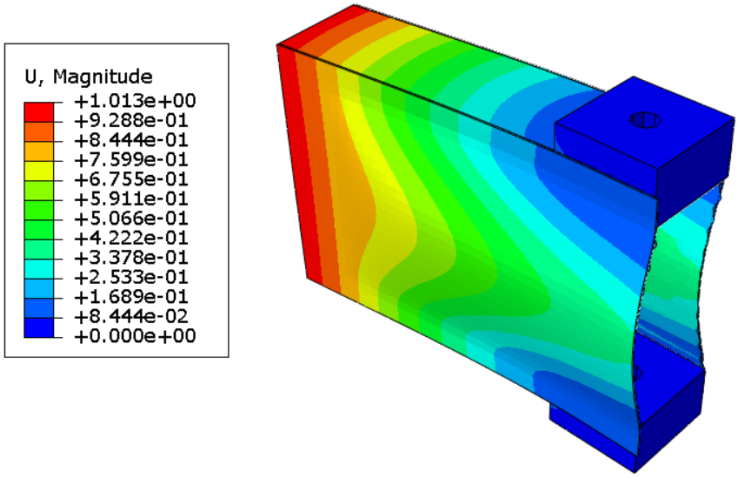

Figure 5-6 Internal resonance of T1 for BC-1, 1479 Hz

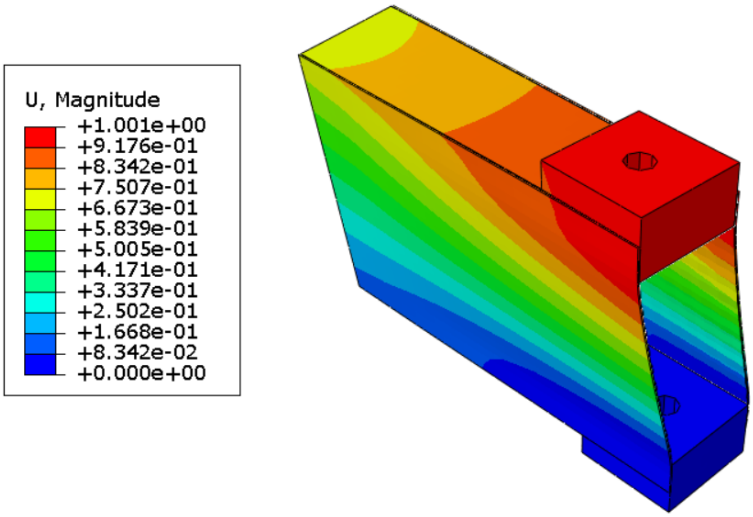

Figure 5-7 Internal resonance of T1 for BC-2, 484 Hz

5.2. Detailed Design of T2

Firstly, design of metallic part of T2 is performed by determining the dimensions of parameters which are depicted in Figure 5-8. These parameters are determined such

that T2 has compliance in three translational axes with stiffness constants given in Table 3-6.

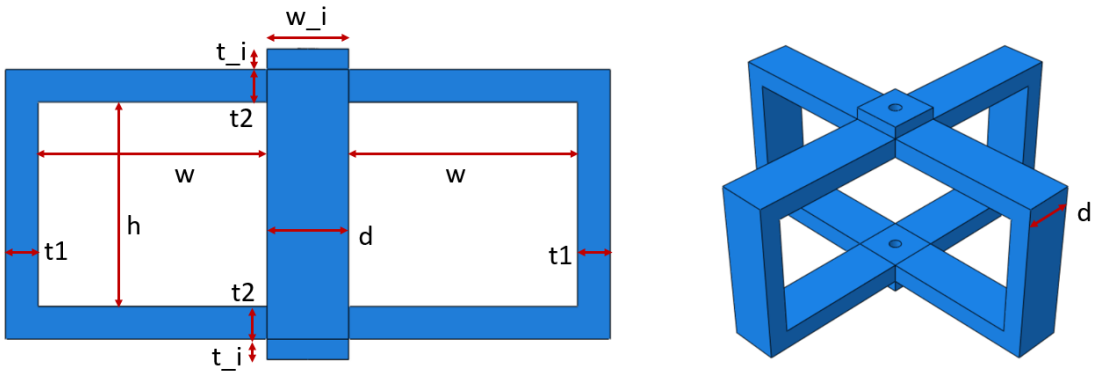

Figure 5-8 Design Parameters of T2-Vibration Isolator

Static load analyses of T2-vibration isolator with different sets of design parameters are performed using Abaqus in order to understand the effect of design parameters on stiffness constants. The stiffness constants of T2 design alternatives, which are obtained as explained in 5.1, are tabulated in Table 5-7. Design parameters related with interface region are kept constant for all design alternatives such that w_i = 20 mm and t_i = 5 mm. Note that Aluminum 6061 is chosen as isolator material due to its widespread availability.

Table 5-7 The stiffness constants of T2 design alternatives

T2 Design Alternative	**h** [mm]	**w** [mm]	**t1** [mm]	**t2** [mm]	**d** [mm]	**k_x** [N/mm]	**k_y** [N/mm]	**k_z** [N/mm]
T2_A1	40	40	8	8	20	**2846**	**6856**	**2846**
T2_A2	40	50	8	8	20	**2372**	**4146**	**2372**
T2_A3	50	40	8	8	20	**2025**	**6399**	**2024**
T2_A4	50	56	8	8	20	**1541**	**2977**	**1541**

T2_A4 design alternative of T2 type vibration isolator is selected since it meets the stiffness requirements. 3M Damping Foil 2552 is applied as in Figure 5-9 and it is named as DT2_v0. The complex stiffness and loss factor of DT2_v0, which are calculated by finite element analyses, are presented in Table 5-8.

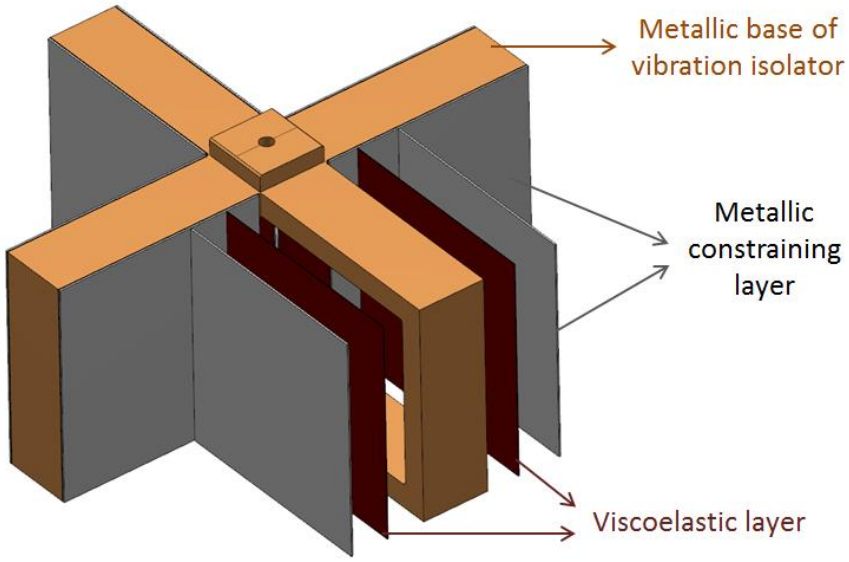

Figure 5-9 T2-Vibration isolator with damping application

Table 5-8 Complex stiffness and loss factor of DT2_v0

Direction	x		y		z	
Frequency [Hz]	Real (K*) [N/mm]	Loss Factor	Real (K*) [N/mm]	Loss Factor	Real (K*) [N/mm]	Loss Factor
0	1540	0.01	3277	0.06	1540	0.01
5	1618	0.05	4382	0.31	1620	0.05
10	1638	0.06	4683	0.34	1640	0.06
15	1658	0.07	4987	0.38	1660	0.07
20	1678	0.07	5291	0.41	1680	0.07
25	1696	0.08	5593	0.43	1699	0.08
30	1714	0.08	5893	0.45	1718	0.08
35	1732	0.08	6191	0.46	1735	0.09

Direction	x		y		z	
Frequency [Hz]	**Real (K*) [N/mm]**	**Loss Factor**	**Real (K*) [N/mm]**	**Loss Factor**	**Real (K*) [N/mm]**	**Loss Factor**
40	1748	0.09	6486	0.48	1752	0.09
45	1764	0.09	6779	0.49	1769	0.09
50	1780	0.09	7069	0.49	1784	0.09
55	1788	0.09	7240	0.50	1793	0.09
60	1796	0.09	7409	0.50	1801	0.10
65	1805	0.09	7578	0.50	1809	0.10
70	1812	0.10	7745	0.50	1817	0.10
75	1820	0.10	7911	0.51	1825	0.10
80	1827	0.10	8076	0.51	1833	0.10
85	1835	0.10	8240	0.51	1840	0.10
90	1842	0.10	8403	0.51	1847	0.10
95	1848	0.10	8565	0.51	1854	0.10
100	1855	0.10	8726	0.51	1861	0.10

As seen from Table 5-8, stiffness constants of damped isolator, DT2_v0, are larger than those of undamped isolator, T2_A4, which are given in Table 5-7. Therefore, dimensions of metallic part of vibration isolator must be updated after damping application to meet stiffness requirement. For this reason, thickness of vibration isolator, i.e. design parameters “t1” and “t2”, is reduced. The dimensions of updated damped vibration isolator, DT2_v1, are given in Table 5-9. The real part of complex stiffness and loss factor of DT2_v1 are presented in Table 5-10.

Table 5-9 The dimensions of DT2_v1

h [mm]	**w** [mm]	**t1** [mm]	**t2** [mm]	**d** [mm]	**w_i** [mm]	**t_i** [mm]
50	56	7	7	20	20	5

Table 5-10 Complex stiffness and loss factor of DT2_v1

Direction	x		y		z	
Frequency [Hz]	Real (K*) [N/mm]	Loss Factor	Real (K*) [N/mm]	Loss Factor	Real (K*) [N/mm]	Loss Factor
0	1191	0.01	2362	0.08	1191	0.01
5	1264	0.06	3325	0.36	1266	0.06
10	1283	0.07	3586	0.39	1285	0.07
15	1302	0.08	3851	0.43	1304	0.08
20	1320	0.08	4114	0.45	1322	0.08
25	1337	0.09	4376	0.48	1339	0.09
30	1353	0.09	4636	0.49	1356	0.09
35	1369	0.09	4894	0.51	1372	0.10
40	1383	0.10	5150	0.52	1387	0.10
45	1398	0.10	5403	0.53	1401	0.10
50	1411	0.10	5654	0.54	1415	0.10
55	1419	0.10	5802	0.54	1422	0.10
60	1426	0.10	5948	0.54	1430	0.10
65	1433	0.10	6093	0.54	1437	0.11
70	1440	0.10	6238	0.54	1444	0.11
75	1446	0.10	6381	0.54	1450	0.11
80	1453	0.11	6524	0.54	1457	0.11
85	1459	0.11	6665	0.54	1463	0.11
90	1465	0.11	6806	0.54	1469	0.11
95	1470	0.11	6945	0.54	1475	0.11
100	1476	0.11	7084	0.54	1481	0.11

The detailed design of T2 type vibration isolator is done and DT2_v1 configuration is chosen. Even though it does not strictly meet the stiffness requirement, it is expected to satisfy system level performance requirements because loss factor of DT2_v1 is high enough. The verification of T2 vibration isolation system, which consist of DT2_v1 vibration isolators, is presented in section 6.2.2 and 6.3.2.

Mass of the T2 vibration isolator, DT2_v1, is 0.3 kg and total mass of the vibration isolation system, which consists of 20 T2 vibration isolator, is 6 kg. Total height of

the vibration isolation system is 74 mm. Hence, T2 vibration isolation system meet system-level physical requirements which are stated in 3.2.

The internal resonances of designed T2 vibration isolator, DT2_v1, are determined for two different boundary conditions given in Figure 3-6. The first internal resonance frequency of T2 is 1055 Hz for BC-1 and 483 Hz for BC-2. The corresponding mode shapes are shown in Figure 5-10 and Figure 5-11 for BC-1 and BC-2, respectively.

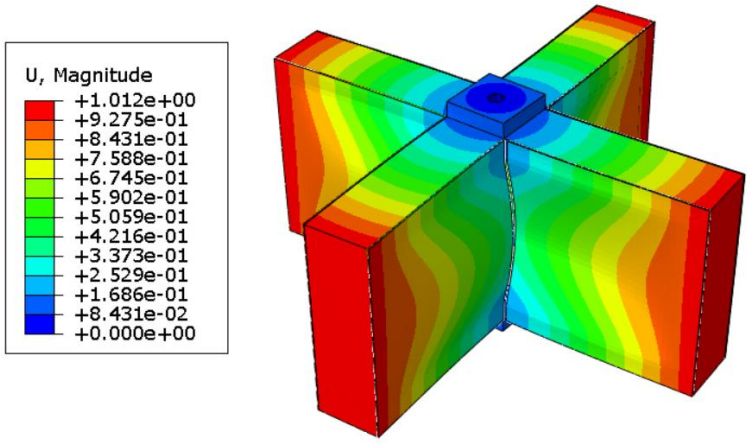

Figure 5-10 Internal resonance of T2 for BC-1, 1055 Hz

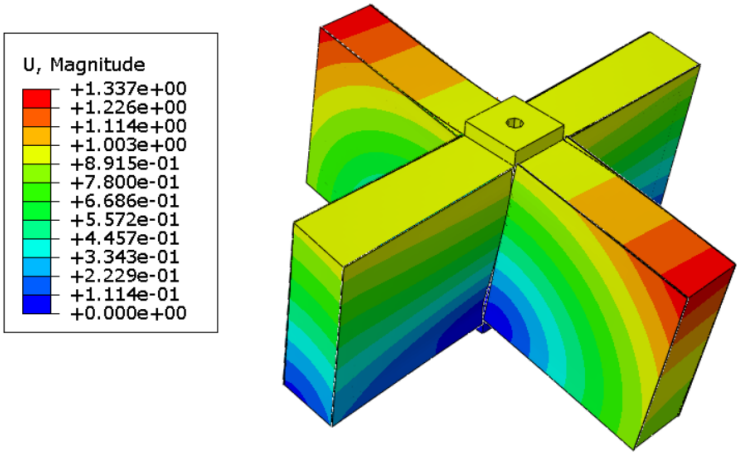

Figure 5-11 Internal resonance of T2 for BC-2, 483 Hz

5.3. Detailed Design of S1

Firstly, design of metallic part of S1 is performed by determining the dimensions of parameters which are shown in Figure 5-12. These parameters are determined such that S1 has compliance in three translational axes with stiffness constants given in Table 3-5.

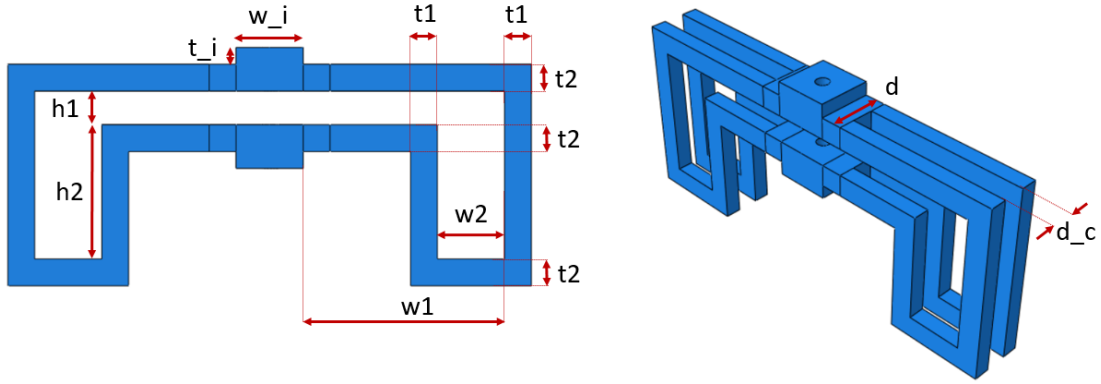

Figure 5-12 Design Parameters of S1-Vibration Isolator

Static load analyses of S1-vibration isolator with different sets of design parameters are performed using Abaqus FEA in order to understand the effect of design parameters on stiffness constants. The stiffness constants of S1 design alternatives, which are obtained as explained in 5.1, are tabulated in Table 5-11. Design parameters related with interface region are kept constant for all design alternatives such that d = 20 mm, w_i = 20 mm and t_i = 5 mm. Note that Aluminum 6061 is chosen as isolator material due to its widespread availability.

Table 5-11 The stiffness constants of S1 design alternatives

S1 Design Alternative	**h1** [mm]	**h2** [mm]	**w1** [mm]	**w2** [mm]	**t1** [mm]	**t2** [mm]	**d_c** [mm]	**k_x** [N/mm]	**k_y** [N/mm]	**k_z** [N/mm]
S1_A1	10	20	80	20	8	8	8	**1759**	**497**	**215**
S1_A2	10	20	60	20	8	8	8	**1925**	**997**	**376**

S1 Design Alternative	h1 [mm]	h2 [mm]	w1 [mm]	w2 [mm]	t1 [mm]	t2 [mm]	d_c [mm]	k_x [N/mm]	k_y [N/mm]	k_z [N/mm]
S1_A3	10	40	60	20	8	8	8	**803**	**895**	**215**
S1_A4	10	20	60	20	12	8	8	**2234**	**1344**	**461**
S1_A5	10	20	60	20	8	12	8	**3254**	**1931**	**487**
S1_A6	10	20	60	20	8	8	4	**2506**	**1256**	**726**
S1_A7	20	20	60	20	8	8	4	**1392**	**1116**	**534**
S1_A8	20	20	60	30	8	8	4	**1215**	**1061**	**487**
S1_A9	20	40	60	30	8	8	4	**592**	**913**	**284**
S1_A10	20	40	50	30	8	8	4	**596**	**1233**	**323**
S1_A11	30	40	50	30	10	7	4	**393**	**1284**	**240**
S1_A12	30	40	50	30	10	7	0	**486**	**1515**	**540**
S1_A13	30	40	60	30	10	7	0	**473**	**1043**	**499**
S1_A14	28	40	60	30	9	7	0	**478**	**958**	**505**
S1_A15	26	40	60	30	9	7	0	**510**	**972**	**530**

S1_A15 design alternative of S1 type vibration isolator is selected since it meets the stiffness requirements. 3M Damping Foil 2552 is applied as in Figure 5-13 and it is named as DS1_v0. The complex stiffness and loss factor of DS1_v0, which are calculated by finite element analyses, are presented in Table 5-12.

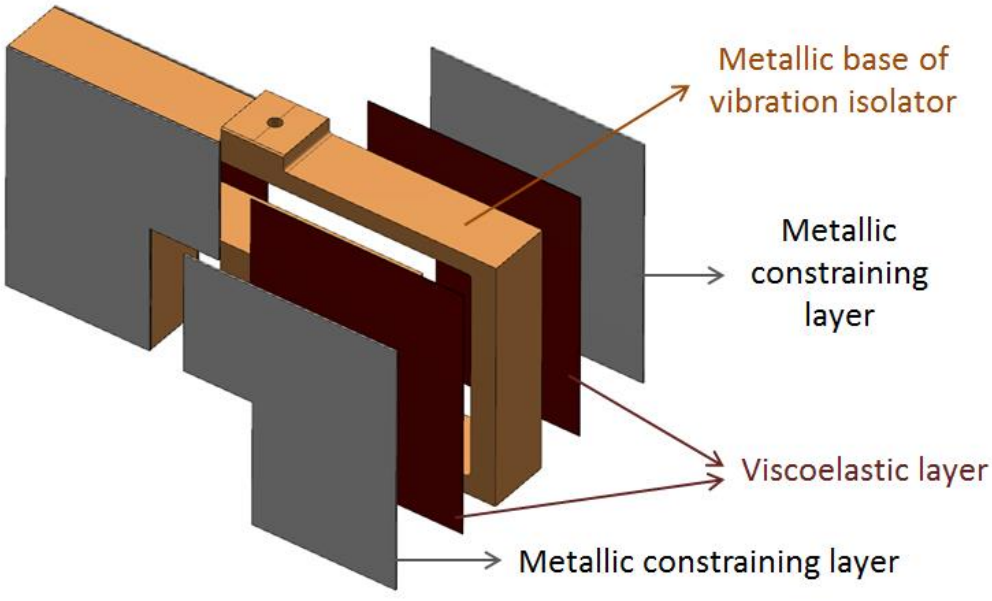

Figure 5-13 S1-Vibration isolator with damping application

Table 5-12 Complex stiffness and loss factor of DS1_v0

Direction	x		y		z	
Frequency [Hz]	Real (K*) [N/mm]	Loss Factor	Real (K*) [N/mm]	Loss Factor	Real (K*) [N/mm]	Loss Factor
0	666	0.12	1232	0.11	556	0.00
5	1076	0.35	1966	0.43	565	0.02
10	1171	0.36	2157	0.45	568	0.02
15	1263	0.36	2348	0.47	570	0.02
20	1349	0.36	2534	0.49	573	0.03
25	1428	0.36	2715	0.50	575	0.03
30	1502	0.36	2892	0.51	578	0.03
35	1570	0.35	3064	0.52	580	0.03
40	1633	0.35	3232	0.52	582	0.04
45	1692	0.34	3395	0.53	585	0.04
50	1747	0.34	3555	0.53	587	0.04
55	1775	0.33	3647	0.53	589	0.04
60	1802	0.33	3738	0.53	591	0.04
65	1827	0.32	3828	0.53	592	0.04
70	1851	0.32	3916	0.53	594	0.04
75	1873	0.32	4004	0.52	596	0.04
80	1894	0.31	4090	0.52	597	0.04
85	1914	0.31	4175	0.52	599	0.05
90	1932	0.31	4259	0.52	601	0.05
95	1949	0.30	4342	0.52	603	0.05
100	1965	0.30	4425	0.52	604	0.05

As seen from Table 5-12, stiffness constants of damped isolator, DS1_v0, are larger than those of undamped isolator, S1_A15, which are given in Table 5-11. Therefore, dimensions of metallic part of vibration isolator must be updated after damping application to meet stiffness requirement. For this reason, thickness of vibration isolator, i.e. design parameters “t1” and “t2”, is reduced. The dimensions of updated damped vibration isolator, DS1_v1, are given in Table 5-13. The real part of complex stiffness and loss factor of DS1_v1 are presented in Table 5-14.

Table 5-13 The dimensions of DS1_v1

h1 [mm]	**h2** [mm]	**w1** [mm]	**w2** [mm]	**t1** [mm]	**t2** [mm]	**d_c** [mm]
26	40	60	30	8	6	0

Table 5-14 Complex stiffness and loss factor of DS1_v1

Direction	**x**		**y**		**z**	
Frequency [Hz]	**Real (K*) [N/mm]**	**Loss Factor**	**Real (K*) [N/mm]**	**Loss Factor**	**Real (K*) [N/mm]**	**Loss Factor**
0	484	0.14	876	0.13	418	0.00
5	845	0.38	1495	0.46	427	0.02
10	924	0.37	1653	0.48	430	0.03
15	1001	0.37	1811	0.50	432	0.03
20	1071	0.37	1965	0.52	434	0.04
25	1135	0.36	2115	0.53	437	0.04
30	1194	0.36	2259	0.53	439	0.04
35	1247	0.35	2400	0.54	442	0.05
40	1296	0.34	2537	0.54	444	0.05
45	1341	0.34	2669	0.54	447	0.05
50	1382	0.33	2798	0.54	449	0.05
55	1403	0.32	2873	0.54	451	0.05
60	1423	0.32	2946	0.54	452	0.05
65	1441	0.32	3019	0.54	454	0.06
70	1458	0.31	3090	0.54	455	0.06
75	1473	0.31	3161	0.54	457	0.06
80	1487	0.30	3230	0.53	458	0.06
85	1500	0.30	3299	0.53	460	0.06
90	1512	0.30	3366	0.53	462	0.06
95	1523	0.29	3433	0.53	463	0.06
100	1532	0.29	3499	0.53	465	0.06

The detailed design of S1 type vibration isolator is done and DS1_v1 configuration is chosen. Even though it does not strictly meet the stiffness requirement, it is expected to satisfy system level performance requirements because loss factor of DS1_v1 is

high enough. The verification of S1 vibration isolation system, which consist of DS1_v1 vibration isolators, is presented in section 6.2.3 and 6.3.3.

Mass of the S1 vibration isolator, DS1_v1, is 0.2 kg and total mass of the vibration isolation system, which consists of 60 S1 vibration isolator, is 12 kg. Height of the vibration isolation system between upper and lower interface is 48 mm. Hence, S1 vibration isolation system meet system-level physical requirements which are stated in 3.2.

The internal resonances of designed S1 vibration isolator, DS1_v1, are determined for two different boundary conditions given in Figure 3-6. The first internal resonance frequency of S1 is 718 Hz for BC-1 and 388 Hz for BC-2. The corresponding mode shapes are shown in Figure 5-14 and Figure 5-15 for BC-1 and BC-2, respectively.

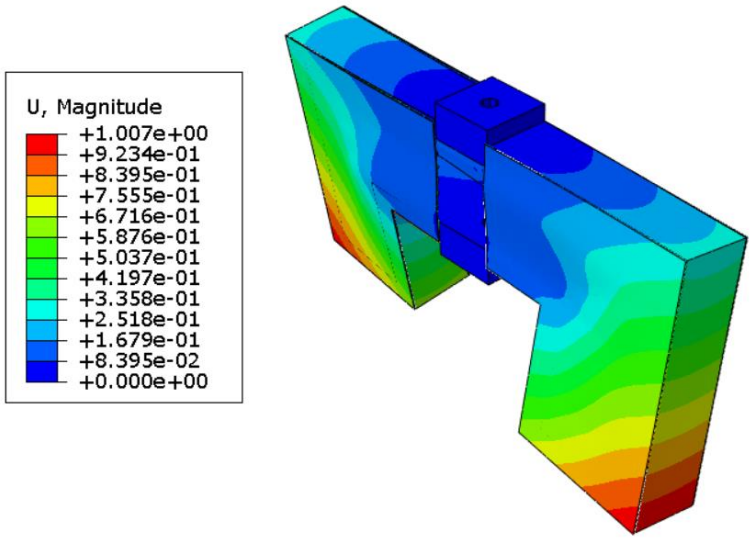

Figure 5-14 Internal resonance of S1 for BC-1, 718 Hz

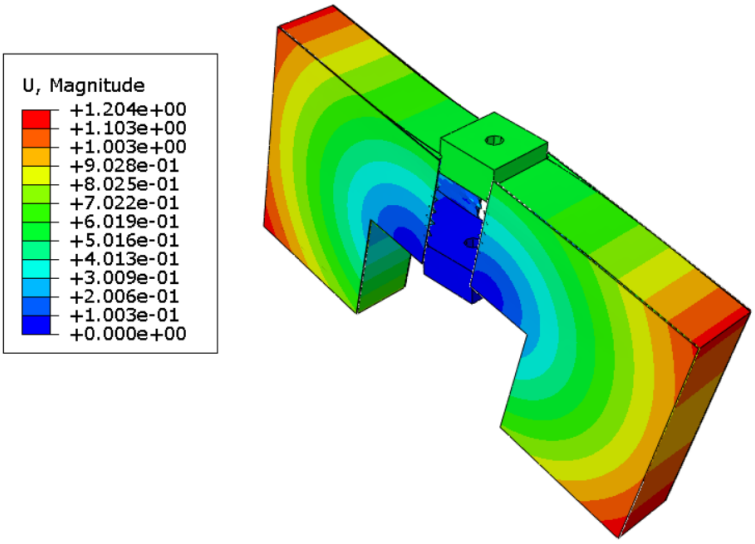

Figure 5-15 Internal resonance of S1 for BC-2, 388 Hz

CHAPTER 6

VERIFICATION OF VIBRATION ISOLATION SYSTEM

6.1. Verification Plan

It is shown that the designed vibration isolation systems, namely T1, T2 and S1, meet all technical requirements by verification process. There are four types of verification method which are analysis, demonstration, inspection and test [67]. The verification method, description of the verification work and success criteria for each requirement are given in Table 6-1 for the vibration isolation systems. Note that tests are performed with scaled-down test configuration due to the limitations of the test equipment used in this thesis work.

Table 6-1 Requirements Verification Matrix

Req. No	**Requirement**	**Verification Method**	**Description of the Verification Work**	**Success Criteria**
R-1	Response RMS acceleration of any point on payload must be lower than 2 gRMS under random vibration input of 6.5 gRMS in longitudinal direction which is given in Table 1-5.	Analysis/Test	Random vibration analysis/test is performed for vibration isolation system by applying acceleration base motion of 6.5 gRMS in y direction as shown in Figure 6-2.	Response RMS accelerations of CG of payload and 3 outer points from lower, middle and upper regions of payload in y direction are lower than 2 gRMS.

Req. No	Requirement	Verification Method	Description of the Verification Work	Success Criteria
R-2	Response RMS acceleration of any point on payload must be lower than 2 gRMS under random vibration input of 6.5 gRMS in lateral direction which is given in Table 1-5.	Analysis/Test	Random vibration analysis/test is performed for vibration isolation system by applying acceleration base motion of 6.5 gRMS in x direction as shown in Figure 6-2.	Response RMS accelerations of CG of payload and 3 outer points from lower, middle and upper regions of payload in x direction are lower than 2 gRMS.
R-3	Harmonic displacement amplitude of any point on payload must be lower than 20 mm under harmonic vibration input in longitudinal direction which is given in Table 1-3.	Analysis/Test	Harmonic vibration analysis/test is performed for vibration isolation system shown in Figure 6-2 by applying acceleration base motion in y direction with an amplitudes given in Table 1-3.	Displacement amplitudes of 3 outer points from lower, middle and upper regions of payload in y direction are lower than 20 mm.
R-4	Harmonic displacement amplitude of any point on payload must be lower than 20 mm under harmonic vibration input in lateral direction which is given in Table 1-4.	Analysis/Test	Harmonic vibration analysis/test is performed for vibration isolation system shown in Figure 6-2 by applying acceleration base motion in x	Displacement amplitudes of 3 outer points from lower, middle and upper regions of payload in x direction are lower than 20 mm.

Req. No	Requirement	Verification Method	Description of the Verification Work	Success Criteria
			direction with an amplitudes given in Table 1-4.	
R-5	Static load capacity of VIS shall be 1200 kg.	Analysis	Static load analysis is performed for vibration isolation system by applying static force of 11772 N in -y direction at CG of payload as shown in Figure 6-1.	Factor of safety must be larger than 1.25 according to von Mises criterion.
R-6	VIS shall withstand the quasi-static acceleration of 8.3 g in longitudinal direction.	Analysis	Static load analysis is performed for vibration isolation system by applying static force of 97708 N in -y direction at CG of payload as shown in Figure 6-1.	Factor of safety must be larger than 1.25 according to von Mises criterion.
R-7	VIS shall withstand the quasi-static acceleration of 1 g in lateral direction.	Analysis	Static load analysis is performed for vibration isolation system by applying static force of 11772 N	Factor of safety must be larger than 1.25 according to von Mises criterion.

Req. No	Requirement	Verification Method	Description of the Verification Work	Success Criteria
			in x direction at CG of payload as shown in Figure 6-1.	
R-8	Static deflection of vibration isolators shall be lower than 3 mm under the quasi-static acceleration of 8.3 g in longitudinal direction.	Analysis	Static load analysis is performed for vibration isolation system by applying static force of 97708 N in -y direction at CG of payload as shown in Figure 6-1.	Maximum displacement of any point on a vibration isolator must be lower than 3 mm.
R-9	Static deflection of vibration isolators shall be lower than 3 mm under the quasi-static acceleration of 1 g in lateral direction.	Analysis	Static load analysis is performed for vibration isolation system by applying static force of 11772 N in x direction at CG of payload as shown in Figure 6-1.	Maximum displacement of any point on a vibration isolator must be lower than 3 mm.

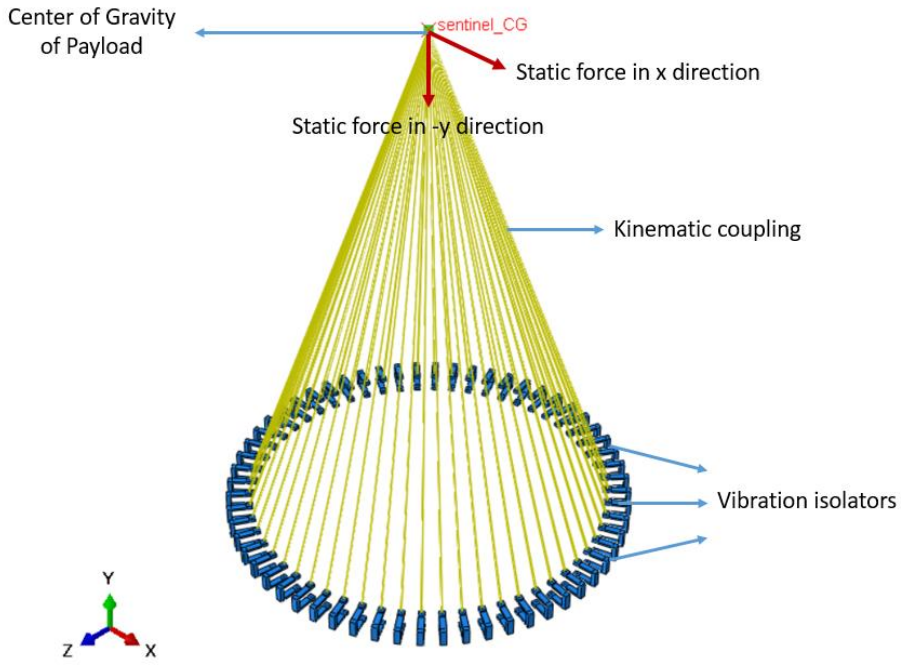

Figure 6-1 Static load analysis for vibration isolation system

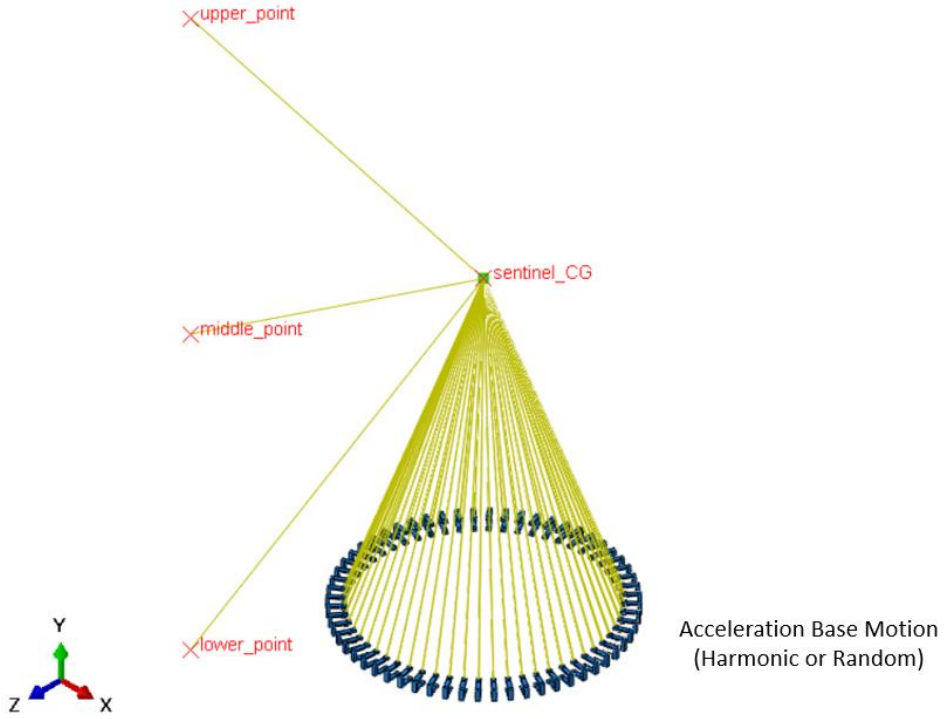

Figure 6-2 Vibration analysis (Harmonic or Random) for vibration isolation system

6.2. Verification of Vibration Isolation Systems by Analysis

The verification of designed vibration isolation systems by analysis are performed using both mathematical model and finite element model. It is also shown that there is a great consistency between the mathematical model and finite element model.

The mathematical models of the vibration isolation systems are developed in MATLAB® using the principles explained in 3.3. In mathematical model, vibration isolators are modelled as massless springs with hysteretic damping. Even though stiffness and loss factor of isolators depend on frequency, they are taken as constant and their values around isolation frequency are used in mathematical model. Note that these spring constants and loss factors of designed vibration isolators are obtained from finite element model as explained in 5.1. Random and harmonic vibration analyses are performed using mathematical model and related technical requirements, which are R-1 to R-4, are verified for each vibration isolation system as presented in subsequent sections.

The finite element models of the vibration isolation systems are constructed using Abaqus®. Payload is modelled as point mass and it is connected to isolators using "kinematic coupling" type of constraint in Abaqus. Metallic part of vibration isolator, VEM layer and constraining layer are connected to each other using "tie" type of constraint. Moreover, three reference points from upper, middle and lower regions of payload are created and they are also connected to CG of payload using "kinematic coupling" as shown in Figure 6-3.

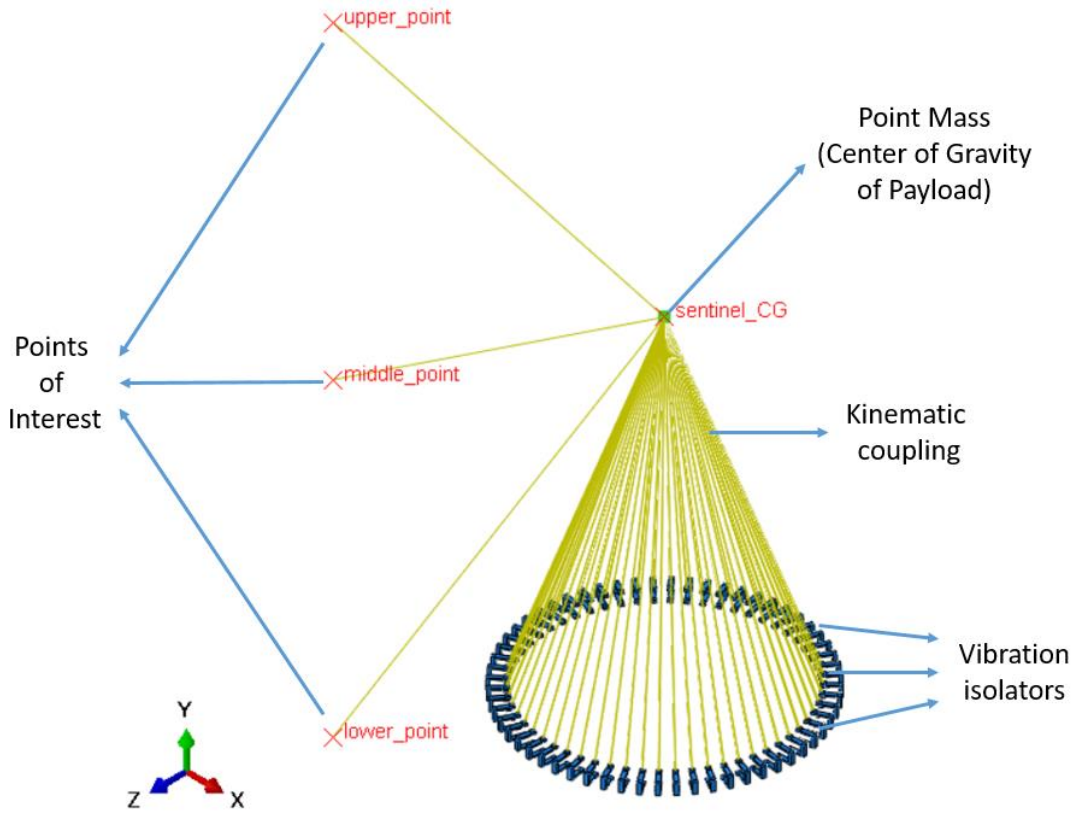

Figure 6-3 Finite element model of vibration isolation system

In finite element analyses which are presented in 6.2.1, 6.2.2 and 6.2.3, material properties of ISD-112 at 20 °C is used. Random vibration analyses in Abaqus are performed using “Random response” step. It is not possible to use frequency dependent viscoelastic material properties in this step. Therefore, elastic modulus of ISD-112 around isolation frequency is used in each analysis since the overall response is mainly driven by the frequency range around isolation frequency. Moreover, damping is defined as loss factor selecting “structural damping” option. The loss factor of VIS for each mode are calculated from the transmissibility curves, which are obtained using mathematical model, by applying the half-power bandwidth method. Half power points are determined as in Figure 6-4.

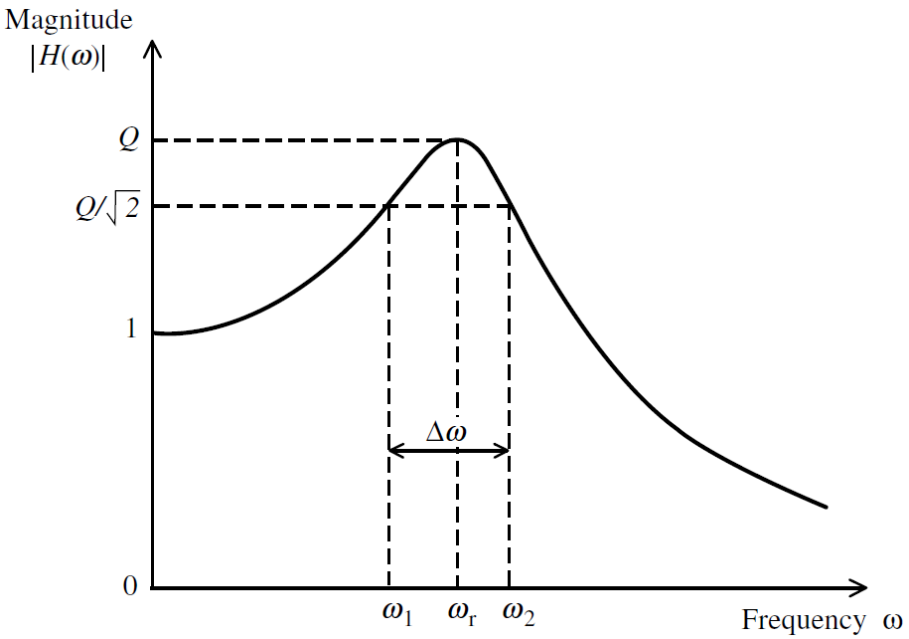

Figure 6-4 Half power points [61]

Then, structural damping loss factor is obtained as

$$\eta = \frac{\omega_2^2 - \omega_1^2}{2\omega_r^2} \tag{6.1}$$

Random vibration analyses, harmonic vibration analyses and static load analyses for quasi-static accelerations are performed using finite element model and related technical requirements, which are R-1 to R-9, are verified for each vibration isolation system as presented in subsequent sections.

6.2.1. Verification of T1 by Analysis

The T1 vibration isolation system, which consist of 60 DT1_A1 vibration isolators, is verified in this section according to verification plan given in 6.1.

Verification of R-1:

The random vibration analysis results of mathematical model for the input in longitudinal direction is given in Figure 6-5.

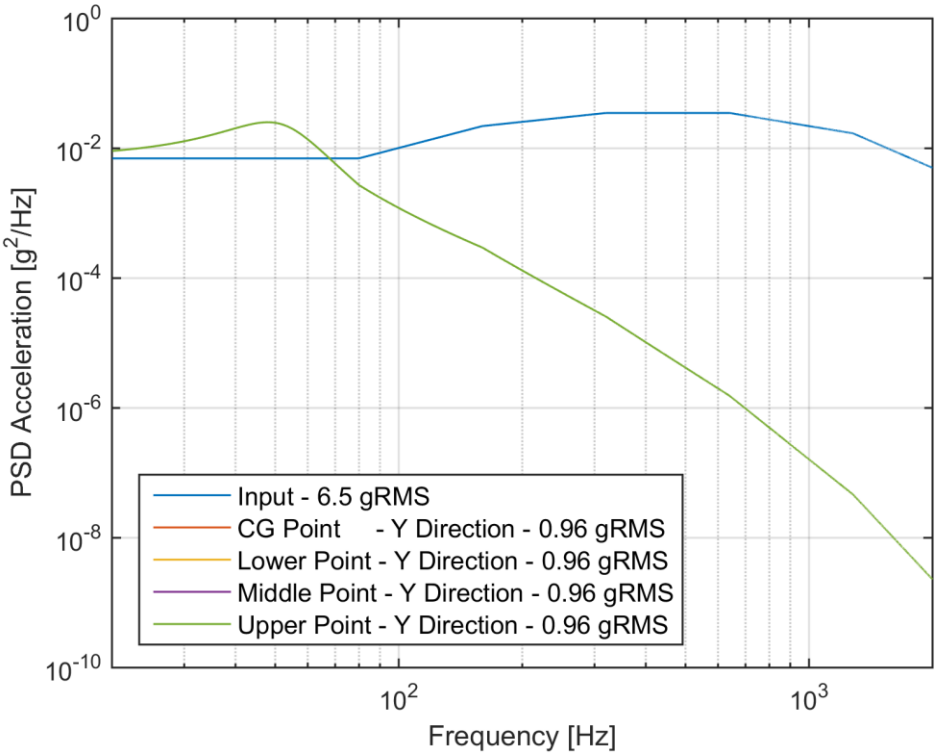

Figure 6-5 T1 VIS - Results of random vibration analysis in longitudinal direction using mathematical model

As seen in Figure 6-5, response RMS acceleration of interested points in longitudinal direction are lower than 2 gRMS. Therefore, the R-1 is satisfied.

Verification of R-2:

The random vibration analysis results of mathematical model and finite element model for the input in lateral direction are given in Figure 6-6 and Figure 6-7, respectively. Note that loss factor, which is used in finite element analysis, is 0.27.

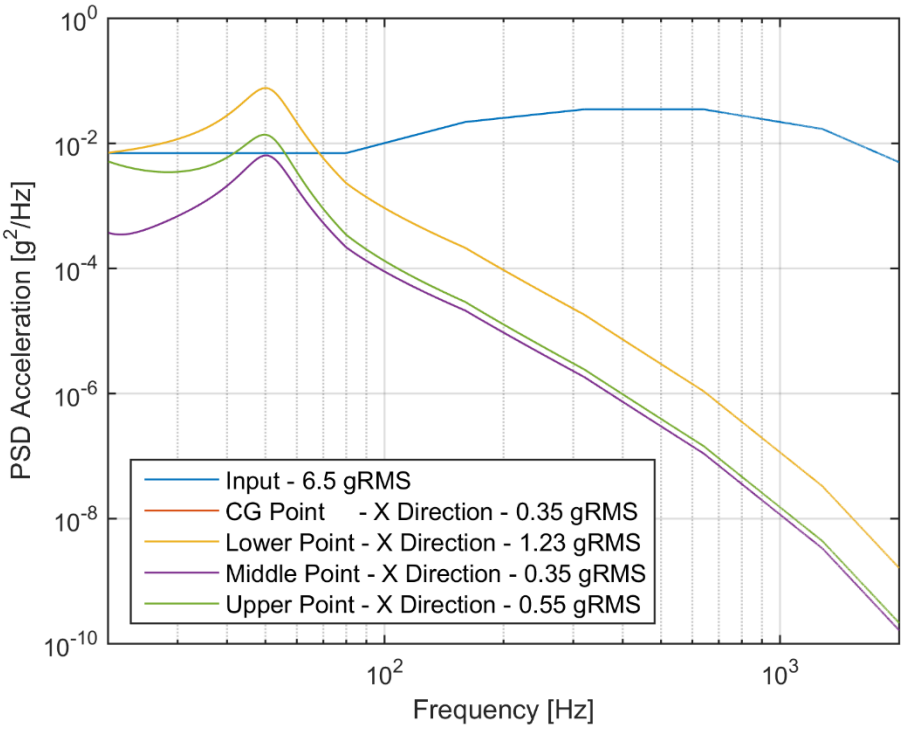

Figure 6-6 T1 VIS - Results of random vibration analysis in lateral direction using mathematical model

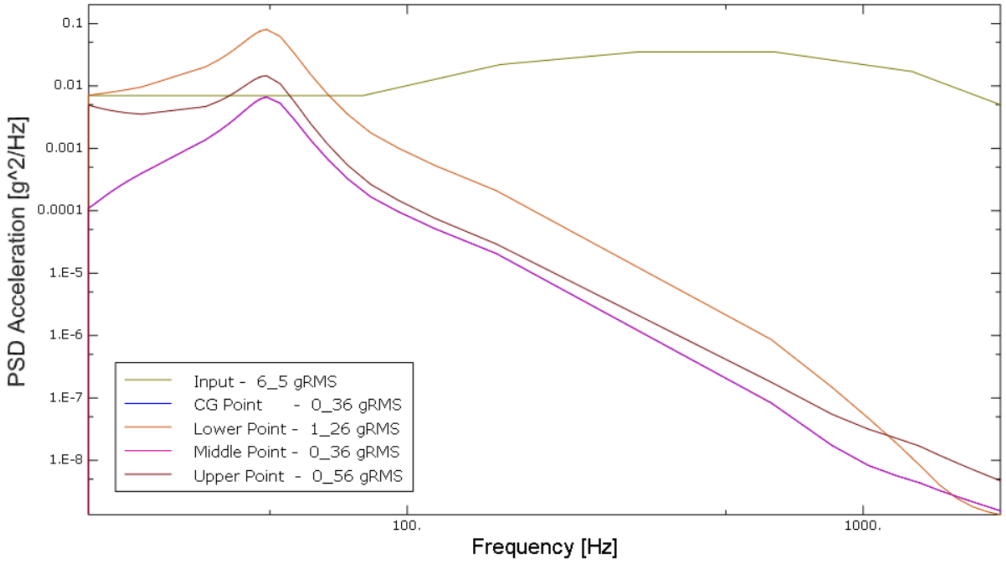

Figure 6-7 T1 VIS - Results of random vibration analysis in lateral direction using finite element model

As seen in Figure 6-6 and Figure 6-7, response RMS acceleration of interested points in lateral direction are lower than 2 gRMS. Therefore, the R-2 is satisfied.

Verification of R-3:

Harmonic vibration analyses for vibration isolation system are performed by using both mathematical model and finite element model. Note that stiffness and loss factor values at 10 Hz is used in both analyses since 10 Hz is at the center of the frequency range of harmonic vibration, which is 2-20 Hz.

The harmonic vibration analysis results of mathematical model for the input in longitudinal direction is given in Figure 6-8.

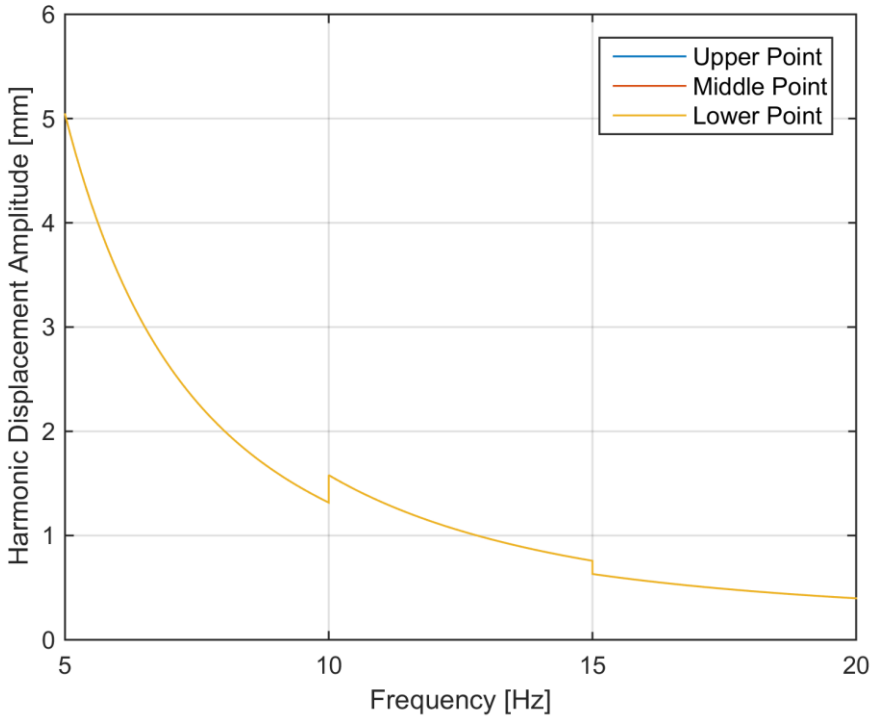

Figure 6-8 T1 VIS - Results of harmonic vibration analysis in longitudinal direction using mathematical model

As seen in Figure 6-8, harmonic displacement amplitudes of interested points in longitudinal direction are lower than 20 mm. Therefore, the R-3 is satisfied.

Verification of R-4:

Harmonic vibration analyses for vibration isolation system are performed by using both mathematical model and finite element model. Note that stiffness and loss factor values at 10 Hz is used in both analyses since 10 Hz is at the center of the frequency range of harmonic vibration, which is 2-20 Hz.

The harmonic vibration analysis results of mathematical model for the input in lateral direction is given in Figure 6-9.

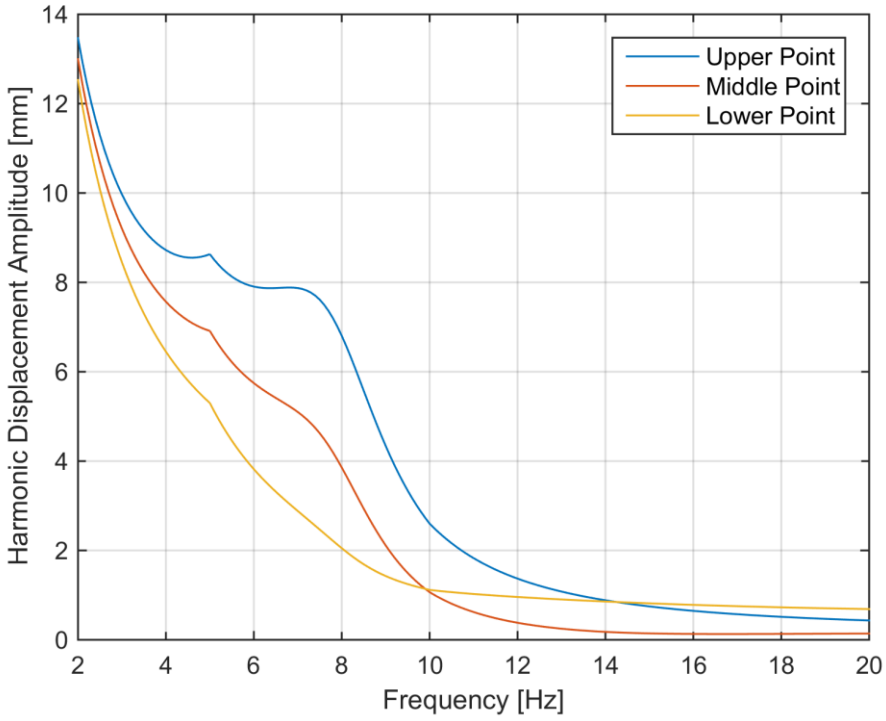

Figure 6-9 T1 VIS - Results of harmonic vibration analysis in lateral direction using mathematical model

As seen in Figure 6-9, harmonic displacement amplitudes of interested points in lateral direction are lower than 20 mm. Therefore, the R-4 is satisfied.

Verification of R-5:

Since R-6 is met, R-5 is automatically satisfied. There is no need to perform any additional verification work for this requirement.

Verification of R-6:

The static load analysis is performed in Abaqus FEA for vibration isolation system by applying static force of 97708 N in -y direction at CG of payload as shown in Figure 6-1. The stress results are presented in Figure 6-10.

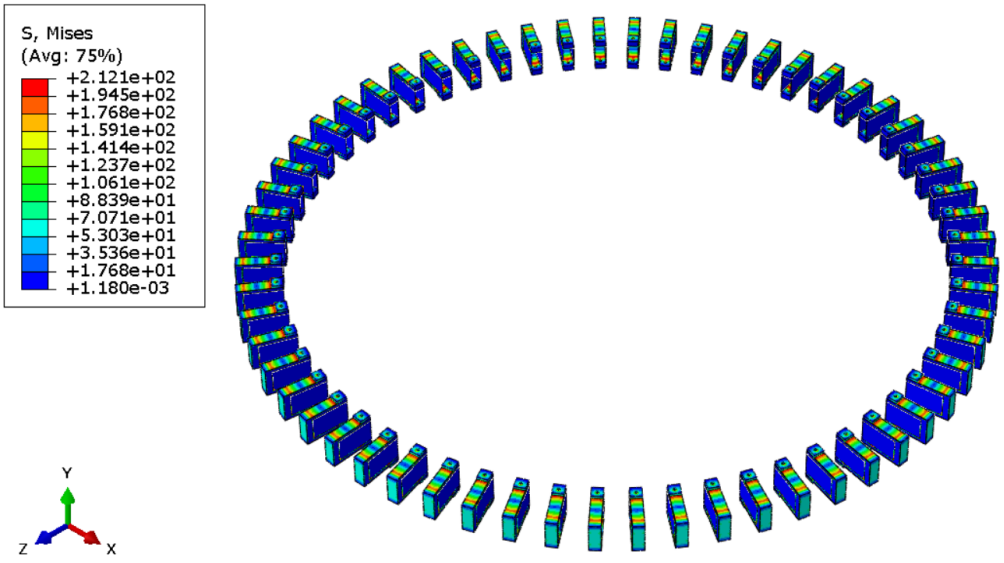

Figure 6-10 T1 VIS – Stress results of quasi-static load analysis in longitudinal direction

As seen in Figure 6-10, the maximum von Mises stress in vibration isolators is 212.2 MPa. The yield strength of isolator material, which is Aluminum 6061-T6, is 276 MPa and factor of safety is 1.3. Therefore, the R-6 is satisfied.

Verification of R-7:

The static load analysis is performed in Abaqus FEA for vibration isolation system by applying static force of 11772 N in x direction at CG of payload as shown in Figure 6-1. The stress results are presented in Figure 6-11.

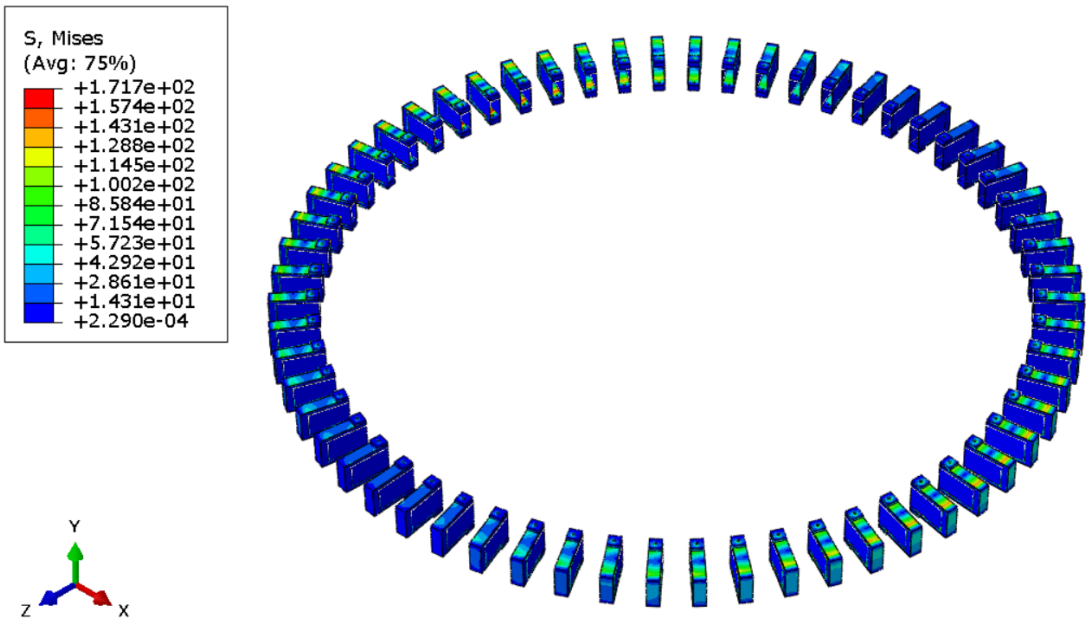

Figure 6-11 T1 VIS – Stress results of quasi-static load analysis in lateral direction

As seen in Figure 6-11, the maximum von Mises stress in vibration isolators is 171.7 MPa. The yield strength of isolator material, which is Aluminum 6061-T6, is 276 MPa and factor of safety is 1.61. Therefore, the R-7 is satisfied.

Verification of R-8:

The static load analysis is performed in Abaqus FEA for vibration isolation system by applying static force of 97708 N in -y direction at CG of payload as shown in Figure 6-1. The displacement results are presented in Figure 6-12.

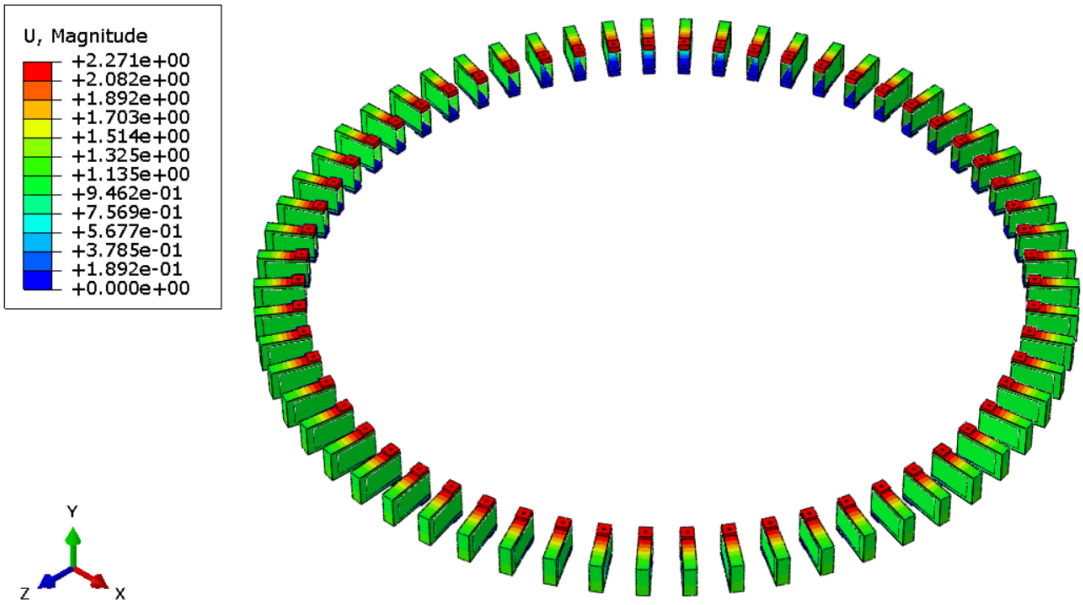

Figure 6-12 T1 VIS – Displacement results of quasi-static load analysis in longitudinal direction

As seen in Figure 6-12, the maximum displacement of vibration isolators is 2.27 mm under the quasi-static acceleration of 8.3 g in longitudinal direction. Therefore, the R-8 is satisfied.

Verification of R-9:

The static load analysis is performed in Abaqus FEA for vibration isolation system by applying static force of 11772 N in x direction at CG of payload as shown in Figure 6-1. The displacement results are presented in Figure 6-13.

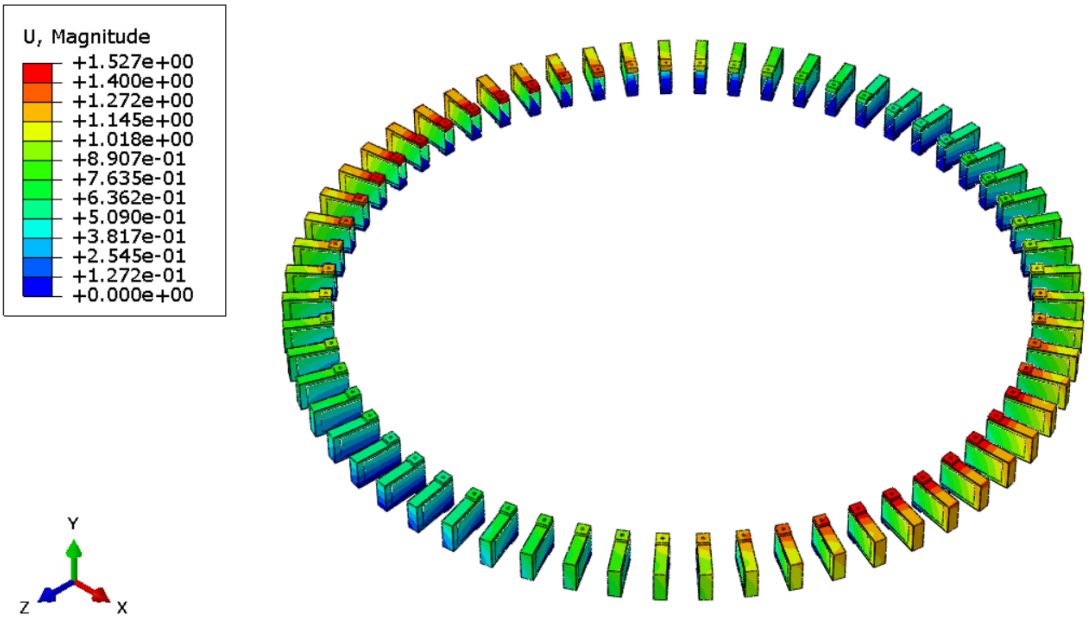

Figure 6-13 T1 VIS – Displacement results of quasi-static load analysis in lateral direction

As seen in Figure 6-13, the maximum displacement of vibration isolators is 1.53 mm under the quasi-static acceleration of 1 g in lateral direction. Therefore, the R-9 is satisfied.

6.2.2. Verification of T2 by Analysis

The T2 vibration isolation system, which consist of 20 DT2_A1 vibration isolators, is verified in this section according to verification plan given in 6.1.

Verification of R-1:

Random vibration analyses for vibration isolation system are performed by using both mathematical model and finite element model. Note that stiffness and loss factor values at isolation frequencies is used in both analyses since it is not possible to use frequency dependent material properties in random vibration analysis.

The random vibration analysis results of mathematical model for the input in longitudinal direction is given in Figure 6-14.

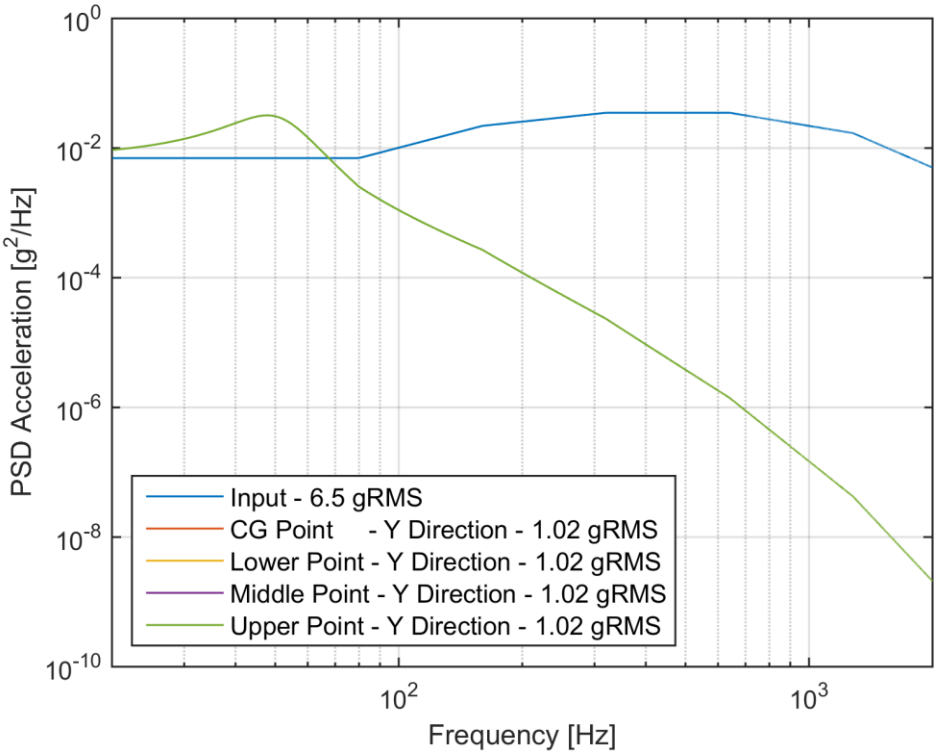

Figure 6-14 T2 VIS - Results of random vibration analysis in longitudinal direction using mathematical model

As seen in Figure 6-14, response RMS acceleration of interested points in longitudinal direction are lower than 2 gRMS. Therefore, the R-1 is satisfied.

Verification of R-2:

The random vibration analysis results of mathematical model and finite element model for the input in lateral direction are given in Figure 6-15 and Figure 6-16, respectively. Note that loss factor, which is used in finite element analysis, is 0.15.

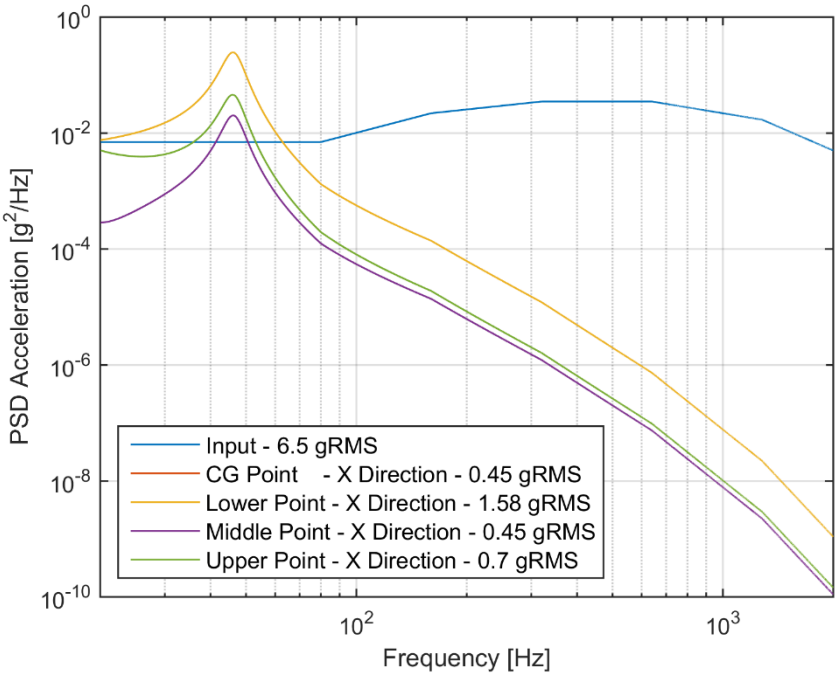

Figure 6-15 T2 VIS - Results of random vibration analysis in lateral direction using mathematical model

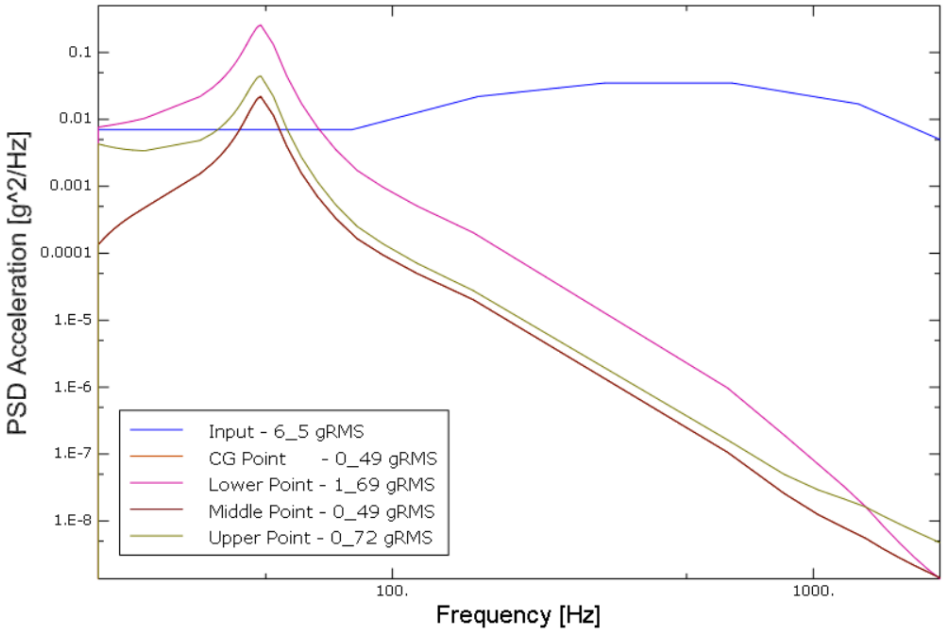

Figure 6-16 T2 VIS - Results of random vibration analysis in lateral direction using finite element model

As seen in Figure 6-15 and Figure 6-16, response RMS acceleration of interested points in lateral direction are lower than 2 gRMS. Therefore, the R-2 is satisfied.

Verification of R-3:

Harmonic vibration analyses for vibration isolation system are performed by using both mathematical model and finite element model. Note that stiffness and loss factor values at 10 Hz is used in both analyses since 10 Hz is at the center of the frequency range of harmonic vibration, which is 2-20 Hz.

The harmonic vibration analysis results of mathematical model for the input in longitudinal direction is given in Figure 6-17.

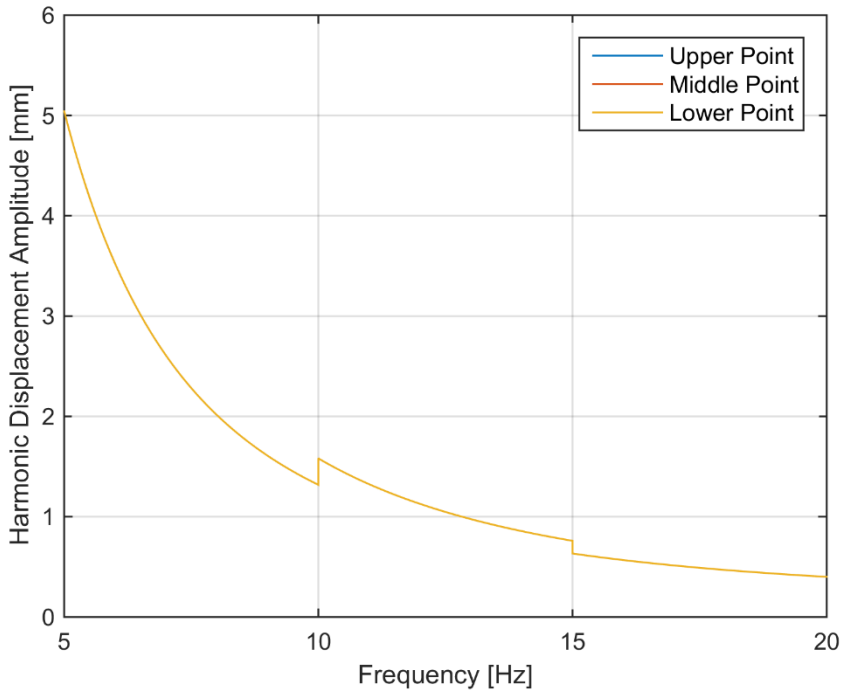

Figure 6-17 T2 VIS - Results of harmonic vibration analysis in longitudinal direction using mathematical model

As seen in Figure 6-17, harmonic displacement amplitudes of interested points in longitudinal direction are lower than 20 mm. Therefore, the R-3 is satisfied.

Verification of R-4:

Harmonic vibration analyses for vibration isolation system are performed by using both mathematical model and finite element model. Note that stiffness and loss factor values at 10 Hz is used in both analyses since 10 Hz is at the center of the frequency range of harmonic vibration, which is 2-20 Hz.

The harmonic vibration analysis results of mathematical model for the input in lateral direction is given in Figure 6-18.

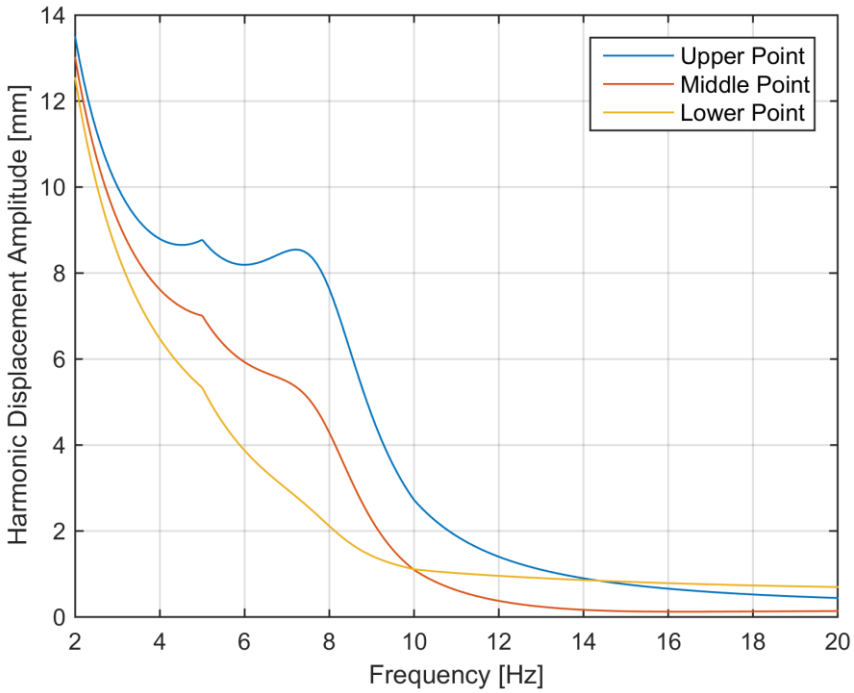

Figure 6-18 T2 VIS - Results of harmonic vibration analysis in lateral direction using mathematical model

As seen in Figure 6-18, harmonic displacement amplitudes of interested points in lateral direction are lower than 20 mm. Therefore, the R-4 is satisfied.

Verification of R-5:

Since R-6 is met, R-5 is automatically satisfied. There is no need to perform any additional verification work for this requirement.

Verification of R-6:

The static load analysis is performed in Abaqus FEA for vibration isolation system by applying static force of 97708 N in -y direction at CG of payload as shown in Figure 6-1. The stress results are presented in Figure 6-19.

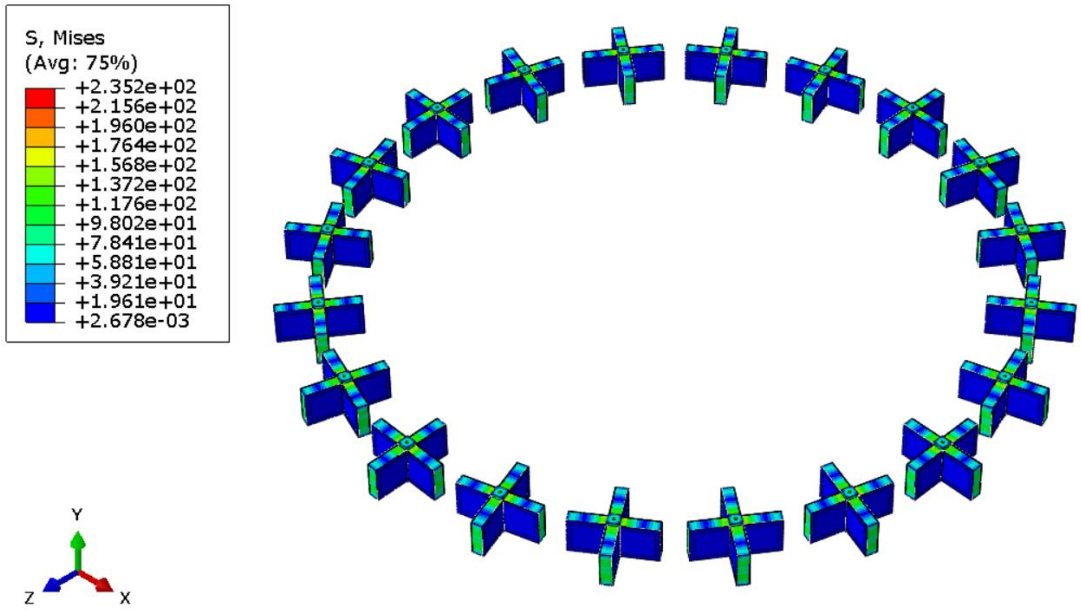

Figure 6-19 T2 VIS – Stress results of quasi-static load analysis in longitudinal direction

As seen in Figure 6-19, the maximum von Mises stress in vibration isolators is 235.2 MPa. The yield strength of isolator material, which is Aluminum 6061-T6, is 276 MPa and factor of safety is 1.17. Therefore, the R-6 is satisfied.

Verification of R-7:

The static load analysis is performed in Abaqus FEA for vibration isolation system by applying static force of 11772 N in x direction at CG of payload as shown in Figure 6-1. The stress results are presented in Figure 6-20.

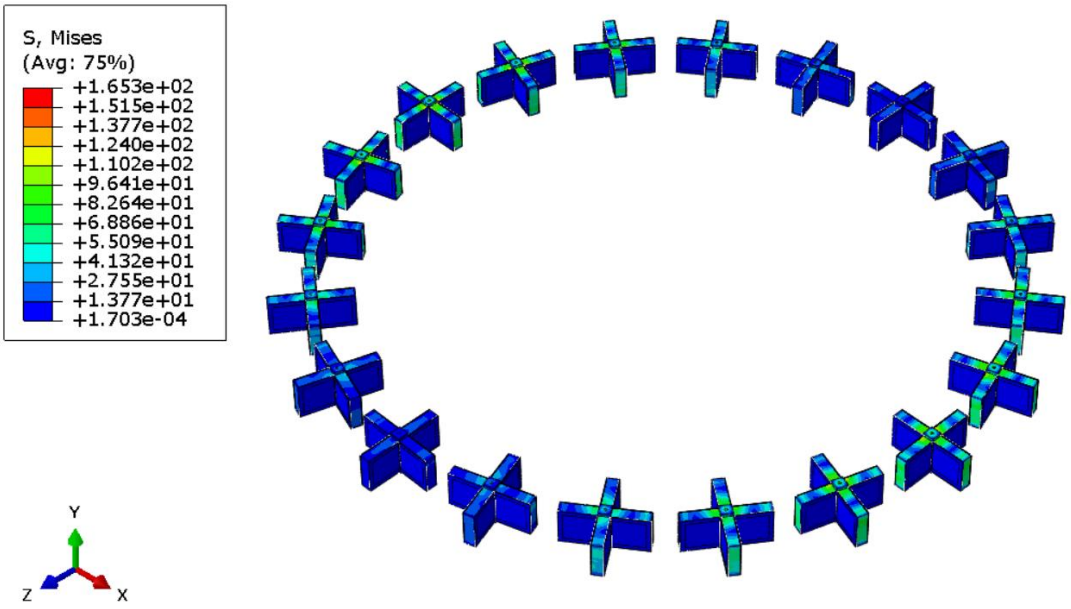

Figure 6-20 T2 VIS – Stress results of quasi-static load analysis in lateral direction

As seen in Figure 6-20, the maximum von Mises stress in vibration isolators is 165.3 MPa. The yield strength of isolator material, which is Aluminum 6061-T6, is 276 MPa and factor of safety is 1.67. Therefore, the R-7 is satisfied.

Verification of R-8:

The static load analysis is performed in Abaqus FEA for vibration isolation system by applying static force of 97708 N in -y direction at CG of payload as shown in Figure 6-1. The displacement results are presented in Figure 6-21.

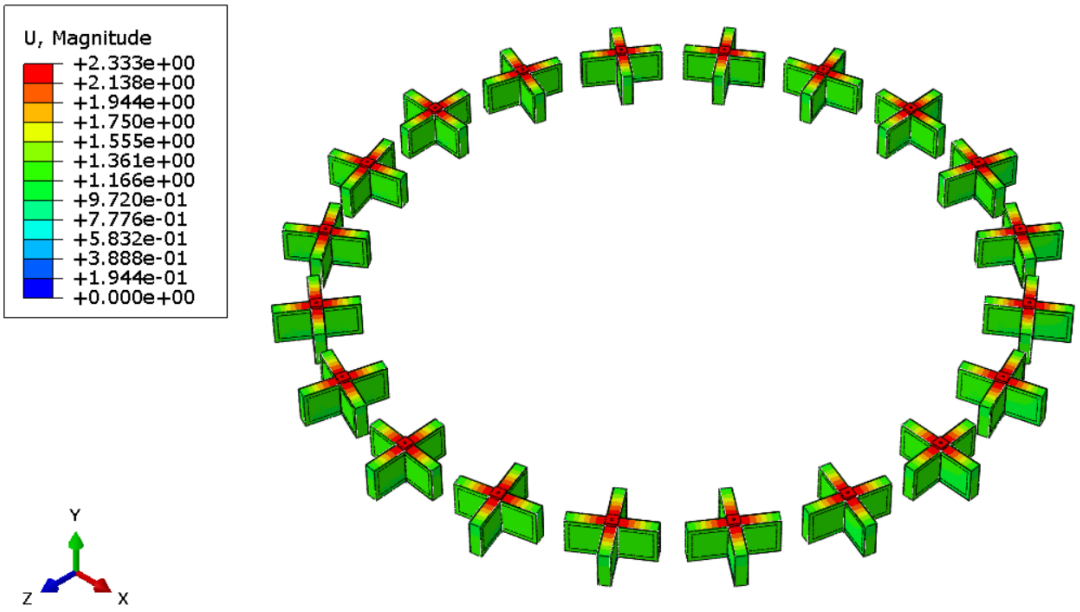

Figure 6-21 T2 VIS – Displacement results of quasi-static load analysis in longitudinal direction

As seen in Figure 6-21, the maximum displacement of vibration isolators is 2.33 mm under the quasi-static acceleration of 8.3 g in longitudinal direction. Therefore, the R-8 is satisfied.

Verification of R-9:

The static load analysis is performed in Abaqus FEA for vibration isolation system by applying static force of 11772 N in x direction at CG of payload as shown in Figure 6-1. The displacement results are presented in Figure 6-22.

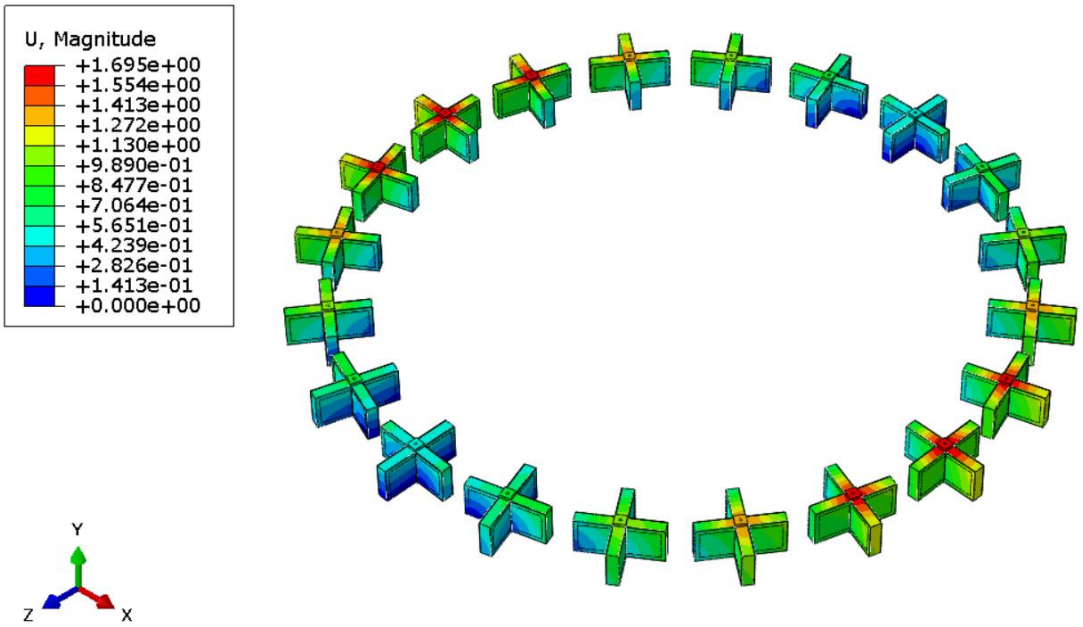

Figure 6-22 T2 VIS – Displacement results of quasi-static load analysis in lateral direction

As seen in Figure 6-22, the maximum displacement of vibration isolators is 1.69 mm under the quasi-static acceleration of 1 g in lateral direction. Therefore, the R-9 is satisfied.

6.2.3. Verification of S1 by Analysis

The S1 vibration isolation system, which consist of 60 DS1_A1 vibration isolators, is verified in this section according to verification plan given in 6.1.

Verification of R-1:

Random vibration analyses for vibration isolation system are performed by using both mathematical model and finite element model. Note that stiffness and loss factor values at isolation frequencies is used in both analyses since it is not possible to use frequency dependent material properties in random vibration analysis.

The random vibration analysis results of mathematical model for the input in longitudinal direction is given in Figure 6-23.

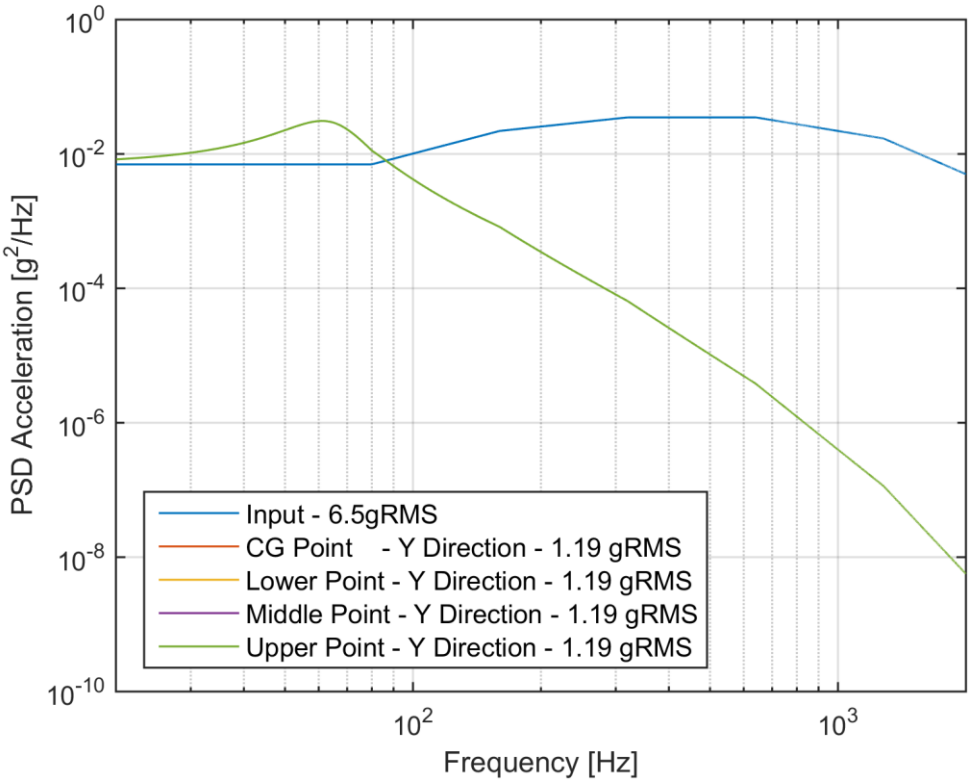

Figure 6-23 S1 VIS - Results of random vibration analysis in longitudinal direction using mathematical model

As seen in Figure 6-23, response RMS acceleration of interested points in longitudinal direction are lower than 2 gRMS. Therefore, the R-1 is satisfied.

Verification of R-2:

The random vibration analysis results of mathematical model and finite element model for the input in lateral direction are given in Figure 6-24 and Figure 6-25, respectively. Note that loss factor used in finite element analysis is 0.28.

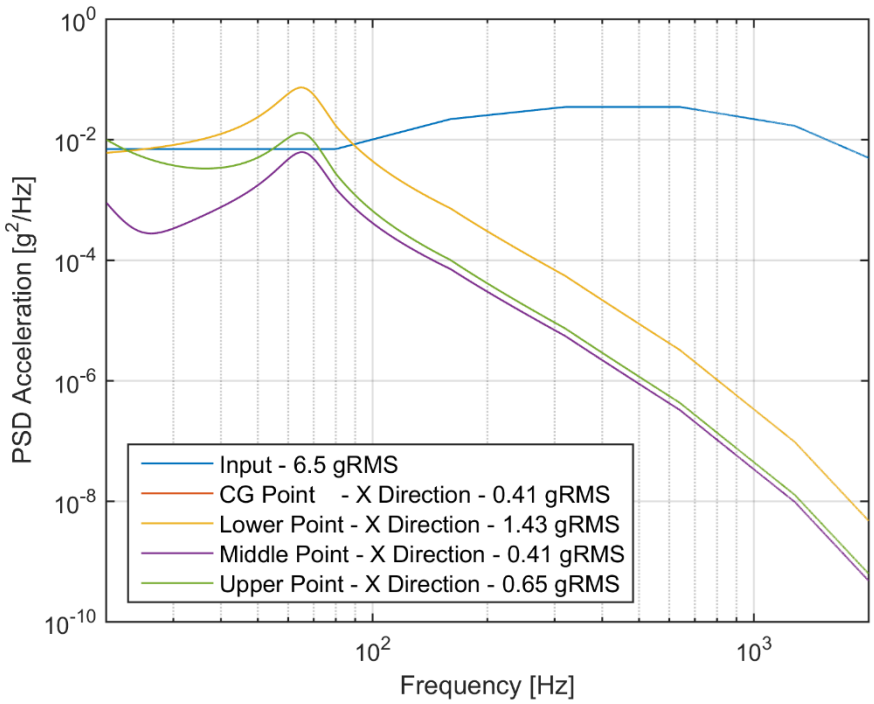

Figure 6-24 S1 VIS - Results of random vibration analysis in lateral direction using mathematical model

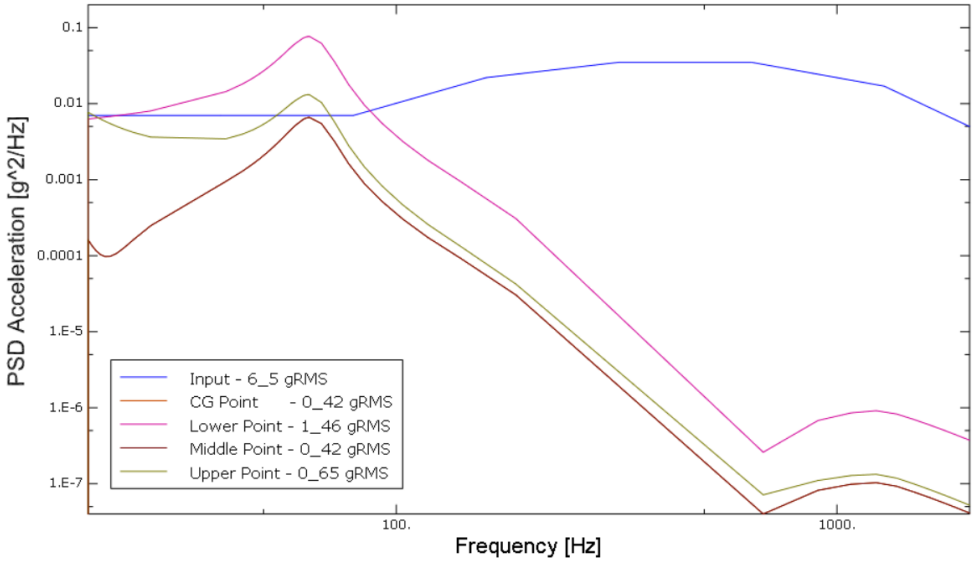

Figure 6-25 S1 VIS - Results of random vibration analysis in lateral direction using finite element model

As seen in Figure 6-24 and Figure 6-25, response RMS acceleration of interested points in lateral direction are lower than 2 gRMS. Therefore, the R-2 is satisfied.

Verification of R-3:

Harmonic vibration analyses for vibration isolation system are performed by using both mathematical model and finite element model. Note that stiffness and loss factor values at 10 Hz is used in both analyses since 10 Hz is at the center of the frequency range of harmonic vibration, which is 2-20 Hz.

The harmonic vibration analysis results of mathematical model for the input in longitudinal direction is given in Figure 6-26.

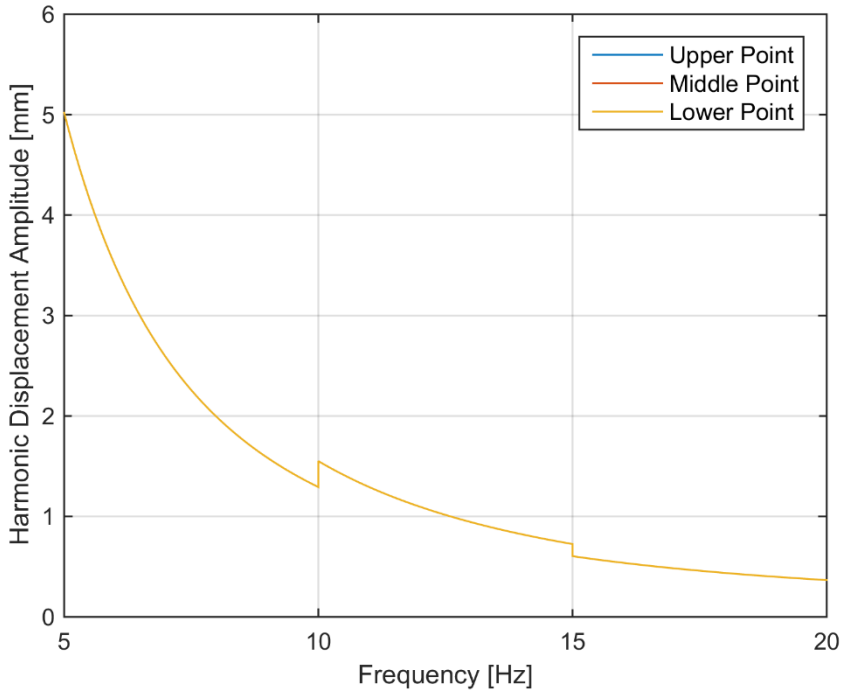

Figure 6-26 S1 VIS - Results of harmonic vibration analysis in longitudinal direction using mathematical model

As seen in Figure 6-26, harmonic displacement amplitudes of interested points in longitudinal direction are lower than 20 mm. Therefore, the R-3 is satisfied.

Verification of R-4:

Harmonic vibration analyses for vibration isolation system are performed by using both mathematical model and finite element model. Note that stiffness and loss factor values at 10 Hz is used in both analyses since 10 Hz is at the center of the frequency range of harmonic vibration, which is 2-20 Hz.

The harmonic vibration analysis results of mathematical model for the input in lateral direction is given in Figure 6-27.

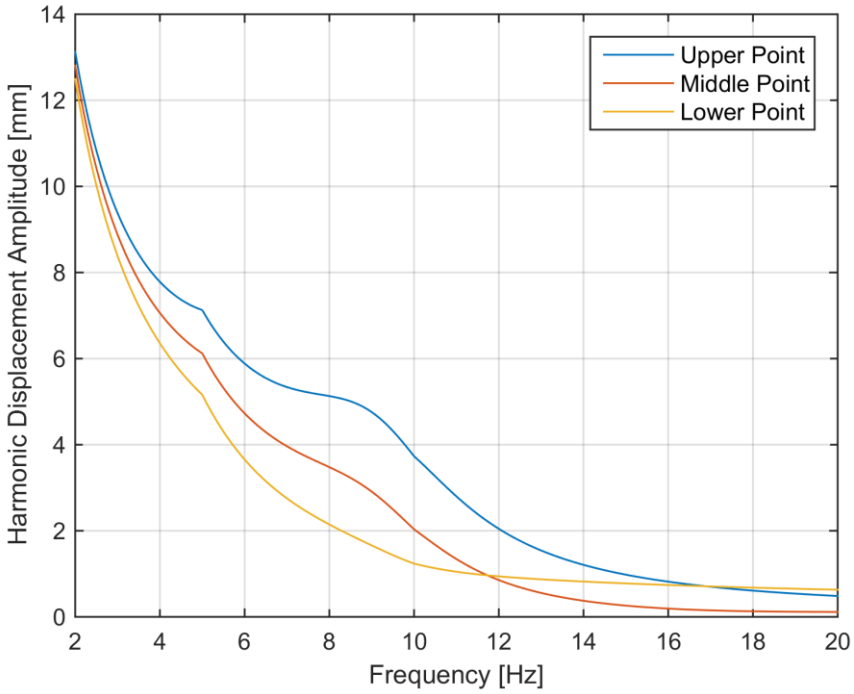

Figure 6-27 S1 VIS - Results of harmonic vibration analysis in lateral direction using mathematical model

As seen in Figure 6-27, harmonic displacement amplitudes of interested points in lateral direction are lower than 20 mm. Therefore, the R-4 is satisfied.

Verification of R-5:

Since R-6 is met, R-5 is automatically satisfied. There is no need to perform any additional verification work for this requirement.

Verification of R-6:

The static load analysis is performed in Abaqus FEA for vibration isolation system by applying static force of 97708 N in -y direction at CG of payload as shown in Figure 6-1. The stress results are presented in Figure 6-28.

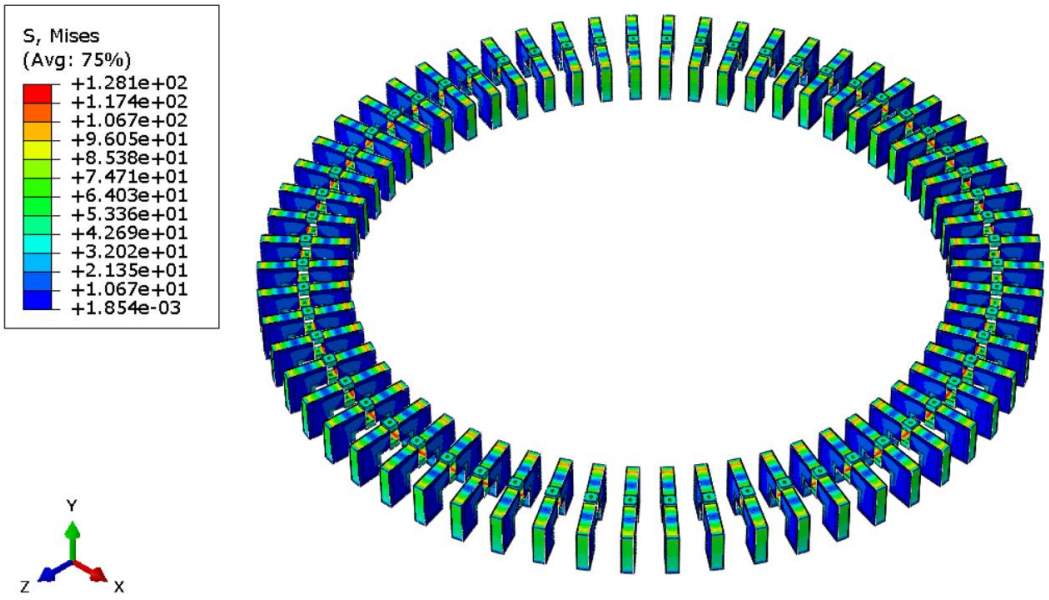

Figure 6-28 S1 VIS – Stress results of quasi-static load analysis in longitudinal direction

As seen in Figure 6-28, the maximum von Mises stress in vibration isolators is 128.1 MPa. The yield strength of isolator material, which is Aluminum 6061-T6, is 276 MPa and factor of safety is 2.15. Therefore, the R-6 is satisfied.

Verification of R-7:

The static load analysis is performed in Abaqus FEA for vibration isolation system by applying static force of 11772 N in x direction at CG of payload as shown in Figure 6-1. The stress results are presented in Figure 6-29.

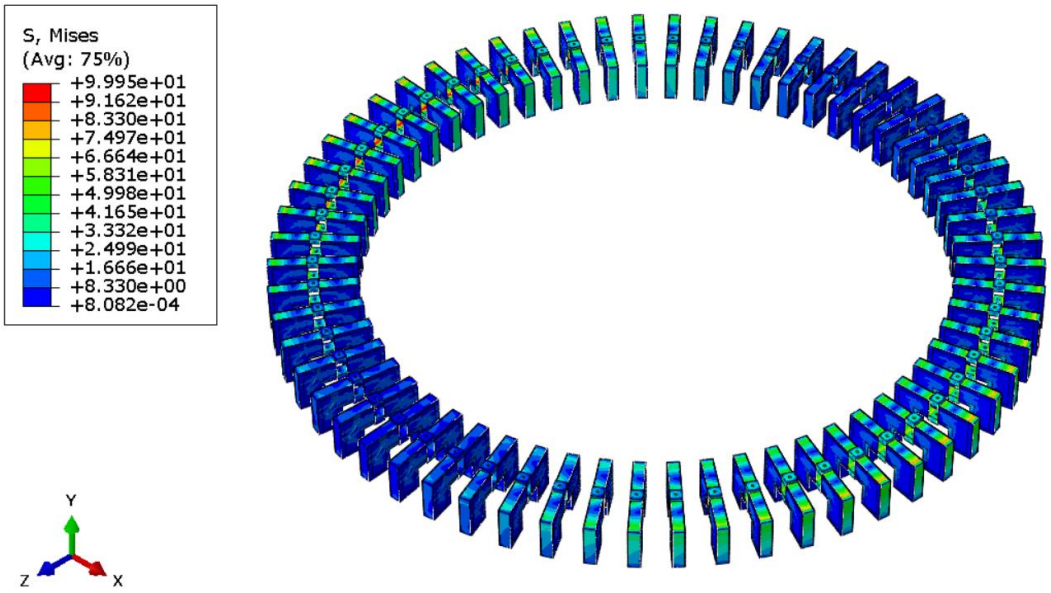

Figure 6-29 S1 VIS – Stress results of quasi-static load analysis in lateral direction

As seen in Figure 6-29, the maximum von Mises stress in vibration isolators is 99.9 MPa. The yield strength of isolator material, which is Aluminum 6061-T6, is 276 MPa and factor of safety is 2.76. Therefore, the R-7 is satisfied.

Verification of R-8:

The static load analysis is performed in Abaqus FEA for vibration isolation system by applying static force of 97708 N in -y direction at CG of payload as shown in Figure 6-1. The displacement results are presented in Figure 6-30.

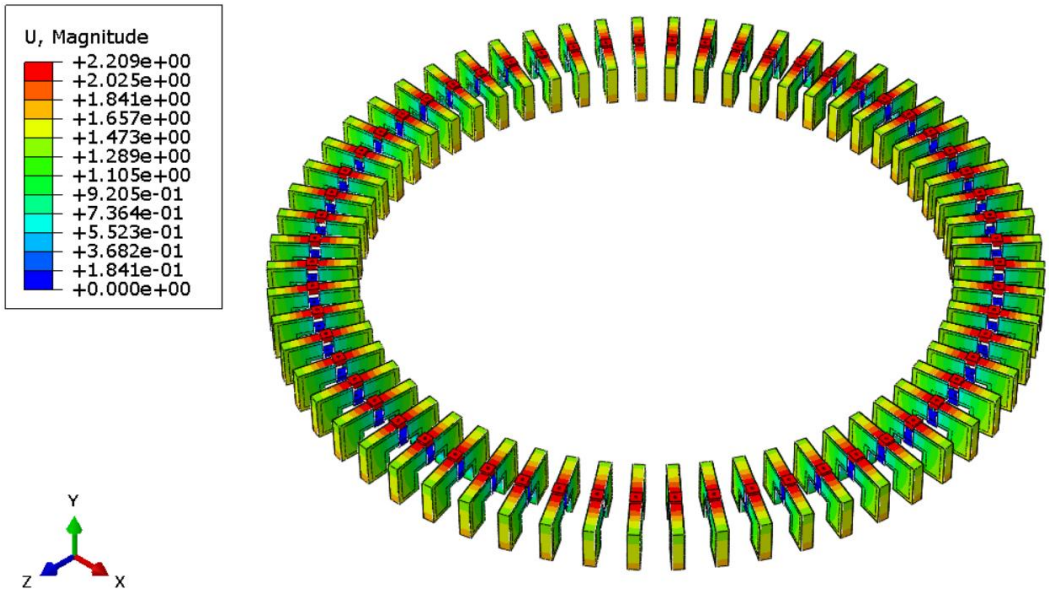

Figure 6-30 S1 VIS – Displacement results of quasi-static load analysis in longitudinal direction

As seen in Figure 6-30, the maximum displacement of vibration isolators is 2.21 mm under the quasi-static acceleration of 8.3 g in longitudinal direction. Therefore, the R-8 is satisfied.

Verification of R-9:

The static load analysis is performed in Abaqus FEA for vibration isolation system by applying static force of 11772 N in x direction at CG of payload as shown in Figure 6-1. The displacement results are presented in Figure 6-31.

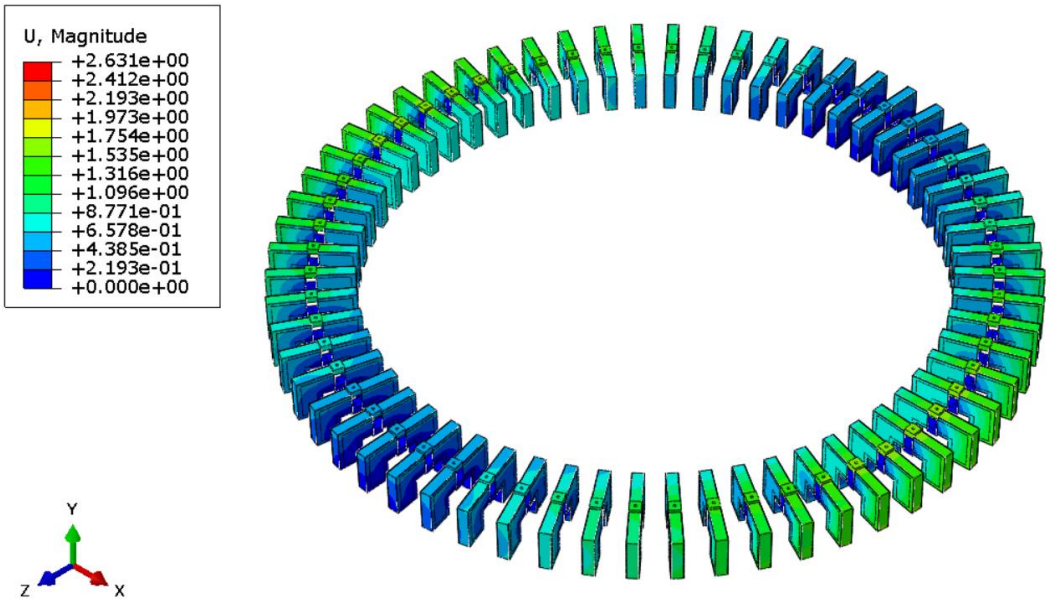

Figure 6-31 S1 VIS – Displacement results of quasi-static load analysis in lateral direction

As seen in Figure 6-31, the maximum displacement of vibration isolators is 2.63 mm under the quasi-static acceleration of 1 g in lateral direction. Therefore, the R-9 is satisfied.

6.3. Verification of Vibration Isolation Systems by Test

The verification of designed vibration isolation systems are performed by tests which are tabulated in Appendix B. The main objective of these tests is to achieve TRL-4 for the designed vibration isolation systems as well as to verify the finite element models, which are used in design and verification phases.

The finite element models of the test configuration of vibration isolation systems are constructed using Abaqus® as shown in Figure 6-32. Vibration isolators are connected to test fixture and dummy payload using “kinematic coupling” type of constraint in Abaqus. Metallic part of vibration isolator, VEM layer and constraining layer are connected to each other using “tie” type of constraint.

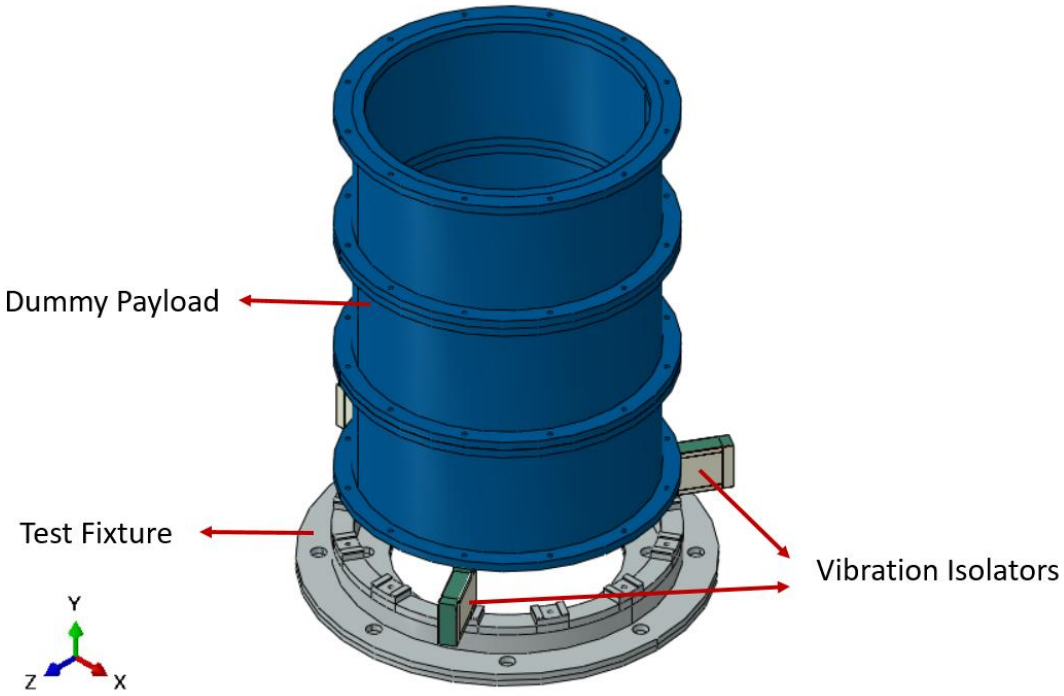

Figure 6-32 Finite element model of test configuration of VIS

In finite element analyses which are presented in 6.3.1, 6.3.2 and 6.3.3, material properties of ISD-112 at 30 °C is used. To obtain transmissibility curves, "Steady-state dynamics, Direct" step is used since it is possible to include frequency-dependent viscoelastic material properties in this analysis type. The loss factor values for each mode are calculated from the transmissibility curves by applying the half-power bandwidth method, which is explained in 6.2. These loss factor values are used in "Random response" step to obtain PSD accelerations and gRMS levels for random vibration input. Note that elastic modulus of ISD-112 around isolation frequency is used in each random vibration analysis since frequency dependent viscoelastic material properties cannot be defined in "Random response" step.

Tests are performed with 1/20-scale model of the vibration isolation system due to the limitations related with test equipment. Therefore, 3 vibration isolators are used for each system instead of 60. Since the mass of the Sentinel-2, which is chosen as payload

for the case study in this thesis work, is 1200 kg, the mass of the dummy payload, which is used in vibration tests, is 60 kg. The dummy payload is designed such that it has same length over diameter ratio with Sentinel-2 in order to represent vibration modes properly. Note that instead of manufacturing a payload in one piece, three identical 20 kg dummy payloads are manufactured from steel and assembled with bolts for ease of handling. The experimental setups for vibration tests in axial and lateral directions are shown in Figure 6-33 and Figure 6-34.

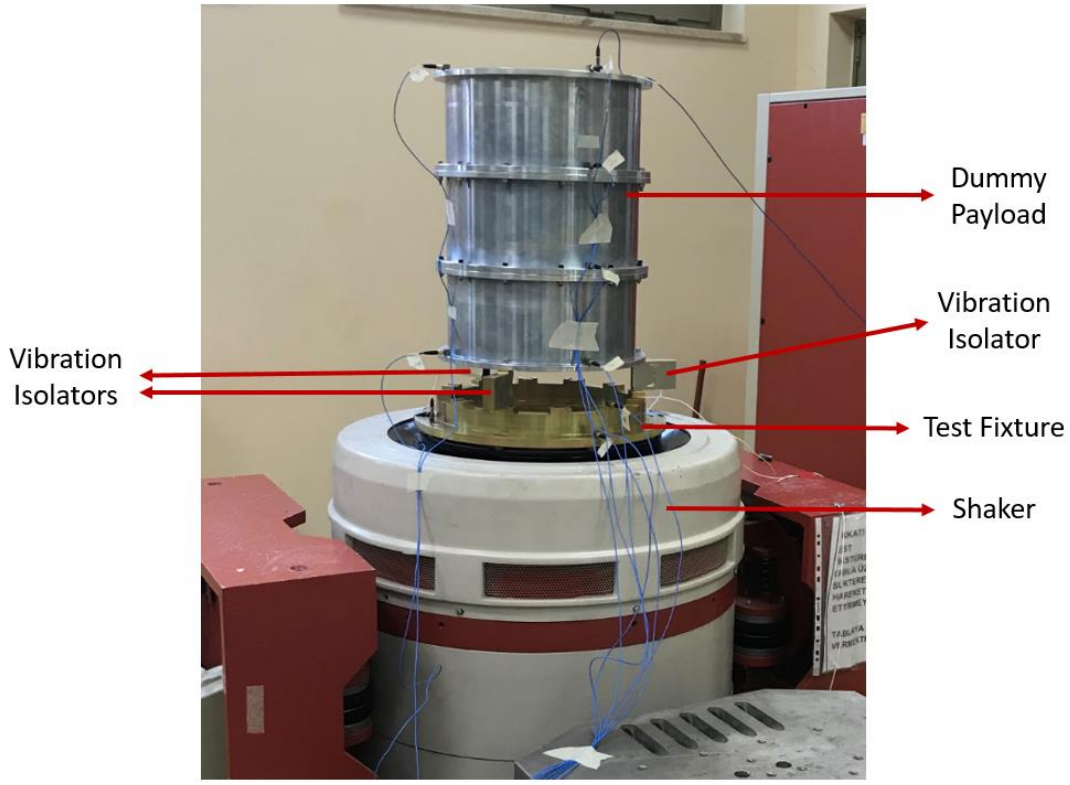

Figure 6-33 The experimental setup for vibration tests in axial direction

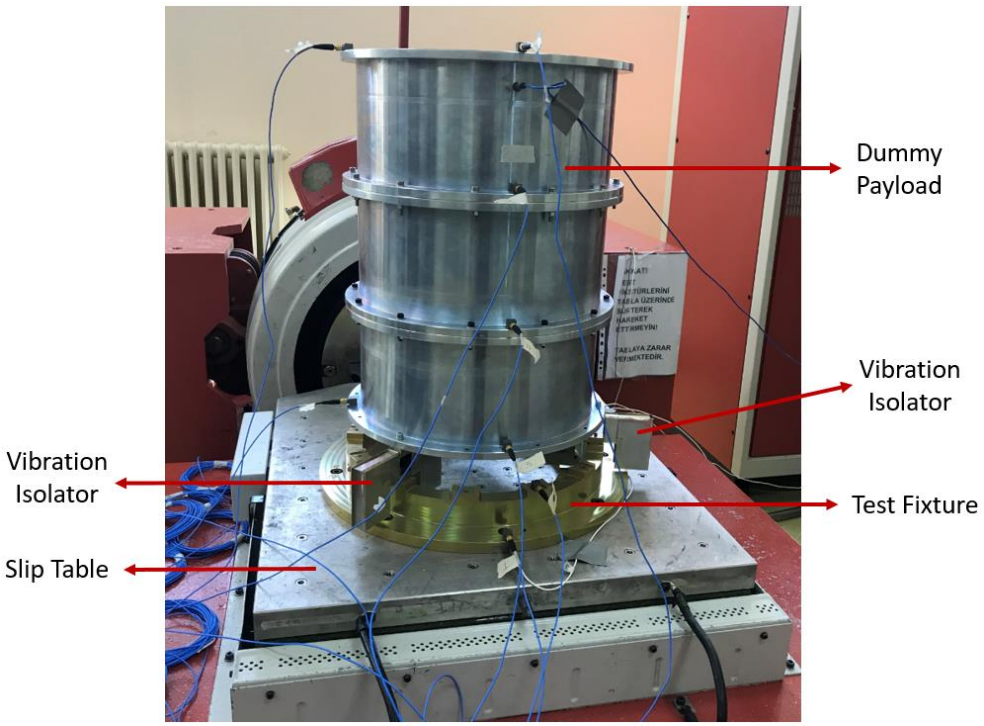

Figure 6-34 The experimental setup for vibration tests in lateral direction

Mechanical connection of vibration isolators with dummy payload and test fixture is shown in Figure 6-35.

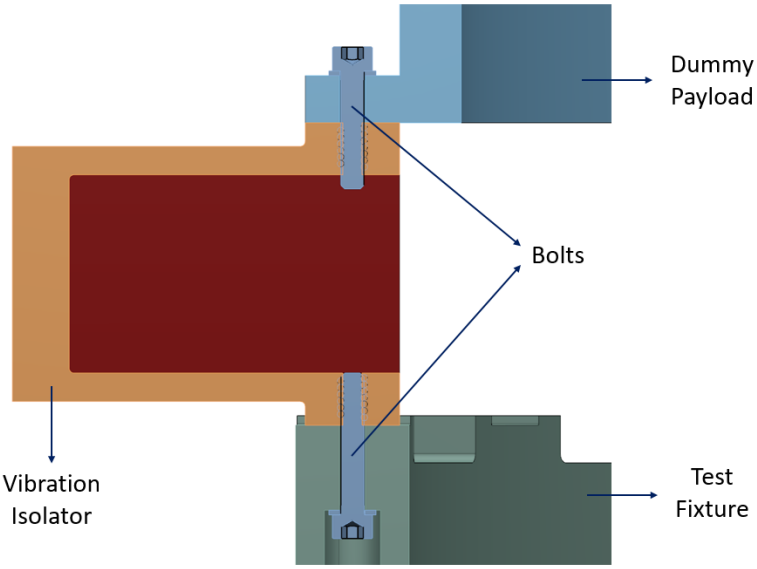

Figure 6-35 Mechanical connection of vibration isolators

The test fixture is designed such that it does not have any vibration mode in frequency range of vibration tests, i.e. its first natural frequency is higher than 2000 Hz to transmit vibration directly. Moreover, it has suitable mechanical interfaces with shaker and vibration isolators. The test fixture is manufactured from Aluminum 6061 and shown in Figure 6-36.

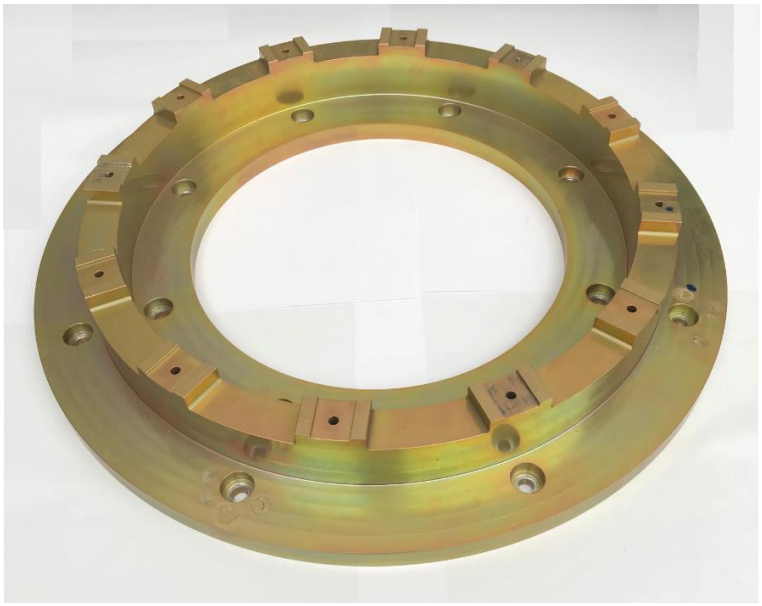

Figure 6-36 Test fixture

The triaxial monitor accelerometers are placed on the test fixture and the different locations on payload as shown in Figure 6-37 to measure the acceleration levels in vibration tests. The model number of triaxial accelerometers is 356A43 and its specifications are given in Appendix C. Moreover, two single-axis control accelerometers are located on the test fixture. Note that average of these two accelerometers is taken to control vibration level produced by shaker.

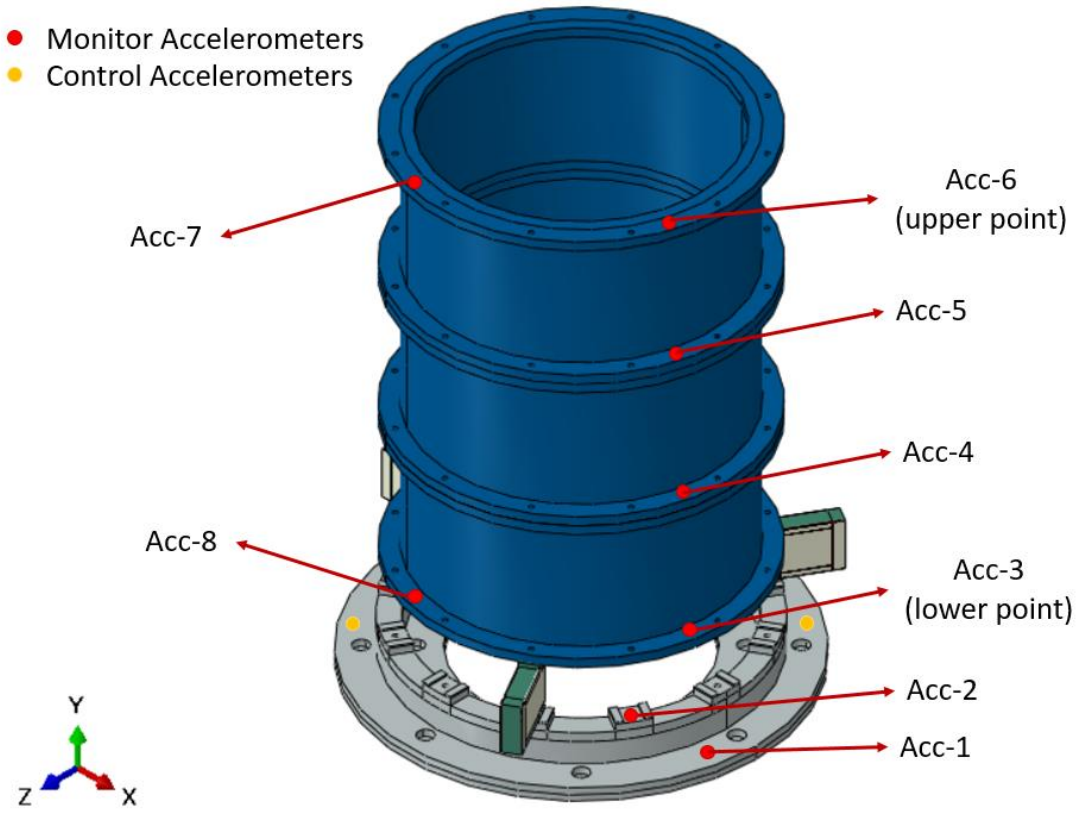

Figure 6-37 The locations of accelerometers

Dewesoft data acquisition system is used in vibration tests. The measured acceleration data are transformed from time domain to the frequency domain using fast Fourier transform (FFT) algorithm. The rectangular window function is used to minimize leakage problem. Then, the transmissibility curves for each vibration isolation system are obtained by dividing the acceleration of an interested point to the input acceleration in frequency domain. The following results are presented in subsequent sections for each vibration isolation systems:

- The transmissibility curves, which are obtained from sine sweep and random vibration tests, to show the functionality of vibration isolation systems
- The comparison of transmissibility curves, which are obtained from sine sweep tests and finite element analyses, to verify the analysis model

- The acceleration data in time domain for 6.5 gRMS random vibration tests to show the functionality of vibration isolation systems
- The PSD accelerations and gRMS levels of interested points for 6.5 gRMS random vibration tests to verify the performance requirements, namely R-1 and R-2
- The comparison of PSD accelerations and gRMS levels of interested points, which are obtained from random vibration tests and finite element analyses, to verify the analysis model
- The displacement amplitudes of interested points for harmonic vibration tests to verify the performance requirements, namely R-3 and R-4.

6.3.1. Verification of T1 by Test

T1 test prototypes are manufactured for vibration tests and shown in Figure 6-38.

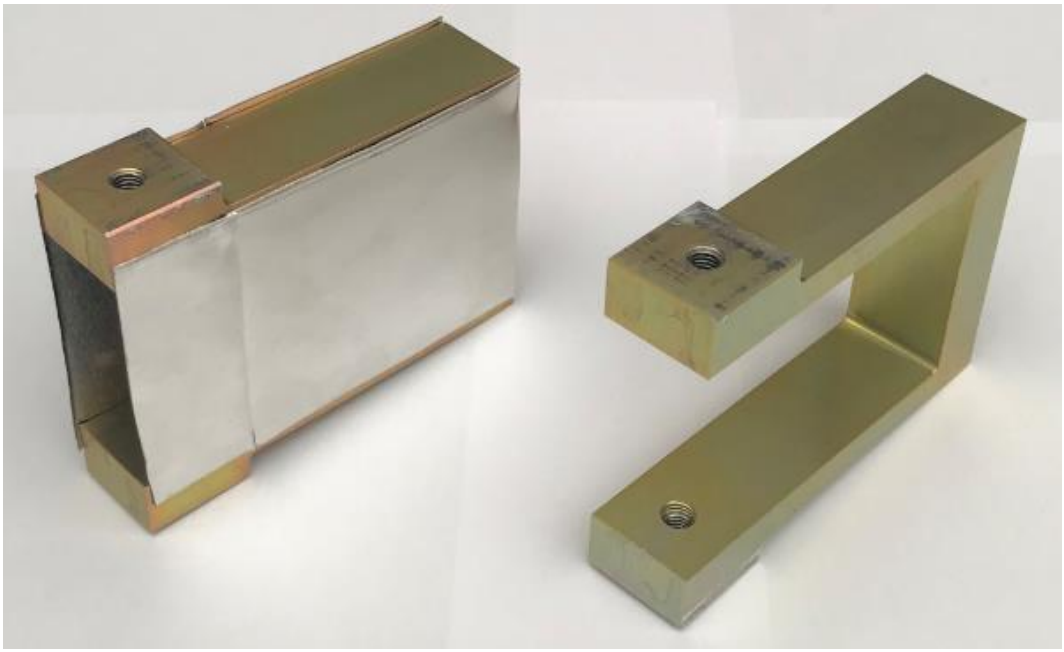

Figure 6-38 T1 test prototypes, with and without damping application

Prior to test results, modal analysis results for test configuration of T1 vibration isolation system are presented in Figure 6-39 to Figure 6-45 for understanding the dynamic behavior of VIS.

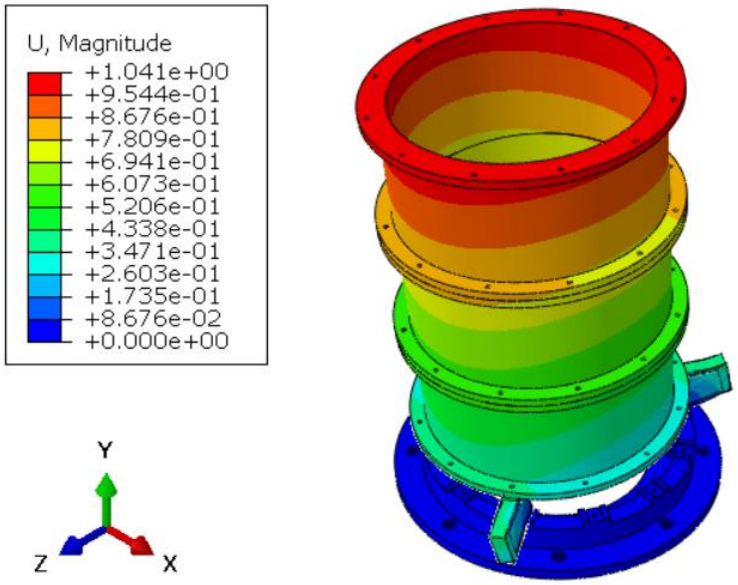

Figure 6-39 Rocking mode shape of T1 test configuration, 14 Hz

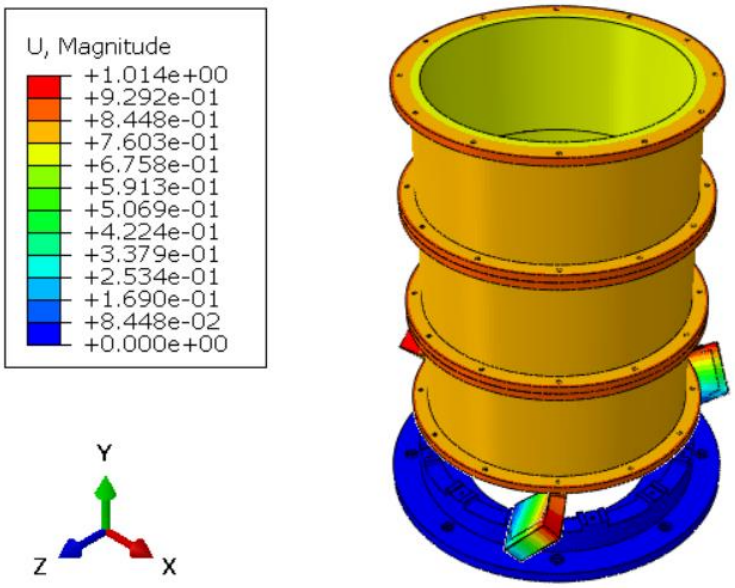

Figure 6-40 Torsional mode shape of T1 test configuration, 30 Hz

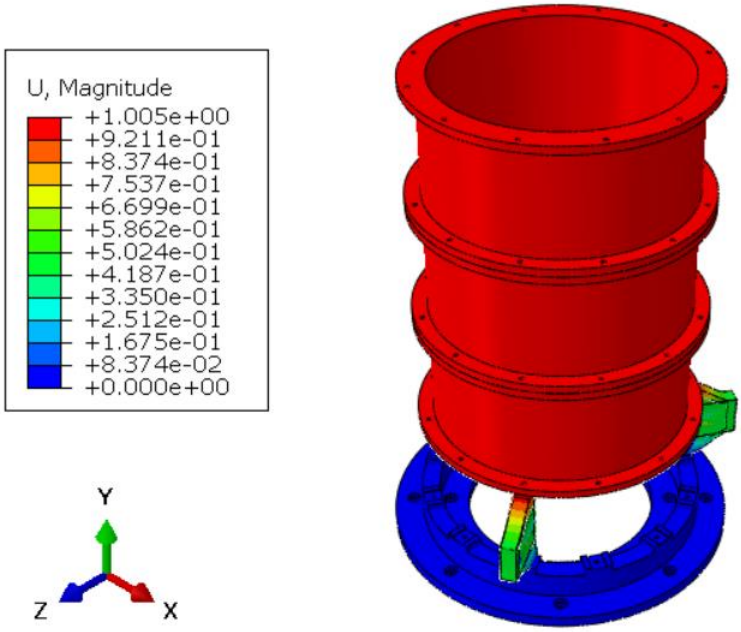

Figure 6-41 Axial mode shape of T1 test configuration, 38 Hz

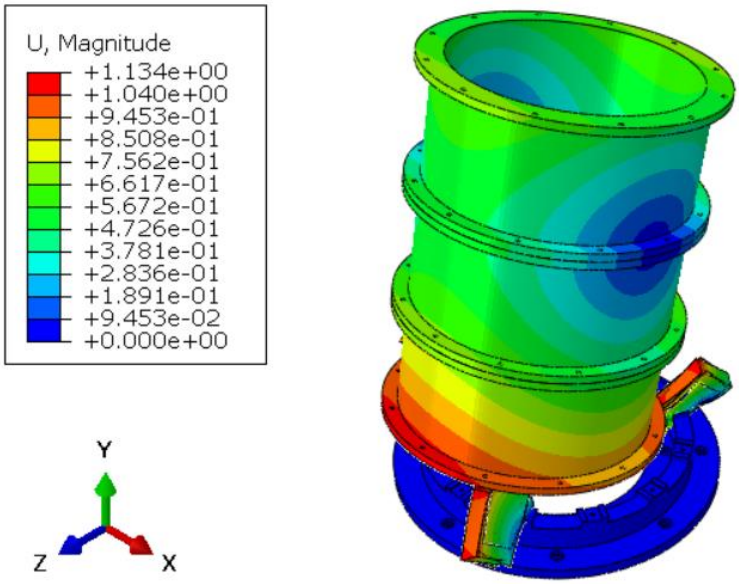

Figure 6-42 Lateral mode shape of T1 test configuration, 50 Hz

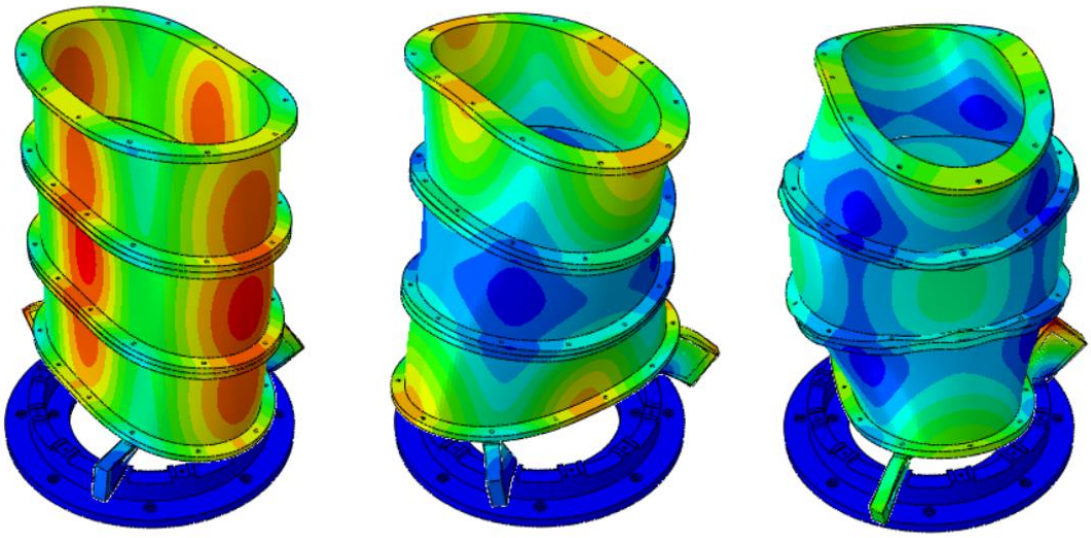

Figure 6-43 Internal modes of dummy payload for T1 test configuration;
506 Hz, 528 Hz, 1096 Hz from left to right

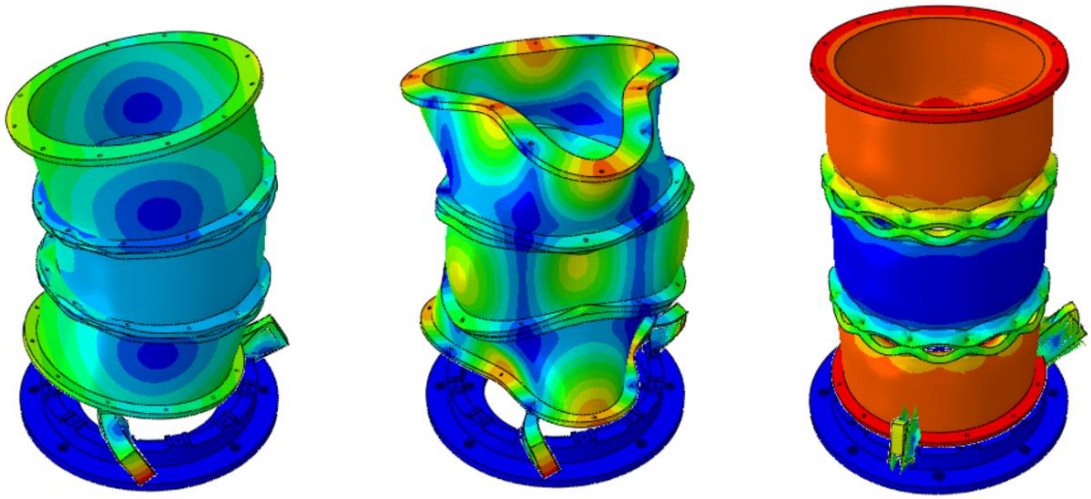

Figure 6-44 Internal modes of dummy payload for T1 test configuration;
1549 Hz, 1629 Hz, 1800 Hz from left to right

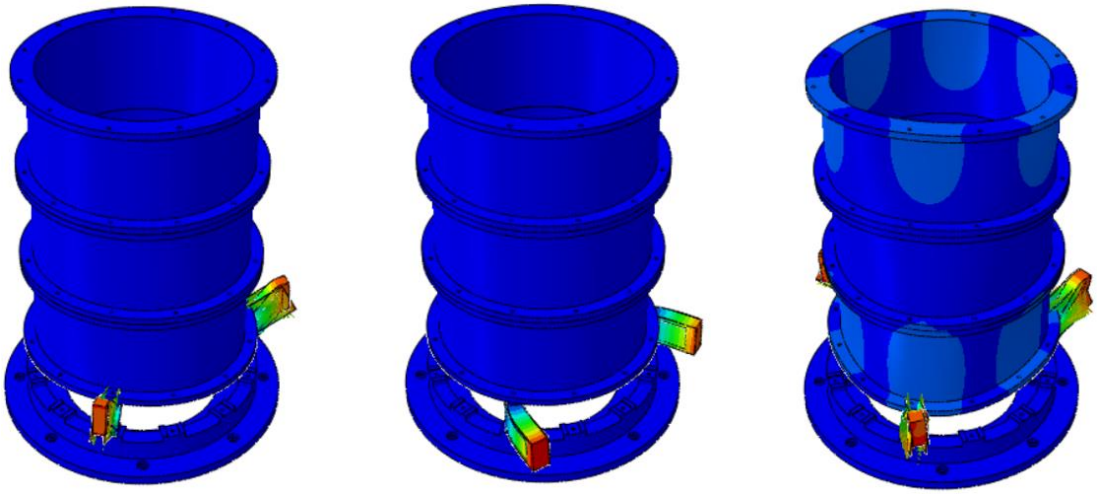

Figure 6-45 Internal resonances of vibration isolators for T1 test configuration;
1291 Hz, 1367 Hz, 1396 Hz from left to right

The transmissibility curves, which are obtained from sine sweep and random vibration tests, for upper and lower points are presented in from Figure 6-46 to Figure 6-48 for axial and lateral directions.

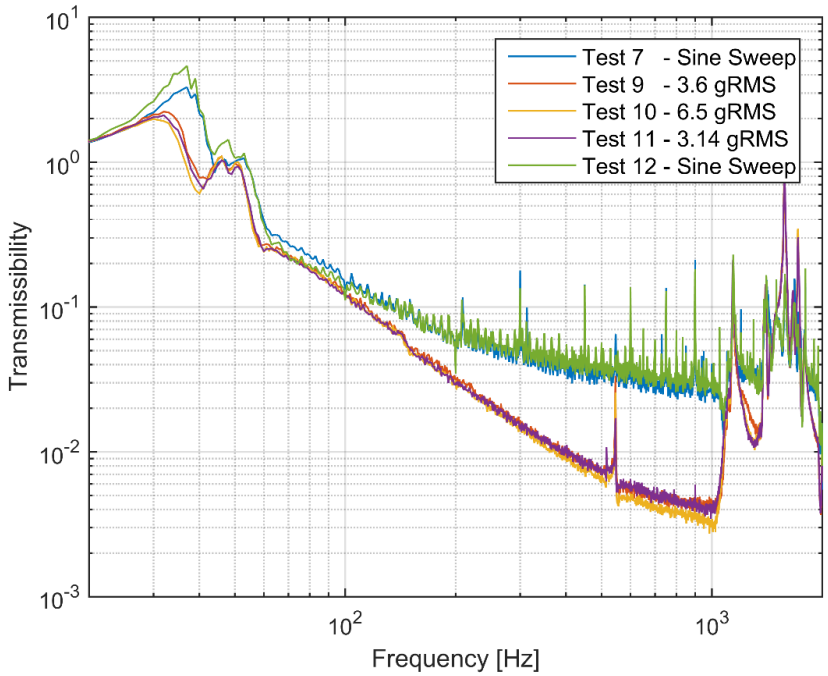

Figure 6-46 T1 - The axial transmissibility curves obtained from vibration tests for upper point

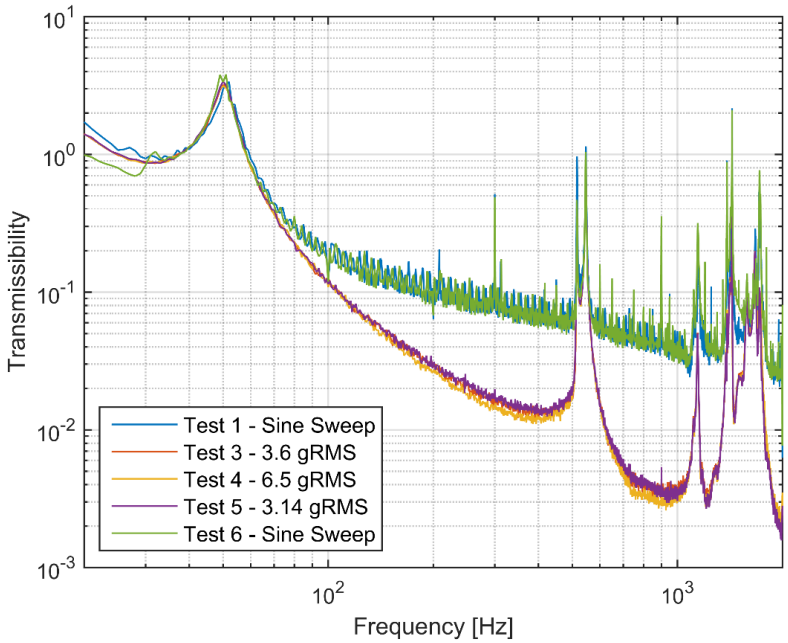

Figure 6-47 T1 - The lateral transmissibility curves obtained from vibration tests for upper point

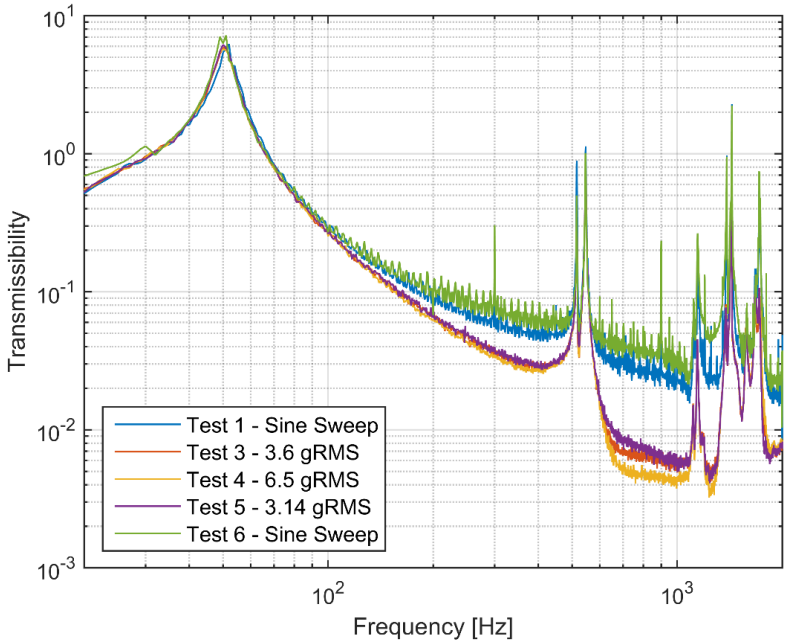

Figure 6-48 T1 - The lateral transmissibility curves obtained from vibration tests for lower point

The comparison of transmissibility curves, which are obtained from sine sweep tests and finite element analyses, for upper and lower points are given in Figure 6-49 to Figure 6-51 for axial and lateral directions.

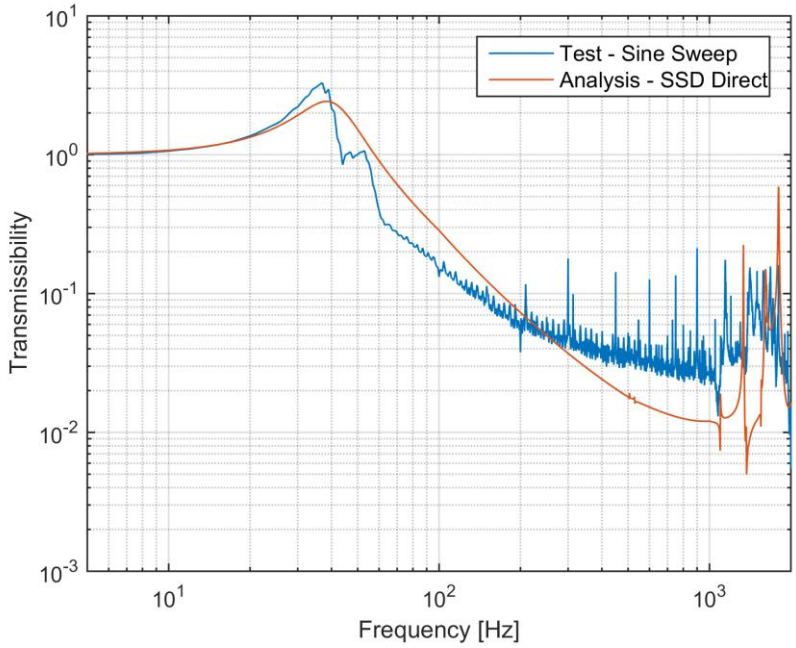

Figure 6-49 T1 – The comparison of axial transmissibility curves obtained from sine sweep test and finite element analysis for upper point

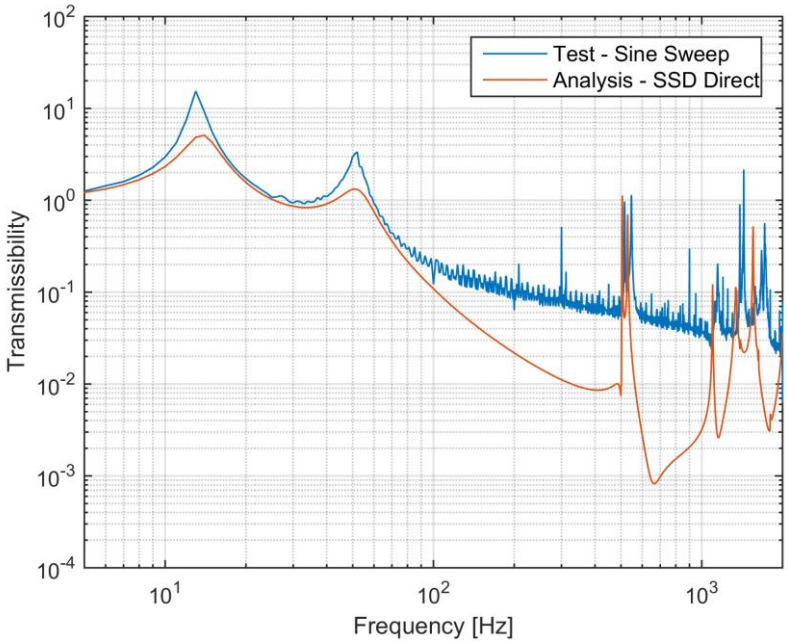

Figure 6-50 T1 – The comparison of lateral transmissibility curves obtained from sine sweep test and finite element analysis for upper point

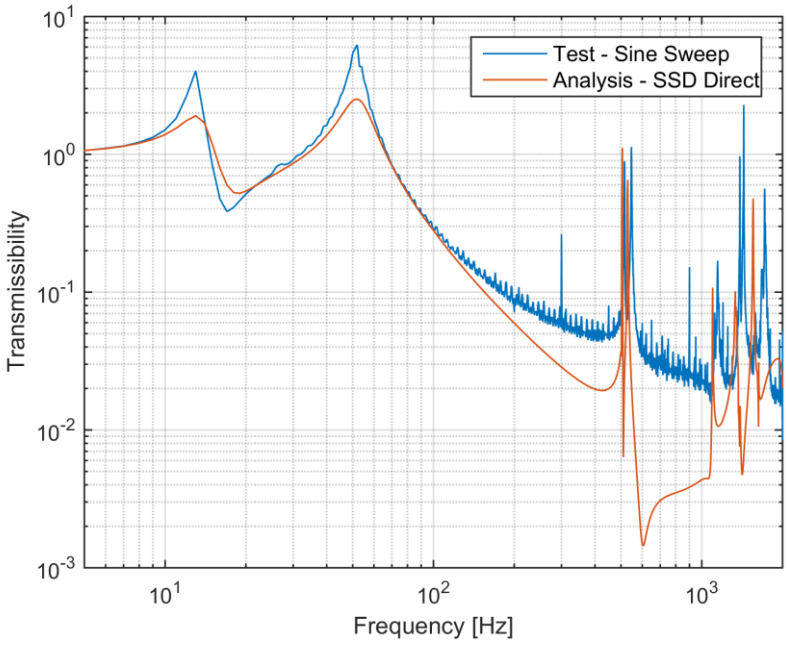

Figure 6-51 T1 – The comparison of lateral transmissibility curves obtained from sine sweep test and finite element analysis for lower point

In Figure 6-49, the peak around 38 Hz is related with the axial mode shape which is given in Figure 6-41. The rocking mode (Figure 6-39) around 14 Hz and lateral mode (Figure 6-42) around 50 Hz can be identified in Figure 6-50 and Figure 6-51. Note that torsional mode of a vibration isolation system, which is shown in Figure 6-40, is not effective for the vibration inputs in axial and lateral directions. Moreover, due to internal resonances of dummy payload and vibration isolators, which are shown in Figure 6-43 to Figure 6-45, there are numerous intense peaks that results in deterioration of transmissibility in the high-frequency range as seen in Figure 6-49 to Figure 6-51.

Figure 6-49 to Figure 6-51 indicates that there is a good consistency between the finite element model and test results. The natural frequencies obtained from finite element analyses and vibration tests are very close to each other. However, there is a slight difference in amplitudes of these resonance frequencies. The amplitudes in tests are slightly higher than the amplitudes in finite element analysis results. It means that loss factor in vibration tests are smaller than the loss factor values, which are calculated by finite element analyses. This difference is mainly caused by uncertainty related with VEM properties. The viscoelastic material properties, which are used in finite element analyses, in datasheet of ISD-112 are obtained for small strain amplitude whereas the strain levels are relatively high in these vibration tests. Moreover, ISD-112 show strong temperature dependence and the exact temperature of viscoelastic material in tests is not known. Obtaining viscoelastic material properties with respect to strain amplitude and locating thermocouples on viscoelastic material during vibration test can minimize the error in finite element model.

The acceleration data in time domain, the PSD accelerations and the comparison of test and random vibration analysis results are presented in Figure 6-52 to Figure 6-55 for Test-10, in which 6.5 gRMS random vibration input is applied in axial direction.

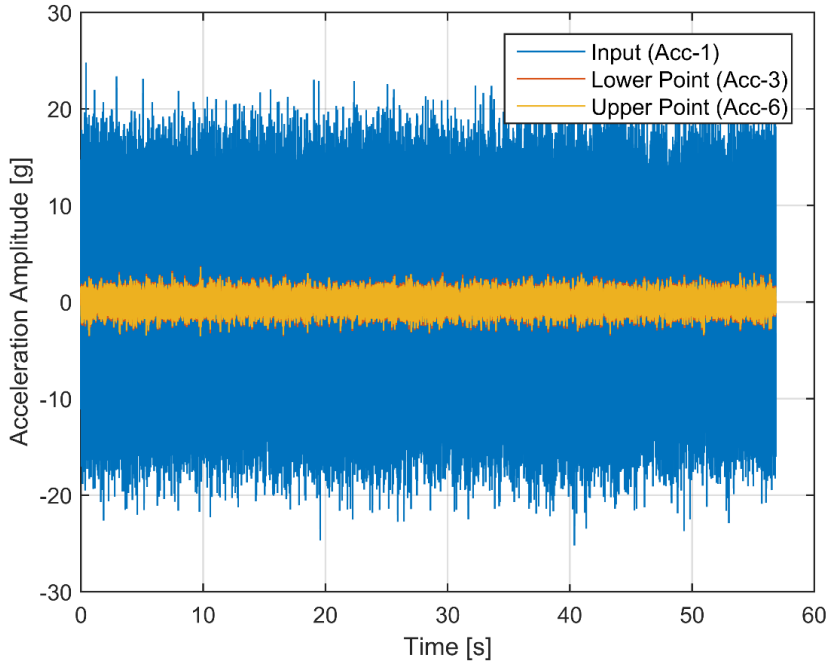

Figure 6-52 T1 – Test 10 - The acceleration data in time domain

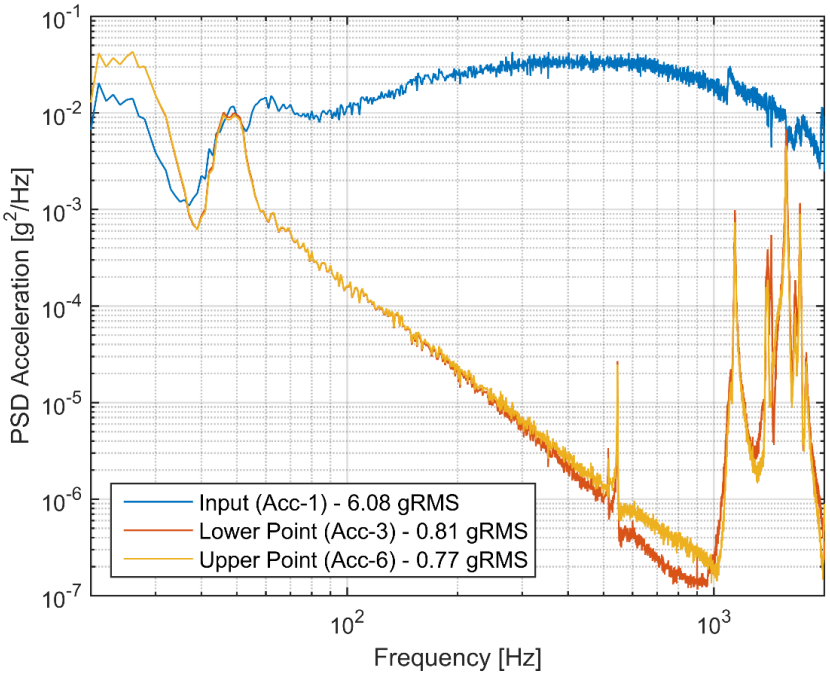

Figure 6-53 T1 – Test 10 - The PSD accelerations in frequency domain

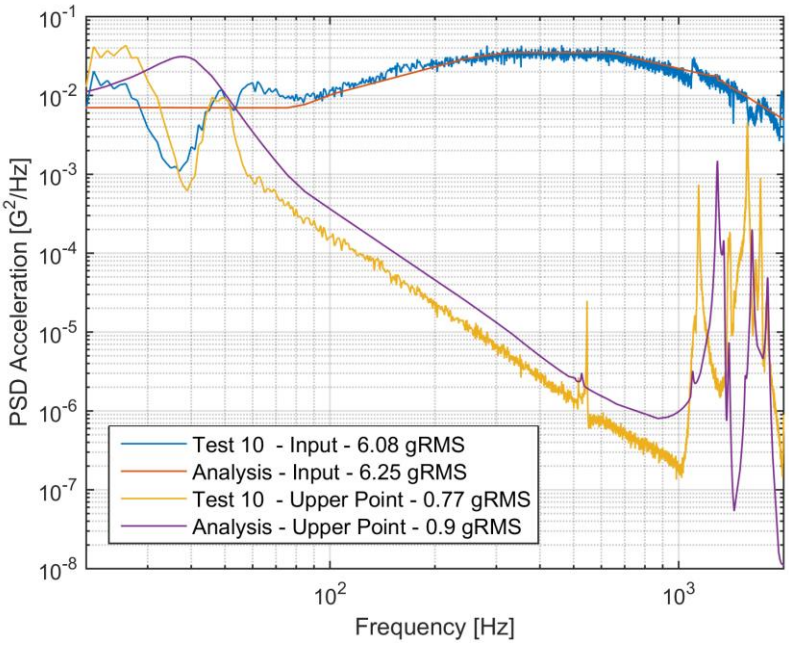

Figure 6-54 T1 – The comparison of Test 10 and random vibration analysis results for upper point

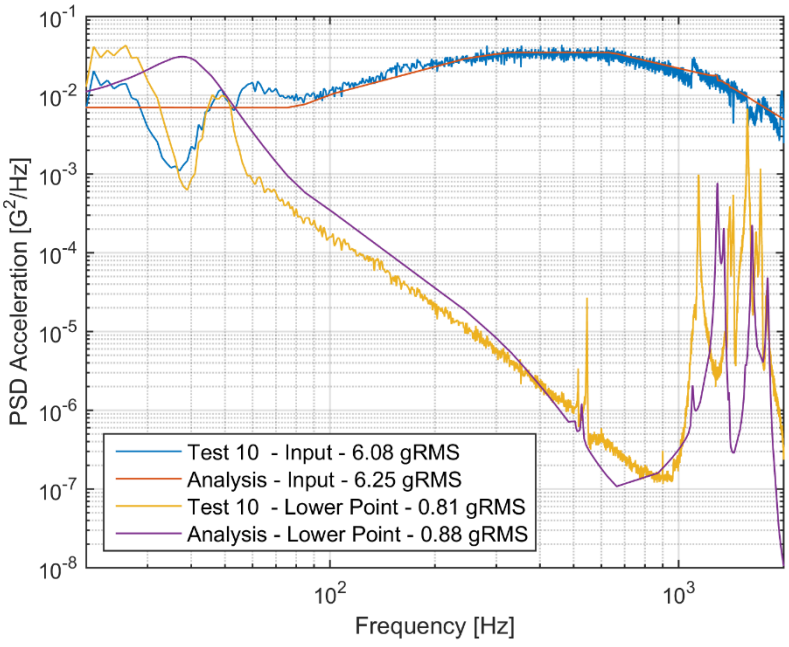

Figure 6-55 T1 – The comparison of Test 10 and random vibration analysis results for lower point

Figure 6-52 indicates that the reduction in acceleration level in axial direction is achieved using T1 vibration isolation system. It can be seen from Figure 6-53 that R-1 is satisfied. Moreover, there is a good consistency between finite element analyses and test results as seen in Figure 6-54 and Figure 6-55.

The acceleration data in time domain, the PSD accelerations and the comparison of test and random vibration analysis results are presented in Figure 6-56 to Figure 6-59 for Test-4, in which 6.5 gRMS random vibration input is applied in lateral direction.

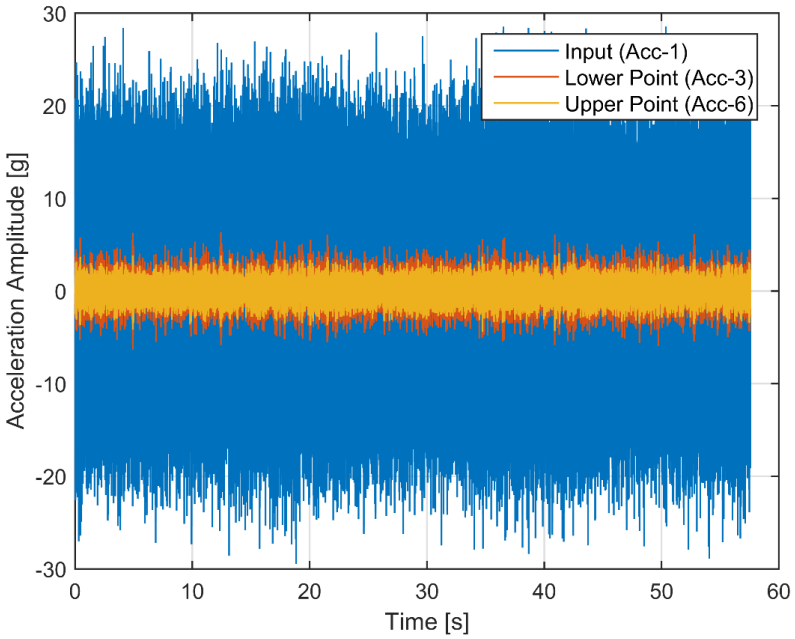

Figure 6-56 T1 – Test 4 - The acceleration data in time domain

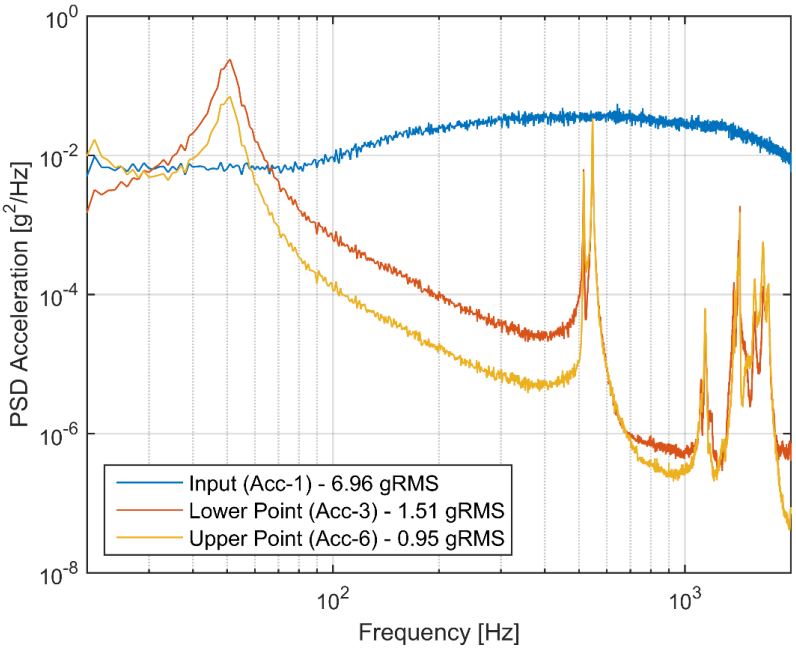

Figure 6-57 T1 – Test 4 - The PSD accelerations in frequency domain

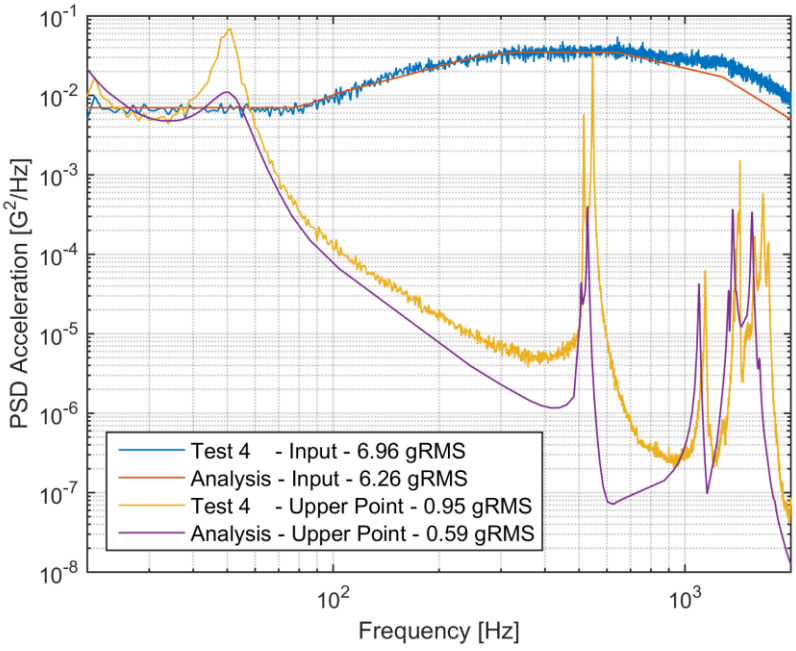

Figure 6-58 T1 – The comparison of Test 4 and random vibration analysis results for upper point

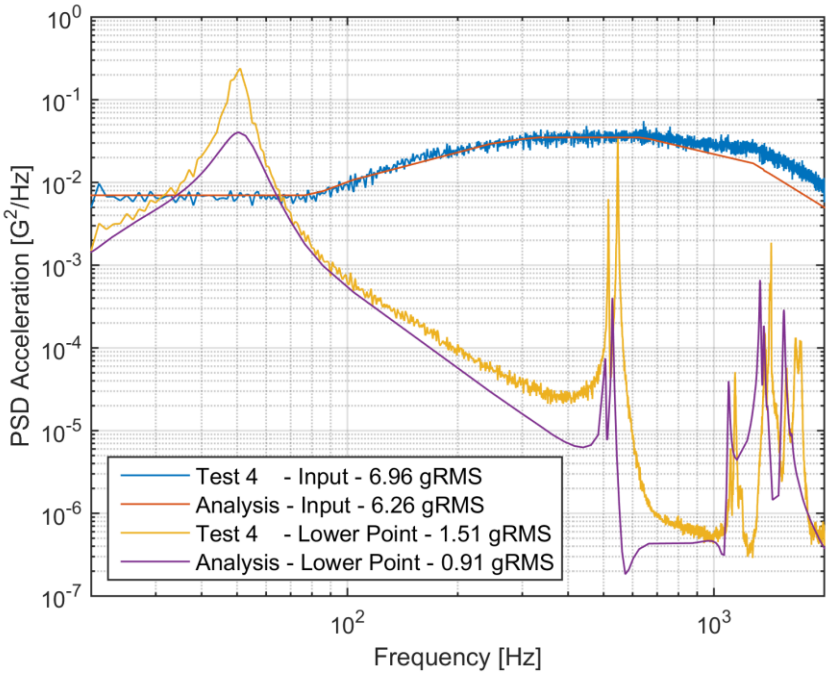

Figure 6-59 T1 – The comparison of Test 4 and random vibration analysis results for lower point

Figure 6-56 indicates that the reduction in acceleration level in lateral direction is achieved using T1 vibration isolation system. It can be seen from Figure 6-57 that R-2 is satisfied. Moreover, there is a good consistency between finite element analyses and test results as seen in Figure 6-58 and Figure 6-59.

The displacement amplitudes of lower and upper points are given in Figure 6-60 and Figure 6-61 for Test-8 and Test-2, which are harmonic vibration tests in axial and lateral directions, respectively.

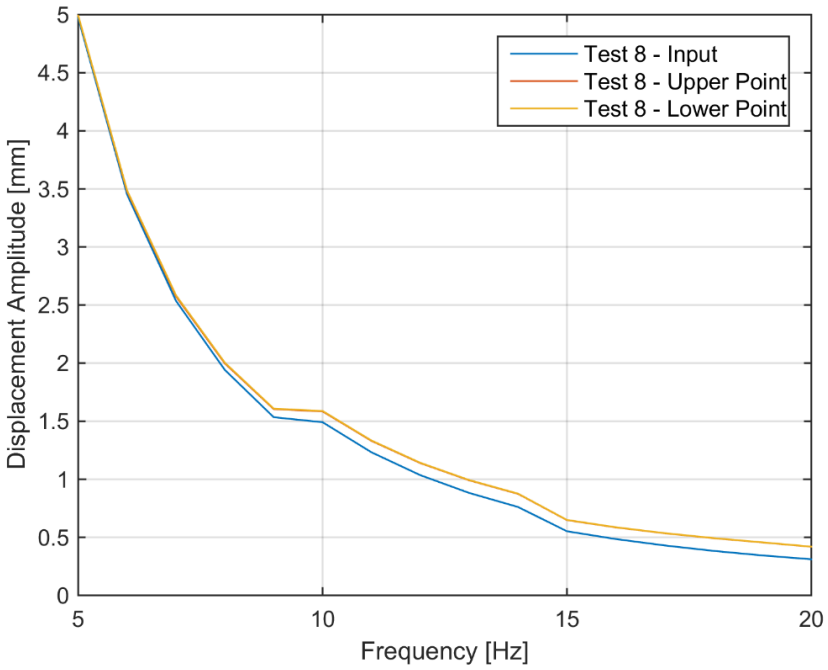

Figure 6-60 T1 - Test 8 – Harmonic displacement results in axial direction

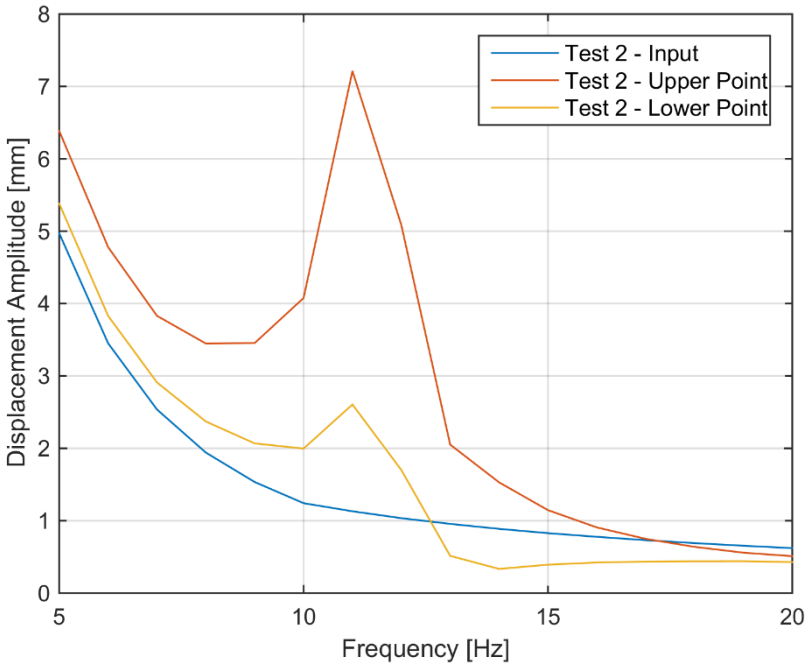

Figure 6-61 T1 - Test 2 – Harmonic displacement results in lateral direction

Figure 6-60 and Figure 6-61 indicate that R-3 and R-4 are met. Harmonic vibration input in axial direction is transmitted directly to the payload as seen in Figure 6-60. On the other hand, there is an amplification, especially for upper point, in lateral direction as seen in Figure 6-61 due to rocking mode of VIS, which is illustrated in Figure 6-39.

After performing all vibration tests with T1 vibration isolators, it is observed that one of the T1 isolators is broken as shown in Figure 6-62. The reason for this failure is high-cycle fatigue since plenty of vibration tests are performed, each test in test matrix has to be repeated more than once due to practical problems related with test set-up, with T1 test configuration.

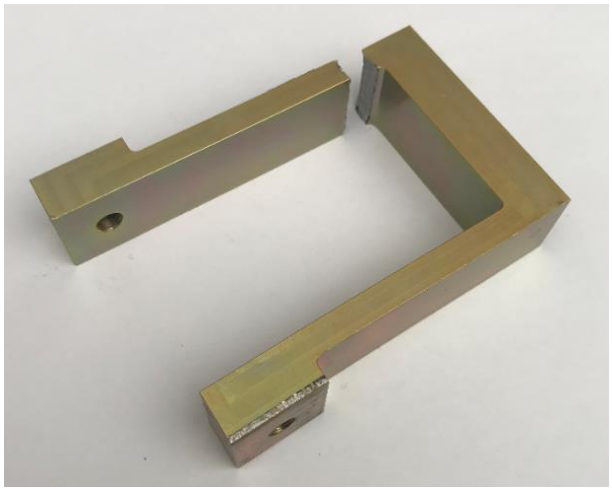

Figure 6-62 Broken T1 vibration isolator

6.3.2. Verification of T2 by Test

T2 test prototypes, which are manufactured for vibration tests, are shown in Figure 6-63.

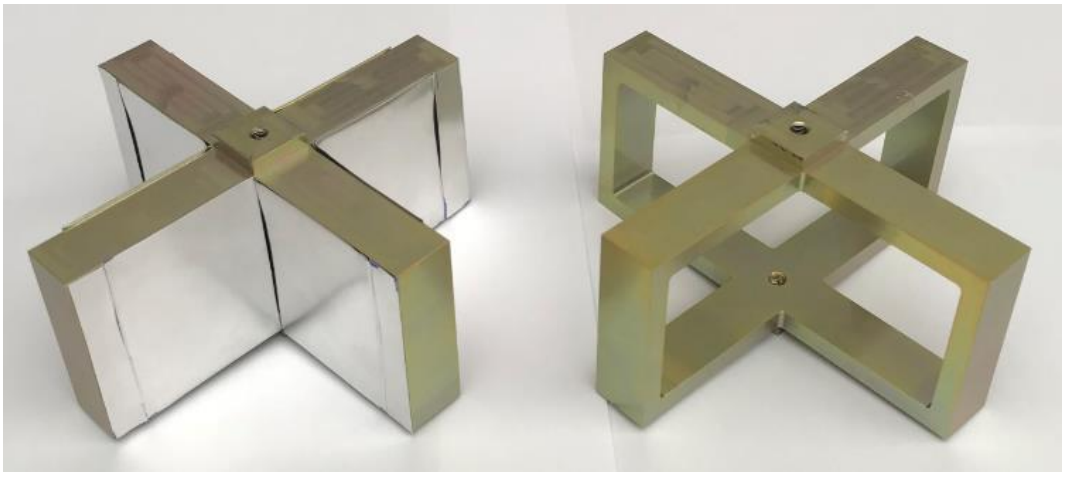

Figure 6-63 T2 test prototypes, with and without damping application

Prior to test results, modal analysis results for test configuration of T2 vibration isolation system are presented in Figure 6-64 to Figure 6-68 for understanding the dynamic behavior of VIS. Note that internal resonances of dummy payload for T2 test configuration is very close to the ones in T1 test configuration, which are shown in Figure 6-43 and Figure 6-44.

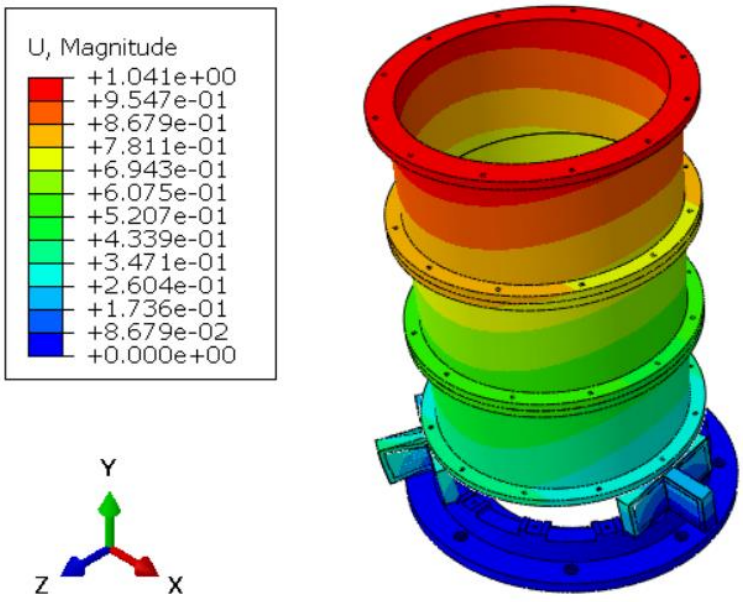

Figure 6-64 Rocking mode shape of T2 test configuration, 23 Hz

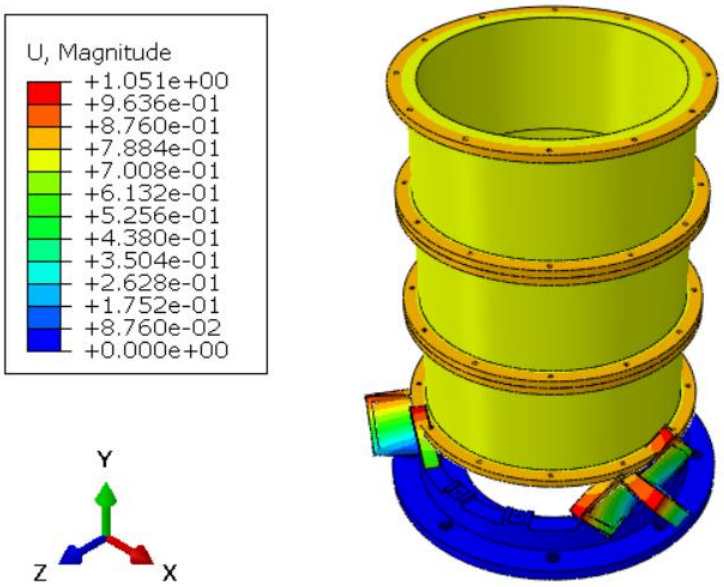

Figure 6-65 Torsional mode shape of T2 test configuration, 48 Hz

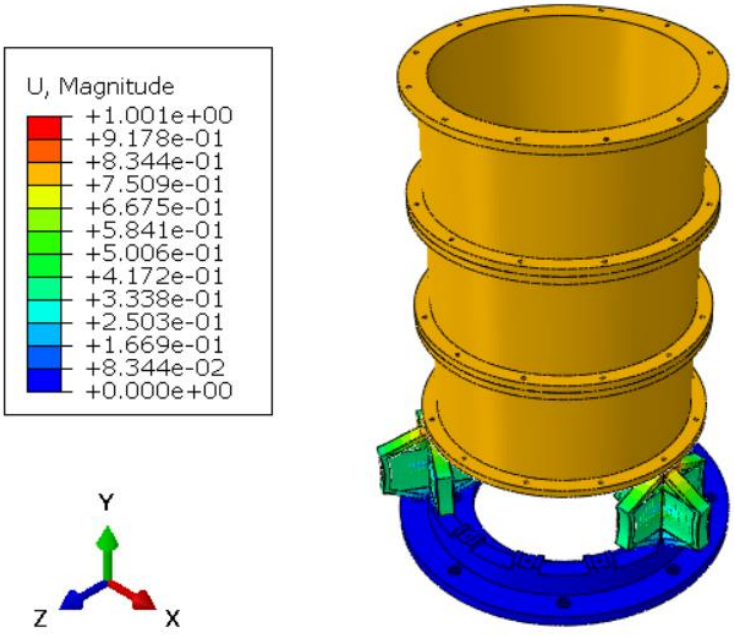

Figure 6-66 Axial mode shape of T2 test configuration, 68 Hz

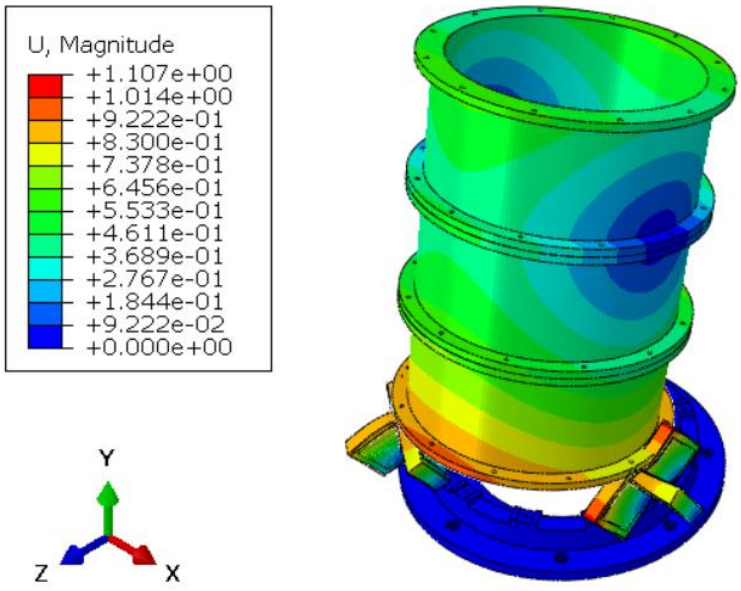

Figure 6-67 Lateral mode shape of T2 test configuration, 84 Hz

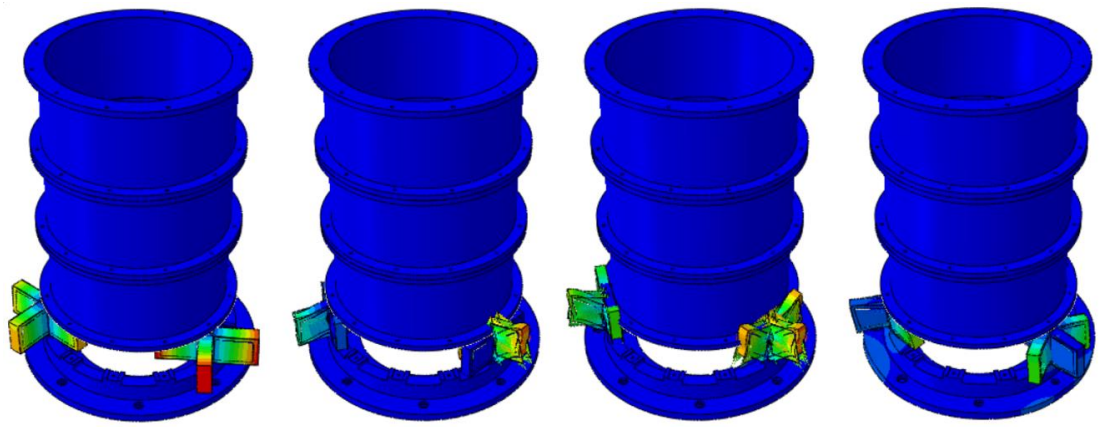

Figure 6-68 Internal resonances of vibration isolators for T2 test configuration;
926 Hz, 1384 Hz, 1426 Hz, 1923 Hz from left to right

The transmissibility curves, which are obtained from sine sweep and random vibration tests, for upper and lower points are presented in from Figure 6-69 to Figure 6-71 for axial and lateral directions.

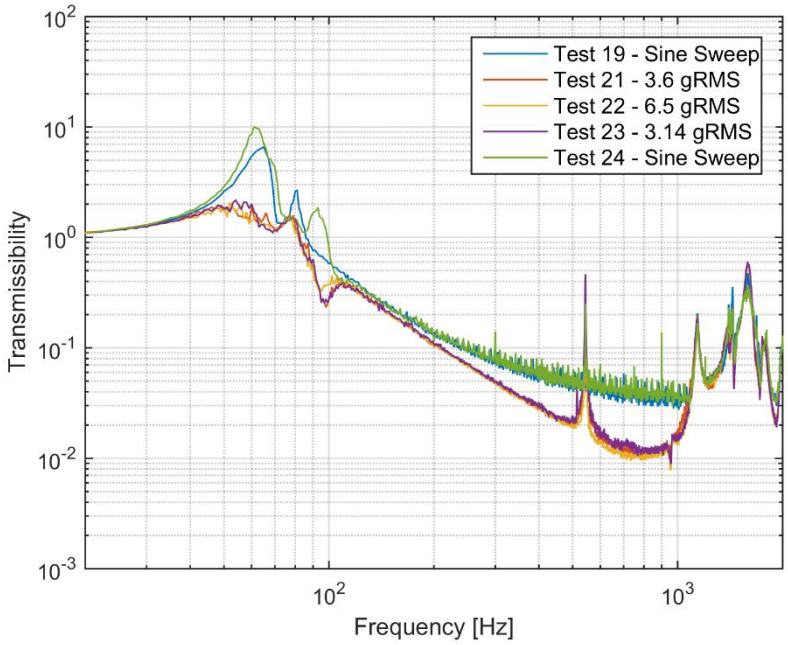

Figure 6-69 T2 - The axial transmissibility curves obtained from vibration tests for upper point

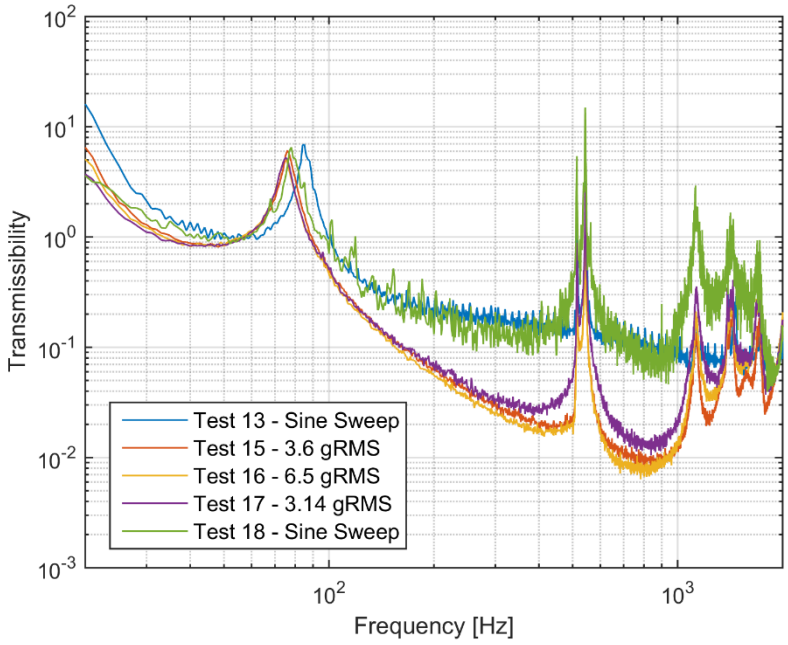

Figure 6-70 T2 - The lateral transmissibility curves obtained from vibration tests for upper point

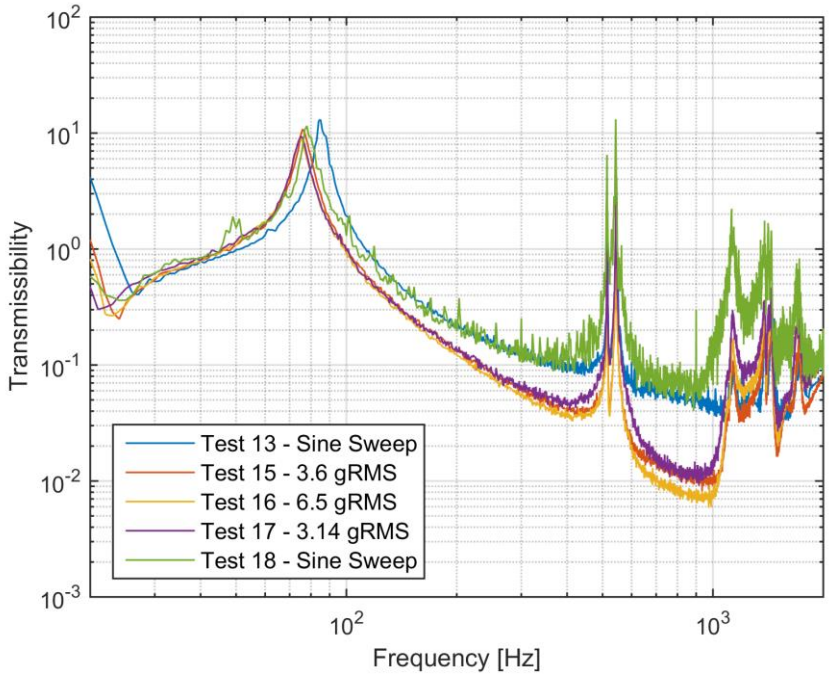

Figure 6-71 T2 - The lateral transmissibility curves obtained from vibration tests for lower point

The comparison of transmissibility curves, which are obtained from sine sweep tests and finite element analyses, for upper and lower points are given in Figure 6-72 to Figure 6-74 for axial and lateral directions.

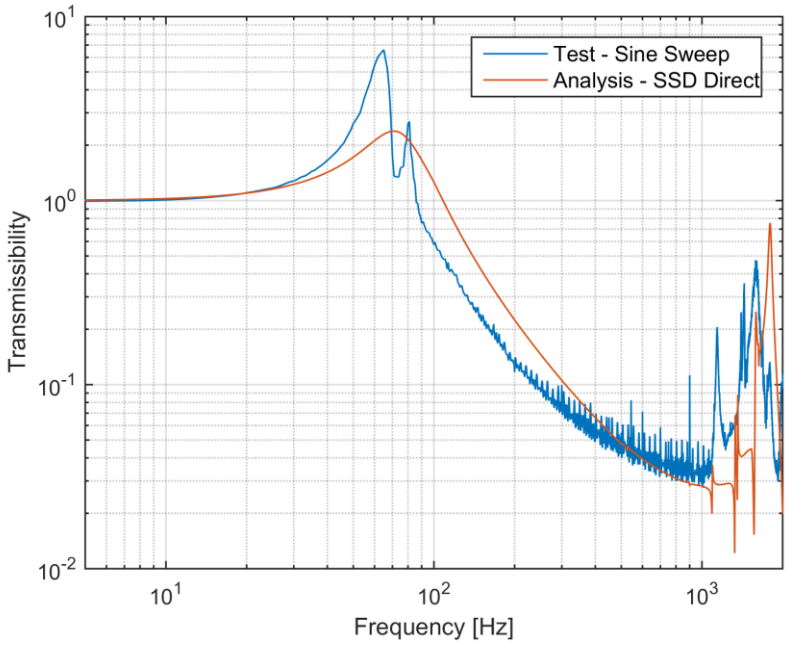

Figure 6-72 T2 – The comparison of axial transmissibility curves obtained from sine sweep test and finite element analysis for upper point

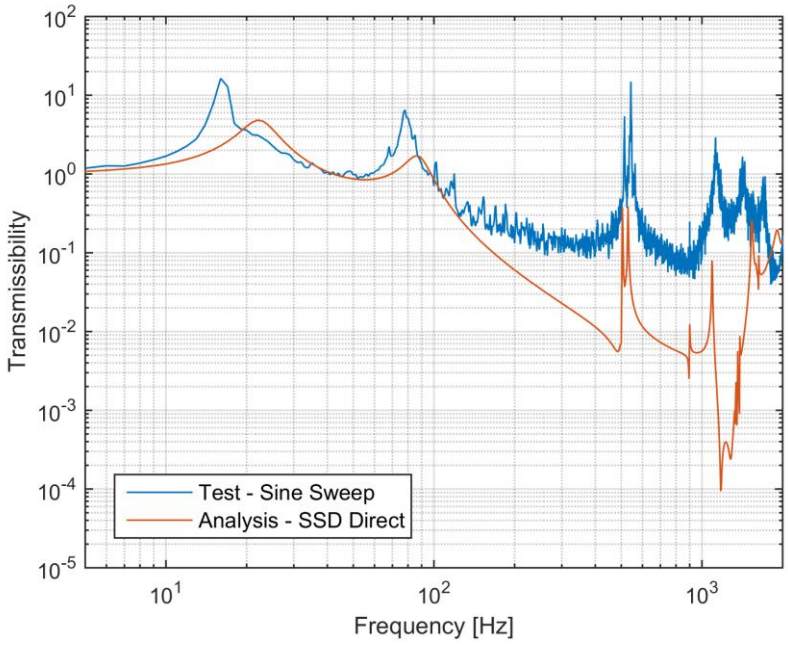

Figure 6-73 T2 – The comparison of lateral transmissibility curves obtained from sine sweep test and finite element analysis for upper point

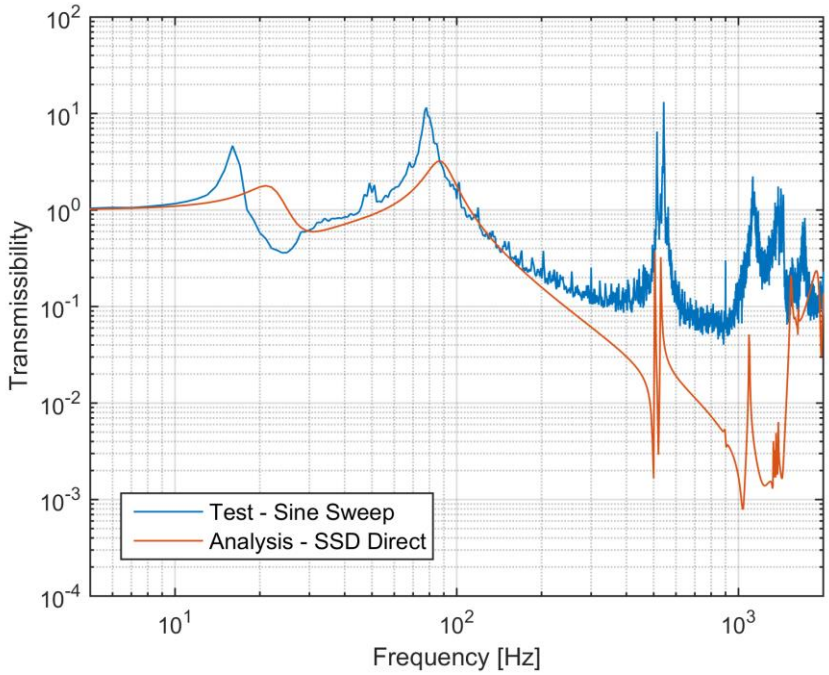

Figure 6-74 T2 – The comparison of lateral transmissibility curves obtained from sine sweep test and finite element analysis for lower point

The acceleration data in time domain, the PSD accelerations and the comparison of test and random vibration analysis results are presented in Figure 6-75 to Figure 6-78 for Test-22, in which 6.5 gRMS random vibration input is applied in axial direction.

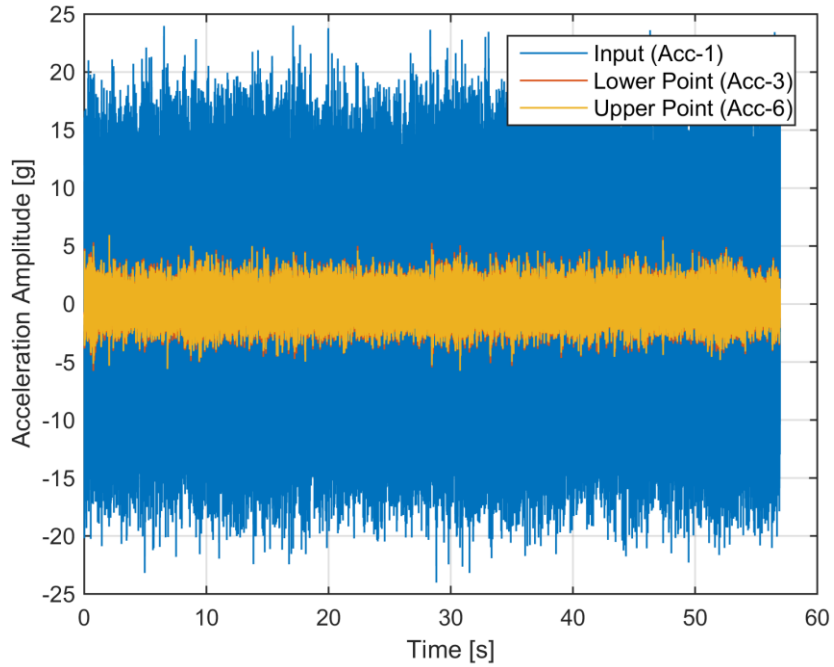

Figure 6-75 T2 – Test 22 - The acceleration data in time domain

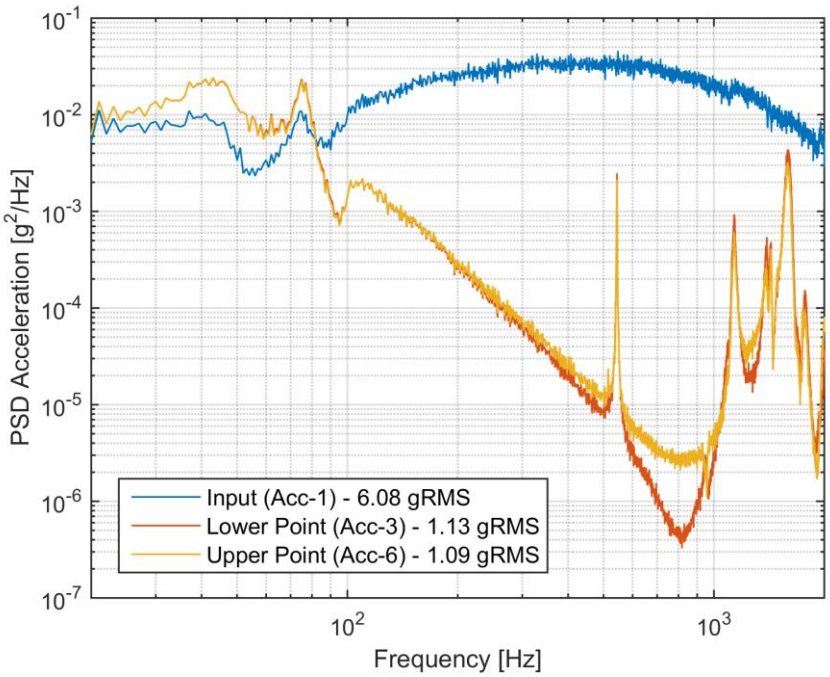

Figure 6-76 T2 – Test 22 - The PSD accelerations in frequency domain

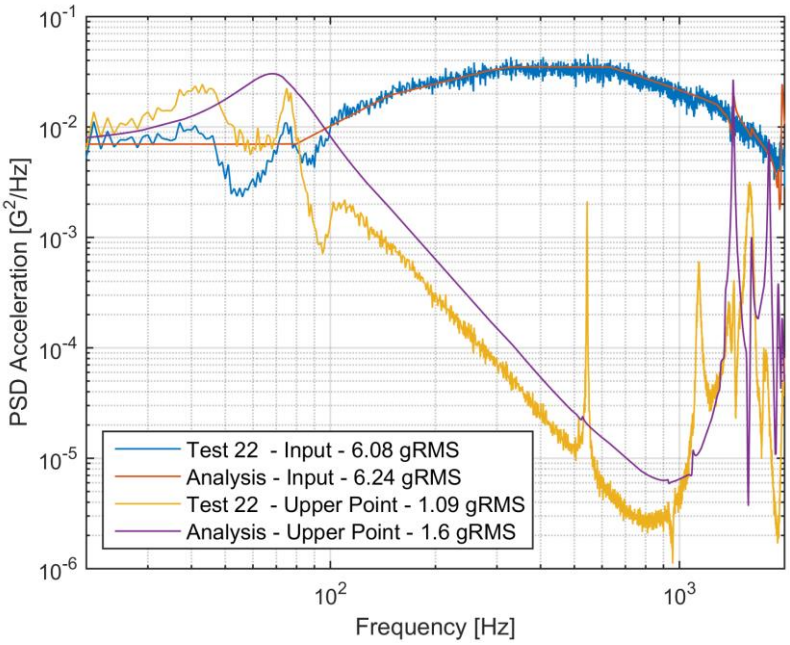

Figure 6-77 T2 – The comparison of Test 22 and random vibration analysis results for upper point

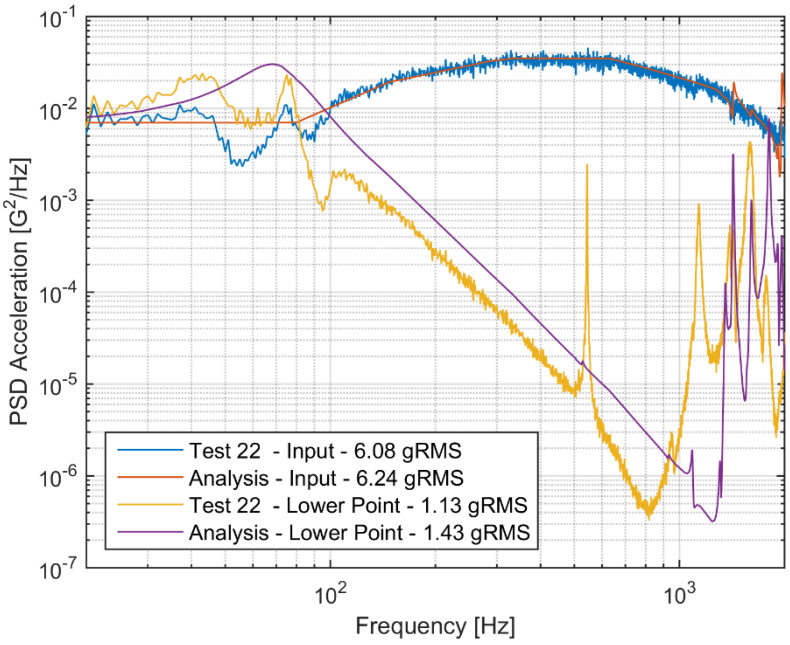

Figure 6-78 T2 – The comparison of Test 22 and random vibration analysis results for lower point

Figure 6-75 indicates that the reduction in acceleration level in axial direction is achieved using T2 vibration isolation system. It can be seen from Figure 6-76 that R-1 is satisfied. Moreover, there is a good consistency between finite element analyses and test results as seen in Figure 6-77 and Figure 6-78.

The acceleration data in time domain, the PSD accelerations and the comparison of test and random vibration analysis results are presented in Figure 6-79 to Figure 6-82 for Test-16, in which 6.5 gRMS random vibration input is applied in lateral direction.

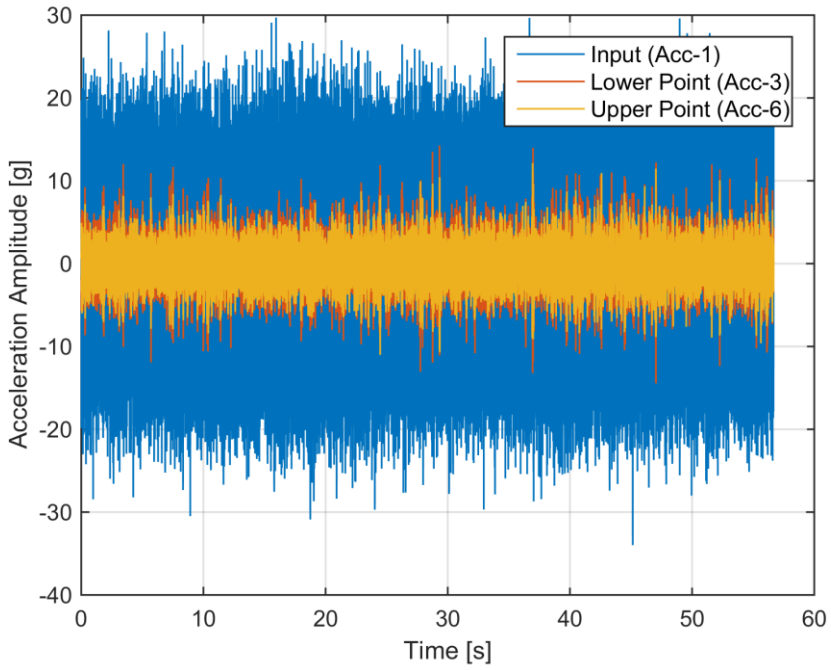

Figure 6-79 T2 – Test 16 - The acceleration data in time domain

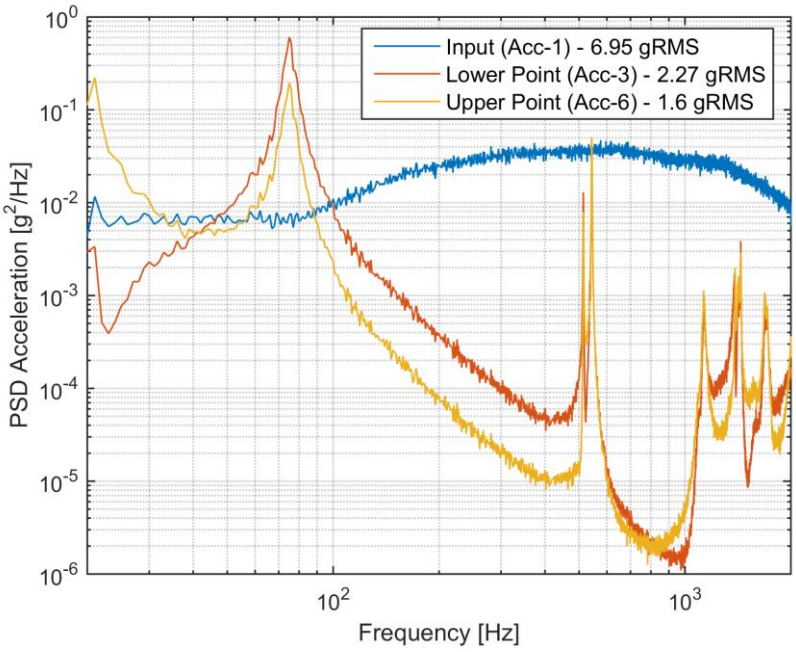

Figure 6-80 T2 – Test 16 - The PSD accelerations in frequency domain

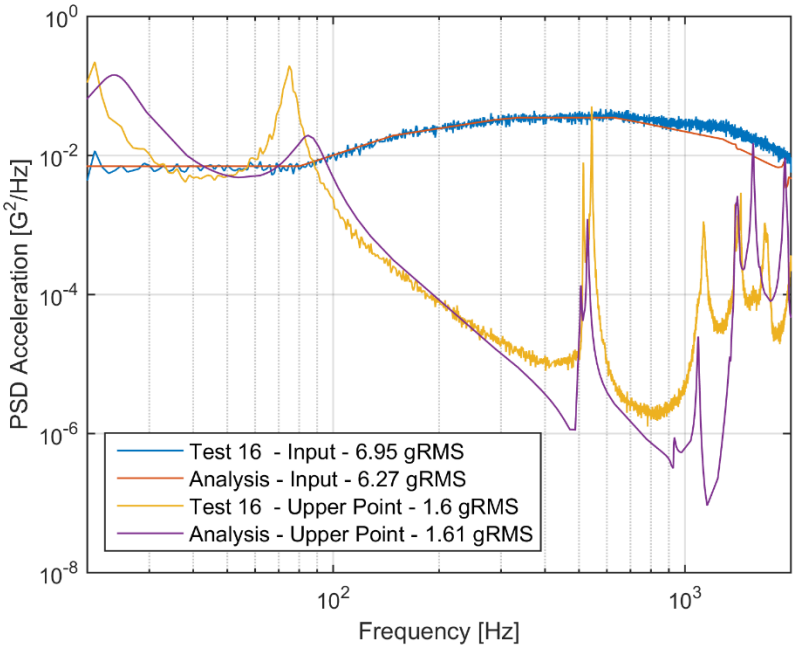

Figure 6-81 T2 – The comparison of Test 16 and random vibration analysis results for upper point

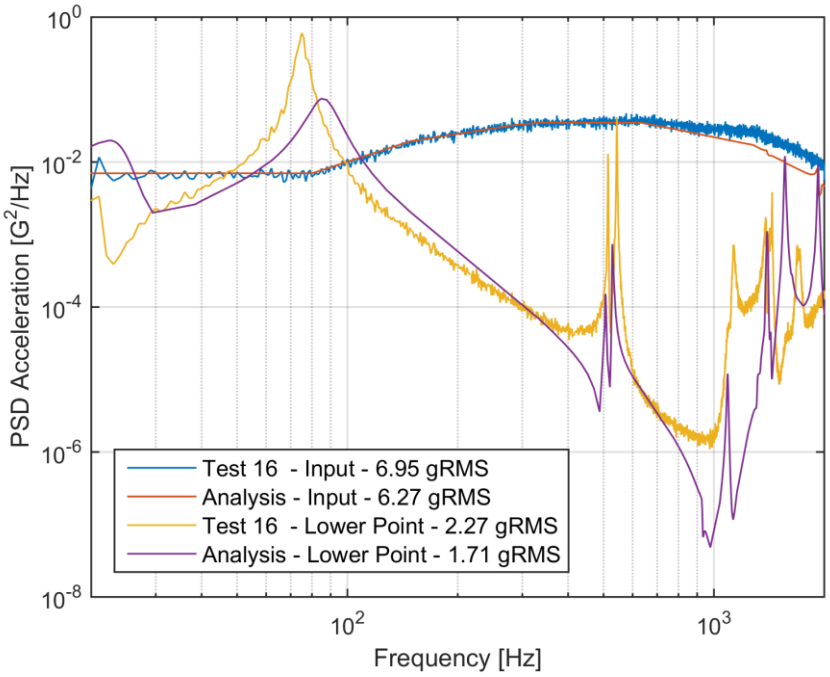

Figure 6-82 T2 – The comparison of Test 16 and random vibration analysis results for lower point

Figure 6-79 indicates that the reduction in acceleration level in lateral direction is achieved using T2 vibration isolation system. Note that the R-2 cannot be verified with results in Figure 6-80 because gRMS level of lower point is higher than 2 gRMS. This is caused by usage of smaller payload for T2 vibration isolation system. Since there is a good consistency between finite element analyses and test results as seen in Figure 6-81 and Figure 6-82, verification of R-2 by analysis, which is stated in 6.2.2, is sufficient.

The displacement amplitudes of lower and upper points are given in Figure 6-83 and Figure 6-84 for Test-20 and Test-14, which are harmonic vibration tests in axial and lateral directions, respectively.

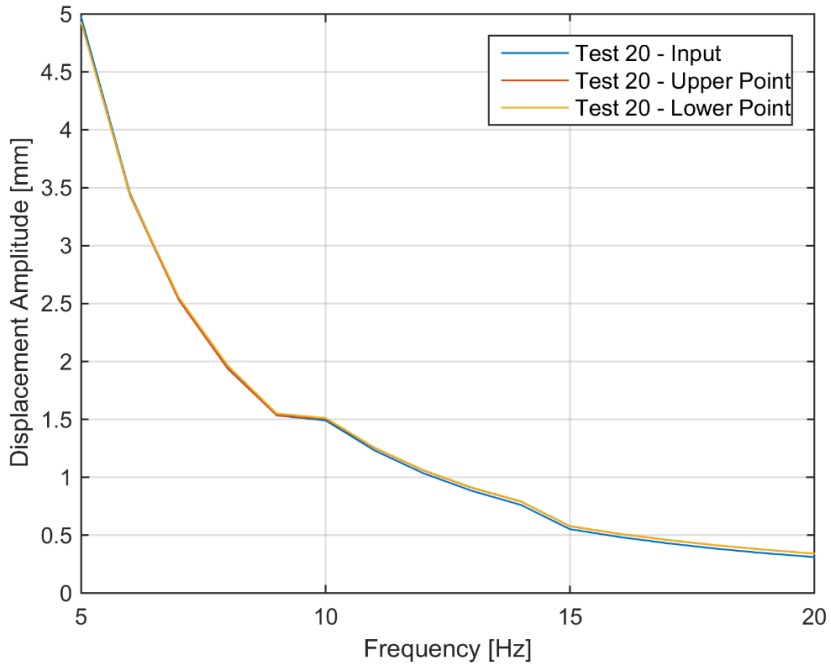

Figure 6-83 T2 - Test 20 – Harmonic displacement results in axial direction

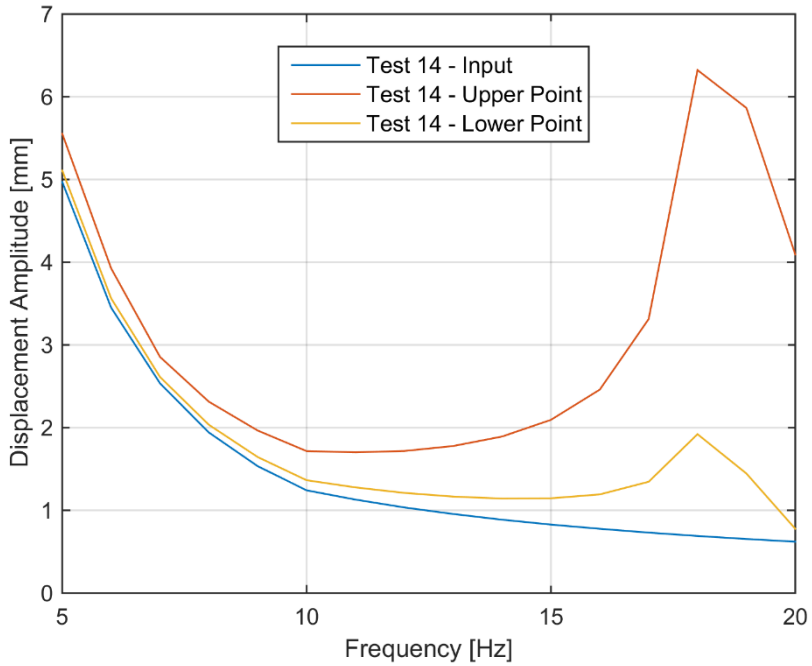

Figure 6-84 T2 - Test 14 – Harmonic displacement results in lateral direction

Figure 6-83 and Figure 6-84 indicate that R-3 and R-4 are met. Harmonic vibration input in axial direction is transmitted directly to the payload as seen in Figure 6-83. On the other hand, there is an amplification, especially for upper point, in lateral direction as seen in Figure 6-84 due to rocking mode of VIS, which is illustrated in Figure 6-64.

6.3.3. Verification of S1 by Test

S1 test prototypes, which are manufactured for vibration tests, are shown in Figure 6-85.

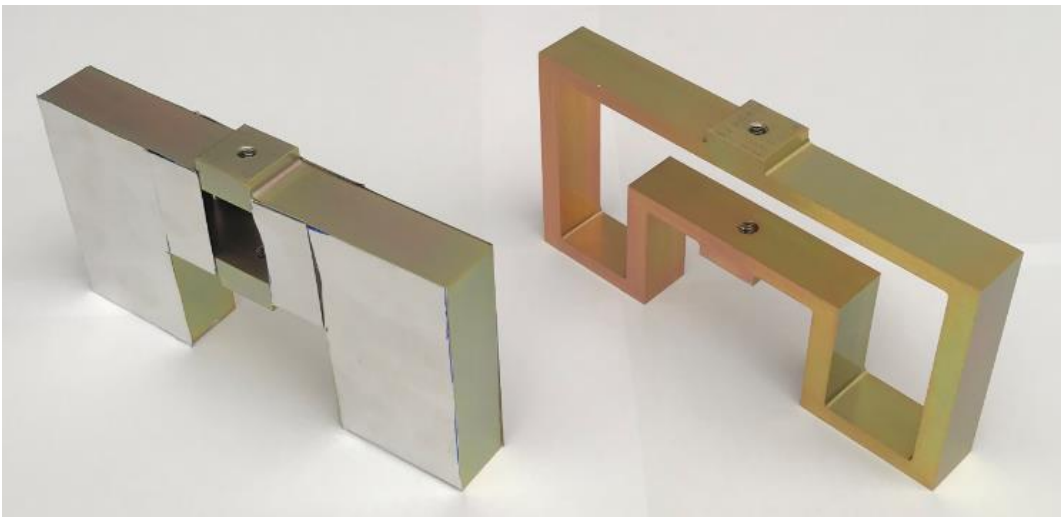

Figure 6-85 S1 test prototypes, with and without damping application

Prior to test results, modal analysis results for test configuration of S1 vibration isolation system are presented in Figure 6-86 to Figure 6-90 for understanding the dynamic behavior of VIS. Note that internal resonances of dummy payload for S1 test configuration are very close to the ones in T1 test configuration, which are shown in Figure 6-43 and Figure 6-44.

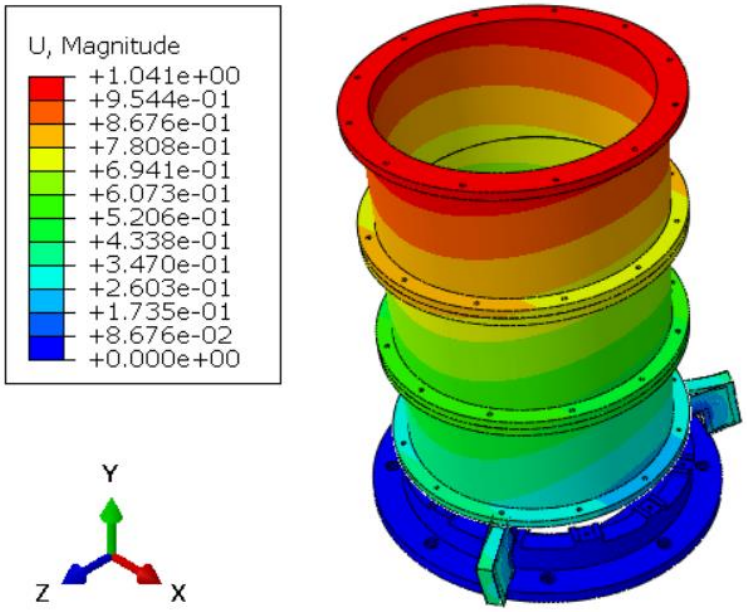

Figure 6-86 Rocking mode shape of S1 test configuration, 16 Hz

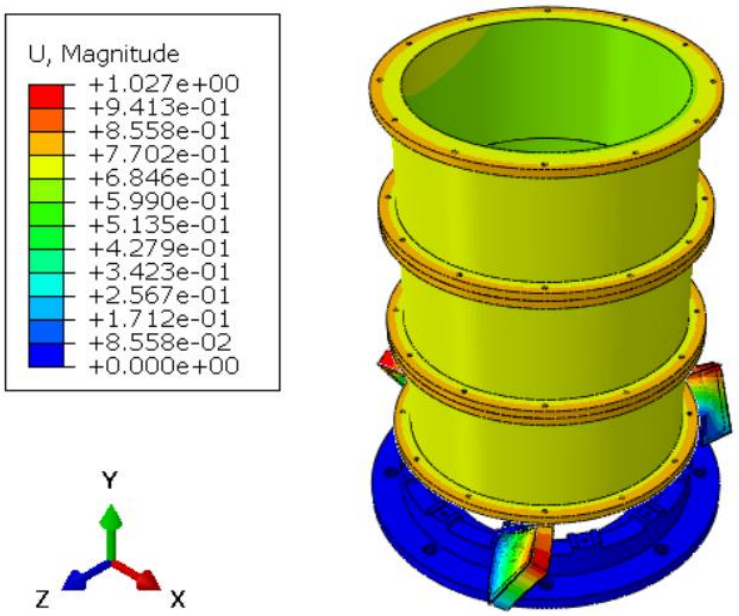

Figure 6-87 Torsional mode shape of S1 test configuration, 30 Hz

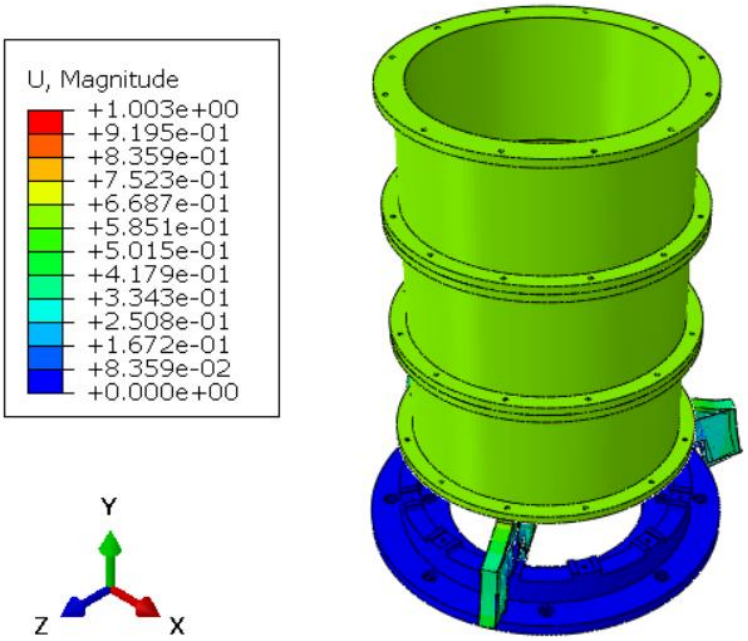

Figure 6-88 Axial mode shape of S1 test configuration, 46 Hz

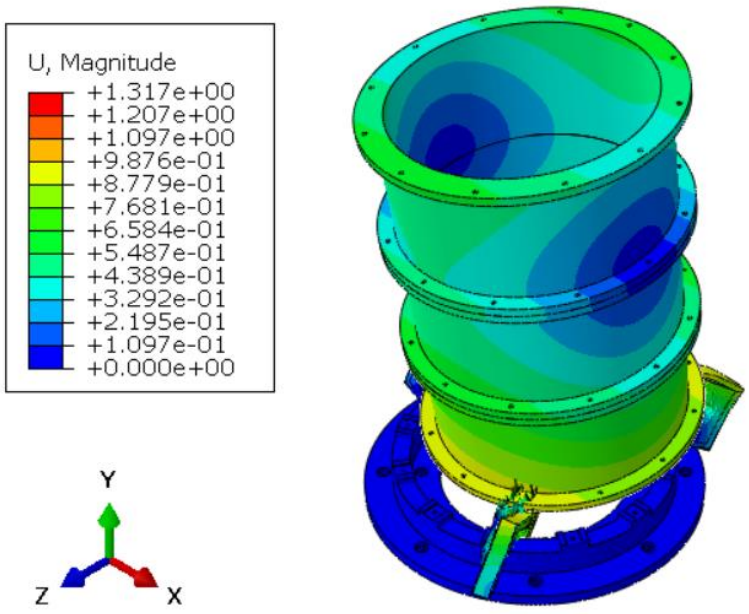

Figure 6-89 Lateral mode shape of S1 test configuration, 60 Hz

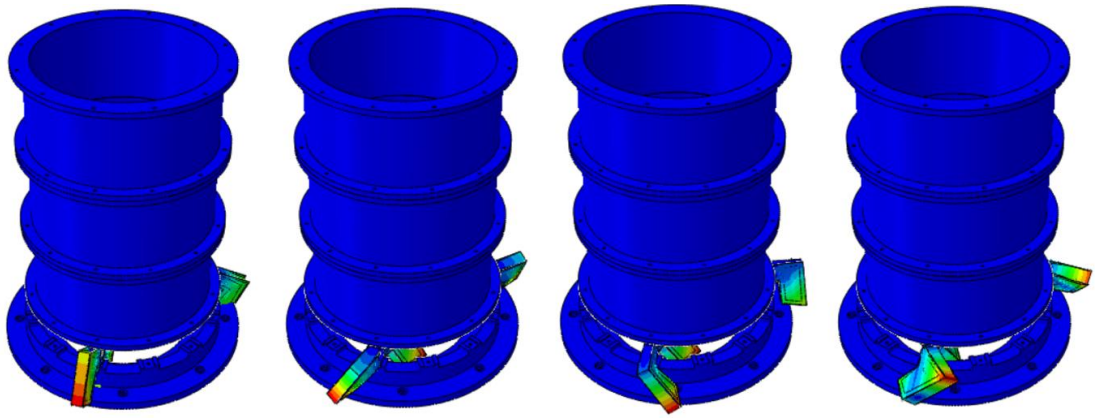

Figure 6-90 Internal resonances of vibration isolators for S1 test configuration; 603 Hz, 692 Hz, 808 Hz, 1368 Hz from left to right

The transmissibility curves, which are obtained from sine sweep and random vibration tests, for upper and lower points are presented in from Figure 6-91 to Figure 6-93 for axial and lateral directions.

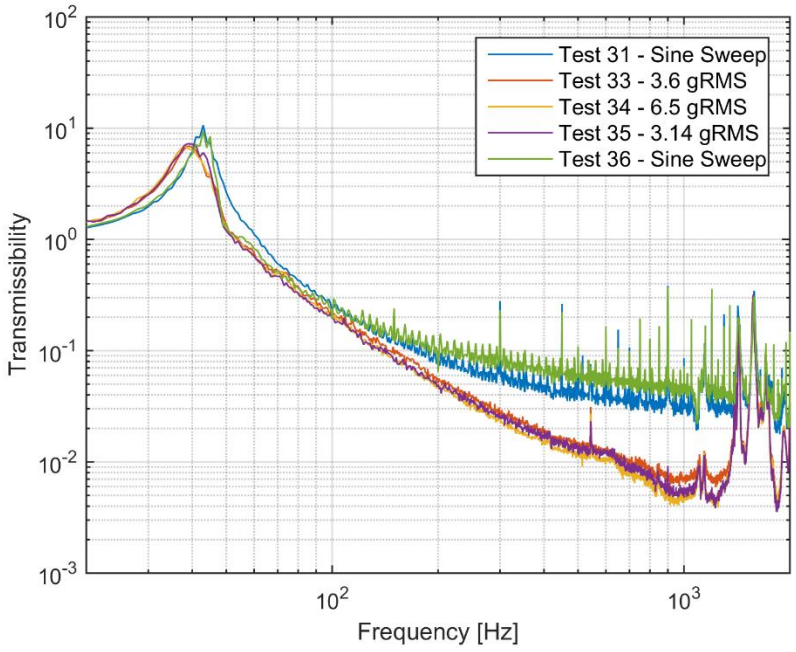

Figure 6-91 S1 - The axial transmissibility curves obtained from vibration tests for upper point

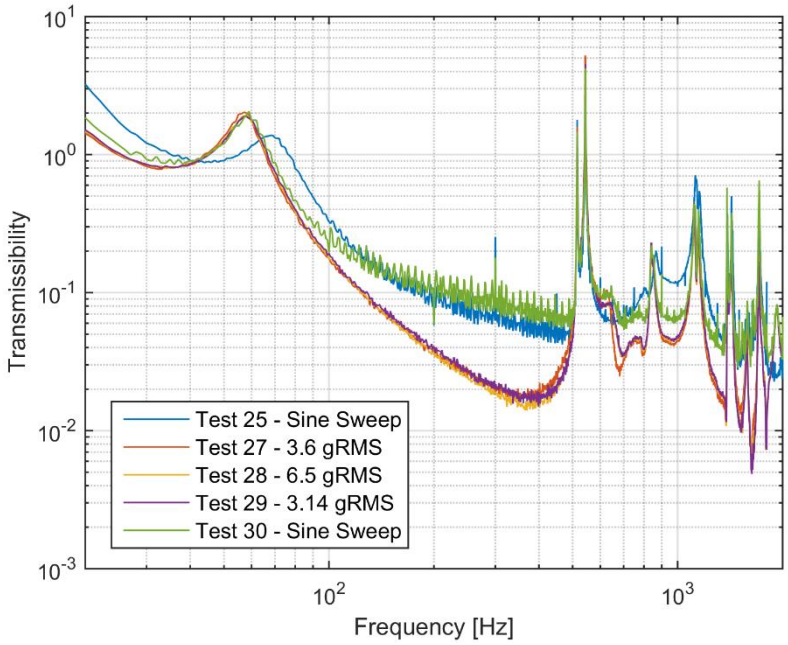

Figure 6-92 S1 - The lateral transmissibility curves obtained from vibration tests for upper point

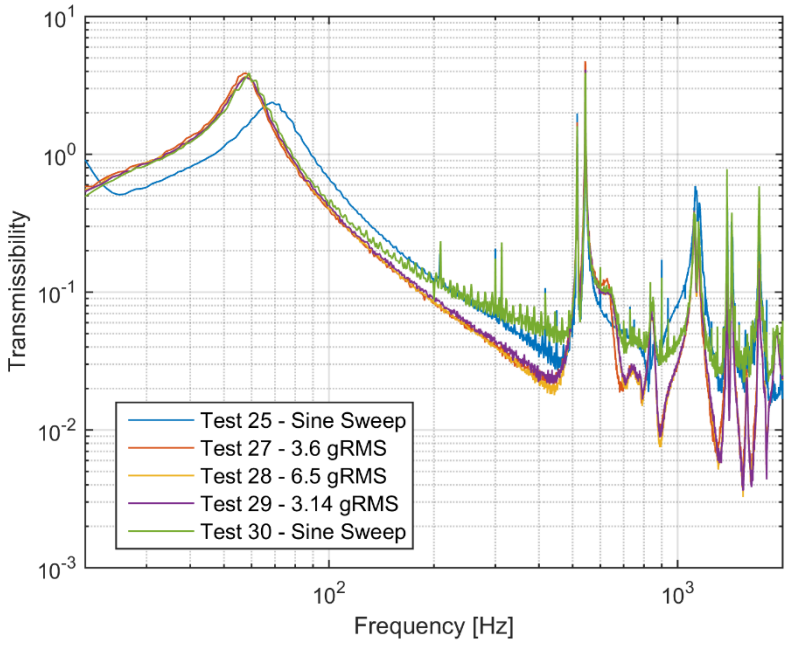

Figure 6-93 S1 - The lateral transmissibility curves obtained from vibration tests for lower point

The comparison of transmissibility curves, which are obtained from sine sweep tests and finite element analyses, for upper and lower points are given in Figure 6-94 to Figure 6-96 for axial and lateral directions.

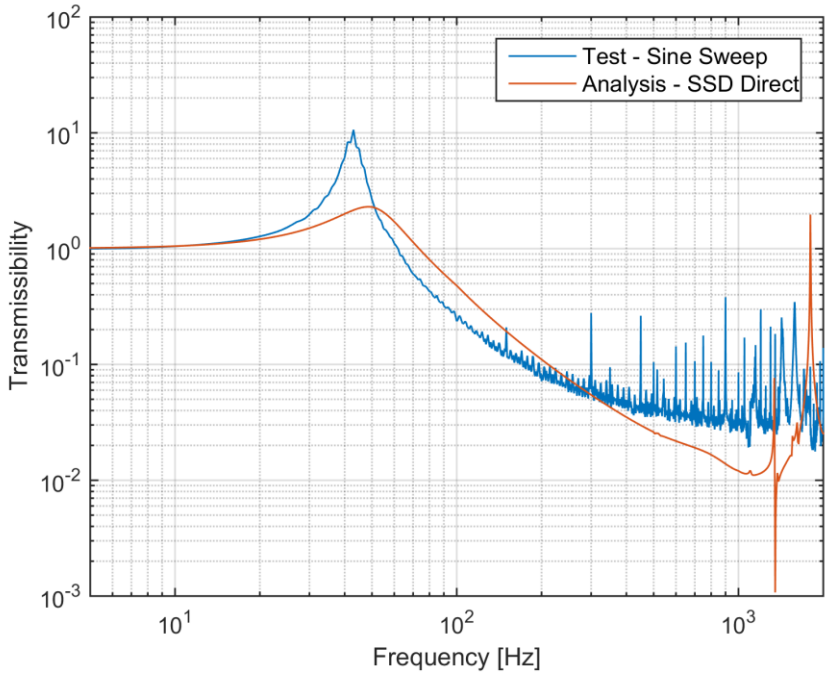

Figure 6-94 S1 – The comparison of axial transmissibility curves obtained from sine sweep test and finite element analysis for upper point

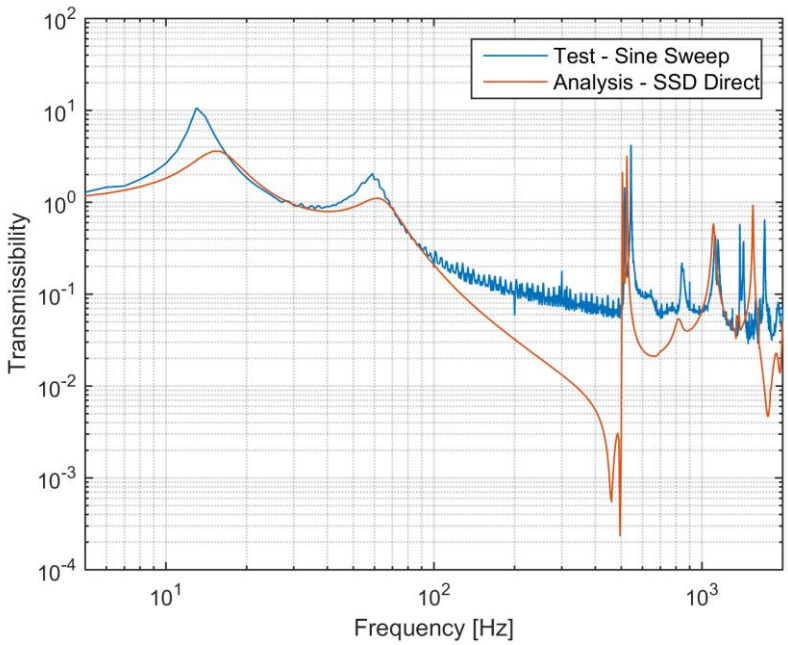

Figure 6-95 S1 – The comparison of lateral transmissibility curves obtained from sine sweep test and finite element analysis for upper point

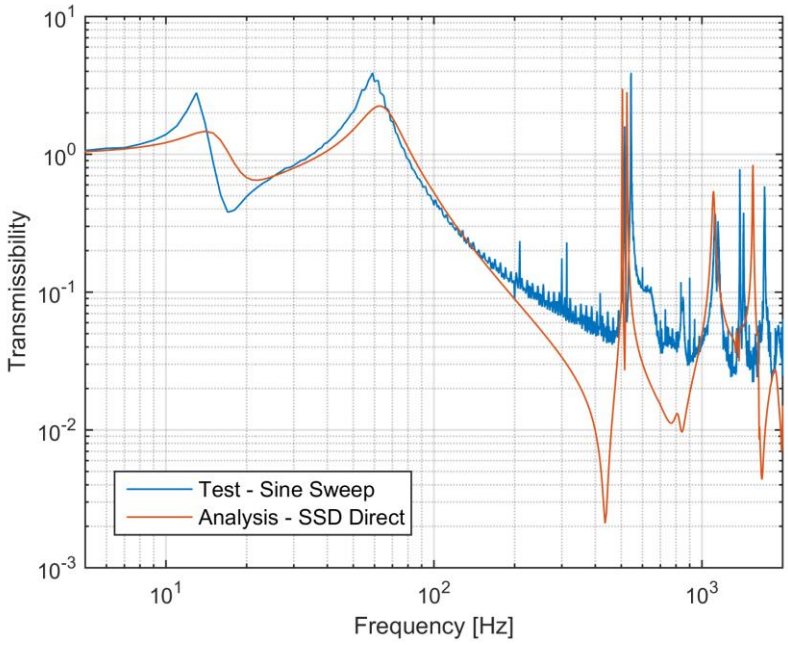

Figure 6-96 S1 – The comparison of lateral transmissibility curves obtained from sine sweep test and finite element analysis for lower point

The acceleration data in time domain, the PSD accelerations and the comparison of test and random vibration analysis results are presented in Figure 6-97 to Figure 6-100 for Test-34, in which 6.5 gRMS random vibration input is applied in axial direction.

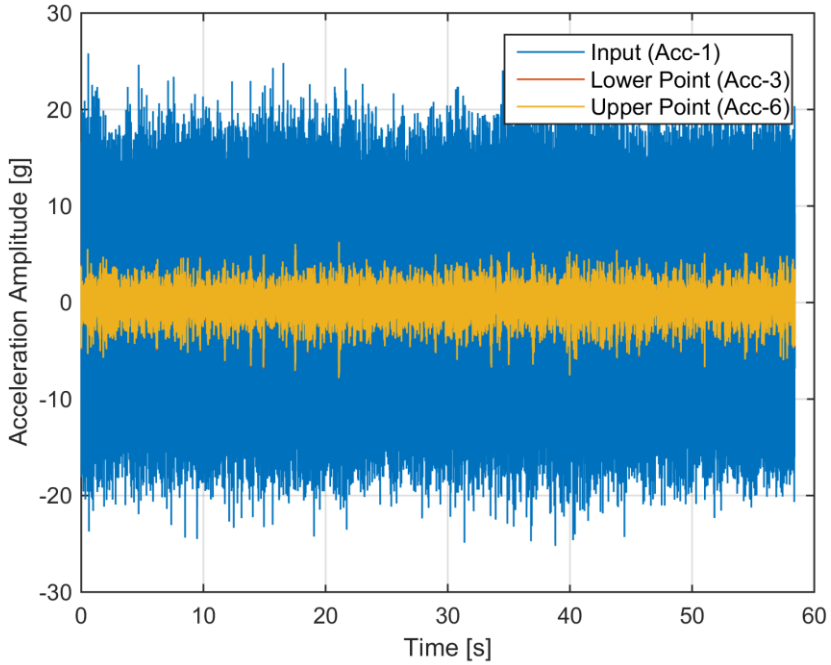

Figure 6-97 S1 – Test 34 - The acceleration data in time domain

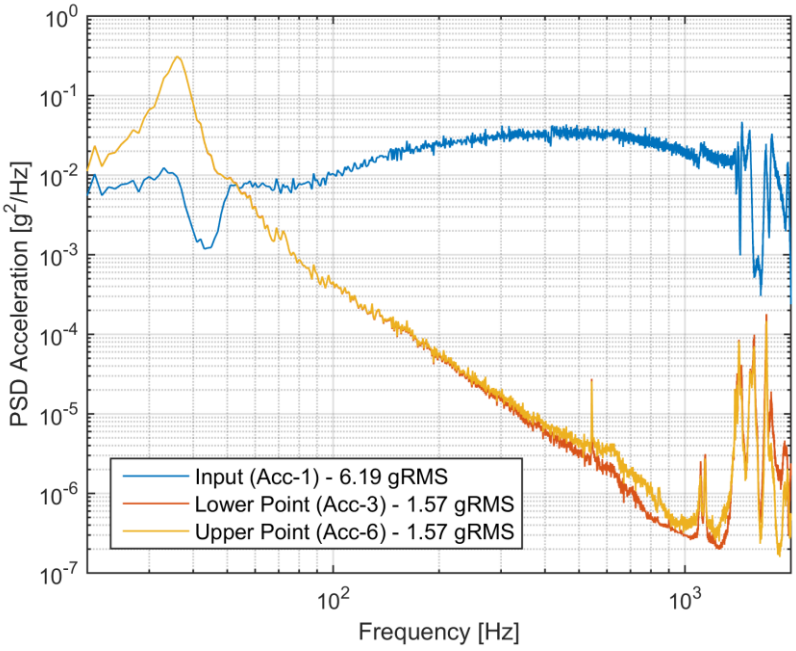

Figure 6-98 S1 – Test 34 - The PSD accelerations in frequency domain

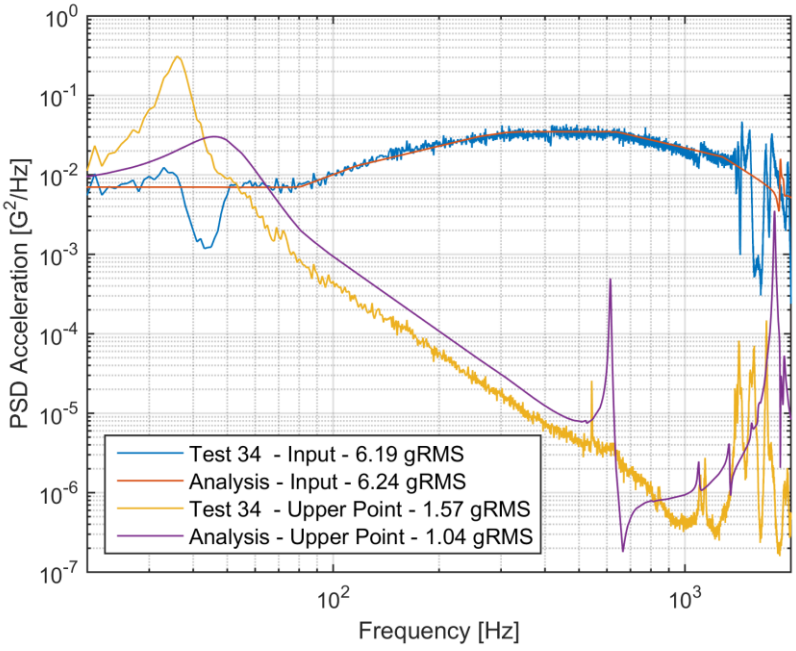

Figure 6-99 S1 – The comparison of Test 34 and random vibration analysis results for upper point

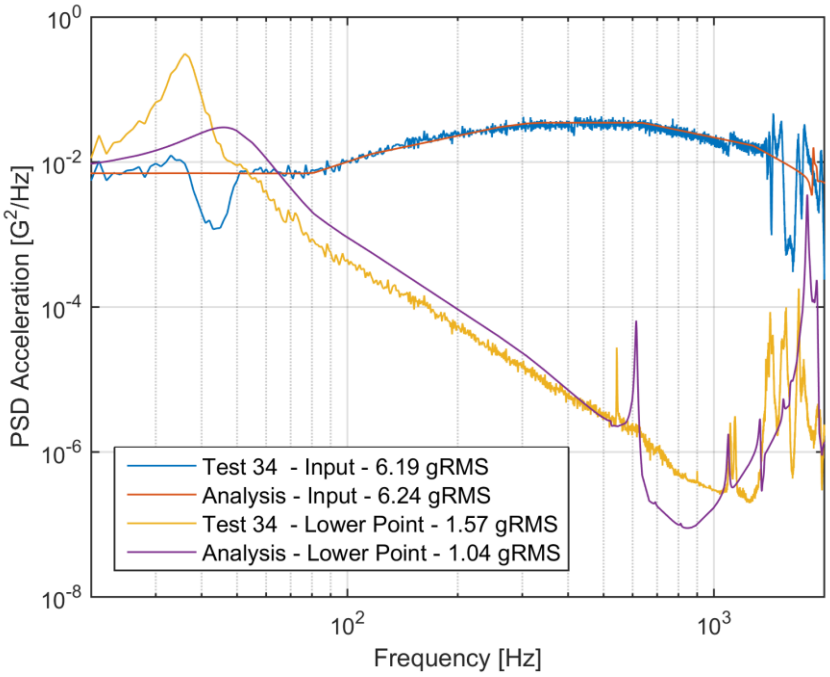

Figure 6-100 S1 – The comparison of Test 34 and random vibration analysis results for lower point

Figure 6-97 indicates that the reduction in acceleration level in axial direction is achieved using S1 vibration isolation system. It can be seen from Figure 6-98 that R-1 is satisfied. Moreover, there is a good consistency between finite element analyses and test results as seen in Figure 6-99 and Figure 6-100.

The acceleration data in time domain, the PSD accelerations and the comparison of test and random vibration analysis results are presented in Figure 6-101 to Figure 6-104 for Test-28, in which 6.5 gRMS random vibration input is applied in lateral direction.

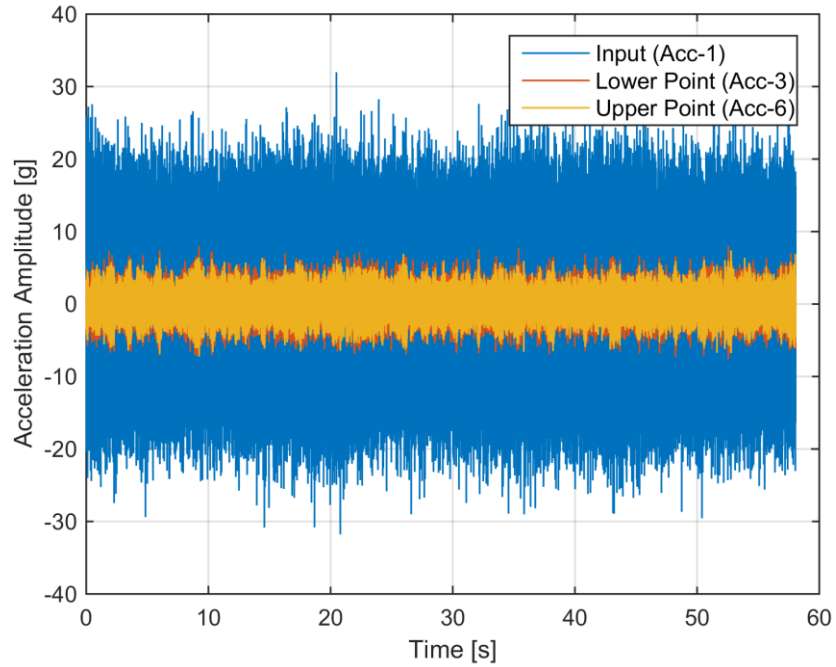

Figure 6-101 S1 – Test 28 - The acceleration data in time domain

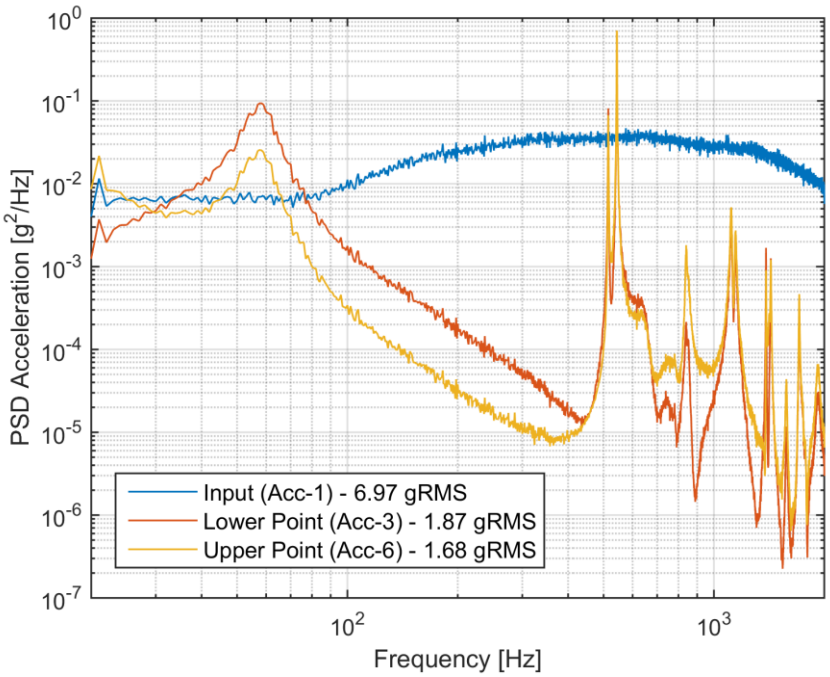

Figure 6-102 S1 – Test 28 - The PSD accelerations in frequency domain

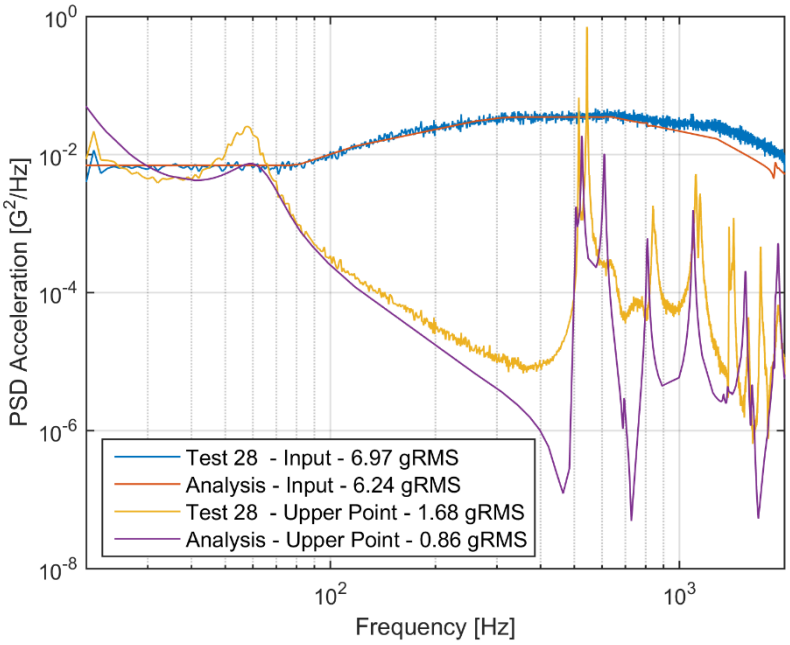

Figure 6-103 S1 – The comparison of Test 28 and random vibration analysis results for upper point

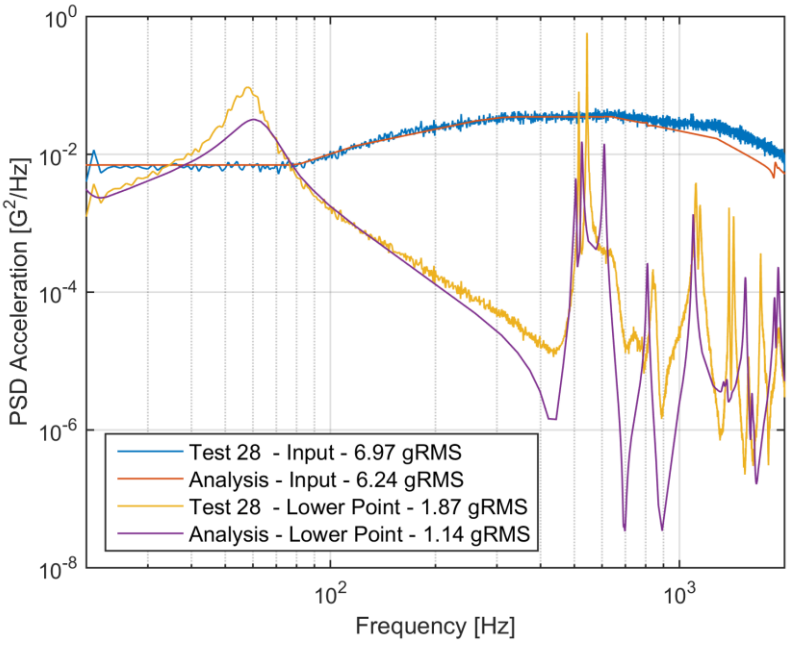

Figure 6-104 S1 – The comparison of Test 28 and random vibration analysis results for lower point

Figure 6-101 indicates that the reduction in acceleration level in lateral direction is achieved using S1 vibration isolation system. It can be seen from Figure 6-102 that R-2 is satisfied. Moreover, there is a good consistency between finite element analyses and test results as seen in Figure 6-103 and Figure 6-104.

The displacement amplitudes of lower and upper points are given in Figure 6-105 and Figure 6-106 for Test-32 and Test-26, which are harmonic vibration tests in axial and lateral directions, respectively.

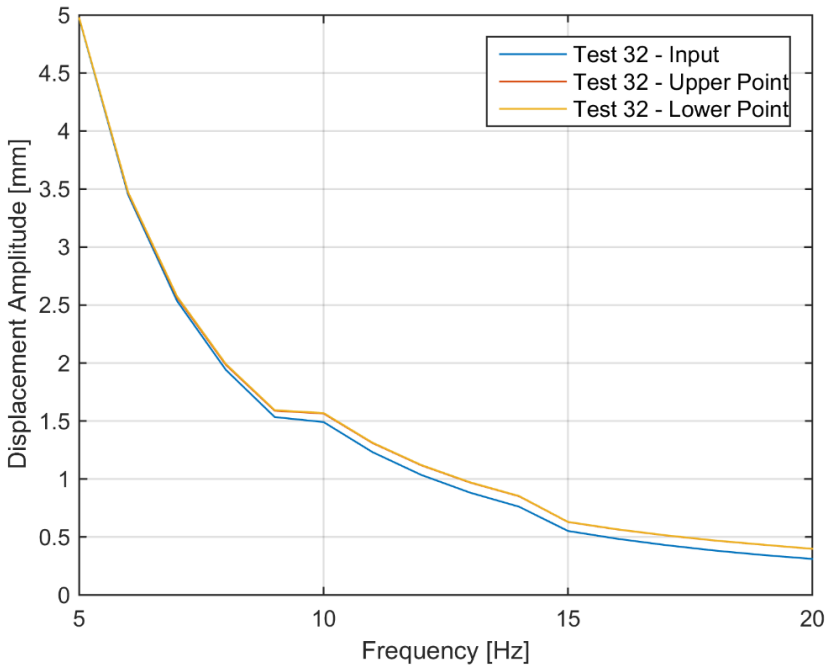

Figure 6-105 S1 - Test 32 – Harmonic displacement results in axial direction

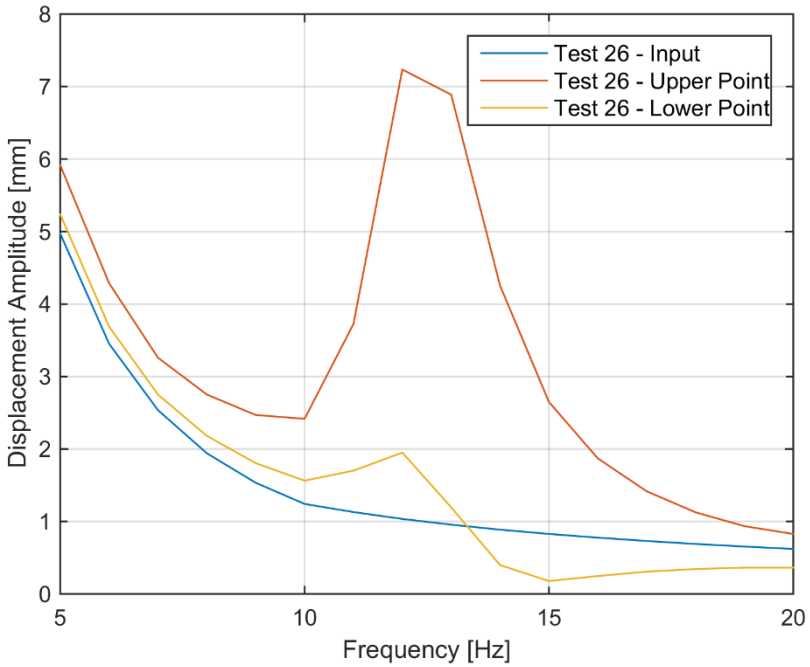

Figure 6-106 S1 - Test 26 – Harmonic displacement results in lateral direction

Figure 6-105 and Figure 6-106 indicate that R-3 and R-4 are met. Harmonic vibration input in axial direction is transmitted directly to the payload as seen in Figure 6-105. On the other hand, there is an amplification, especially for upper point, in lateral direction as seen in Figure 6-106 due to rocking mode of VIS, which is illustrated in Figure 6-86.

CHAPTER 7

CONCLUSIONS AND FUTURE WORK

In this thesis study, novel vibration isolation systems for payload-launch vehicle interface are developed. Dnepr launch vehicle and Sentinel-2 satellite are chosen as a case study for determination of system-level technical requirements of vibration isolation system. It is aimed that VIS can be adaptable to different launch vehicles and payloads. Vibration isolator properties such as stiffness and loss factor are derived from system-level requirements. Then, design of vibration isolation system is performed by following three different methods and 6 different design concepts are created. Among these design concepts, detailed design of 3 vibration isolators are performed. It is shown that mathematical model and finite element model which are constructed in this study are in good consistency with test results. Moreover, vibration tests verify that designed vibration isolation systems satisfy all technical requirements and Technology Readiness Level (TRL)-4 is achieved for this technology.

As a future work, to improve the finite element model of vibration isolation system, the viscoelastic material characterization test can be performed to obtain material properties with respect to strain amplitude. Furthermore, thermocouples can be placed on viscoelastic material during vibration tests in order to measure the exact temperature and update the finite element model with correct material properties since viscoelastic material properties show strong dependency on temperature. On the other hand, launch vehicle is considered as rigid body and dynamics of payload are not taken into consideration in this study. Modelling of payload and launch vehicle as flexible structures, determining technical requirements accordingly and performing coupled load analyses can be planned as a future study. In addition, high-cycle fatigue characteristics of vibration isolators may be investigated for missions with relatively long duration.

REFERENCES

[1] H. Himelblau, J. E. Manning, A. G. Piersol, and S. Rubin, *NASA Technical Handbook - Dynamic Environmental Criteria*. 2001.

[2] "Antares OSP-3 User's Guide," 2013.

[3] "Ariane 5 User's Manual," 2011.

[4] "Minotaur I User's Guide 2.1," 2006.

[5] "Pegasus User's Guide 7.0," 2010.

[6] "Dnepr User's Guide, Issue 2," 2001.

[7] G. T. Zheng, "Parametric Studies of the Whole Spacecraft Vibration Isolation," *AIAA J.*, vol. 41, no. 9, pp. 1839–1841, 2003.

[8] M. F. Winthrop and R. G. Cobb, "Survey of State-of-the-Art Vibration Isolation Research and Technology for Space Applications," in *Smart Structures and Materials 2003: Damping and Isolation*, 2003, vol. 5052, pp. 13–26.

[9] X. Miao and G. Zheng, "Analytical Study of Whole Flexible Spacecraft Vibration Isolation," in *49th AIAA/ASME/ASCE/AHS/ASC Structures, Structural Dynamics, and Materials Conference*, 2008.

[10] Z. Jun, H. Hongxing, and Z. Zhiyi, "An evaluation of the whole-spacecraft passive vibration isolation system," *J. Aerosp. Eng.*, vol. 221, no. 1, pp. 67–72, 2007.

[11] L. K. Liu and G. T. Zheng, "Parameter analysis of PAF for whole-spacecraft vibration isolation," *Aerosp. Sci. Technol.*, vol. 11, no. 6, pp. 464–472, 2007.

[12] G. R. Thomas, C. M. Fadick, and B. J. Fram, "Launch Vehicle Payload Adapter Design with Vibration Isolation Features," in *12th Annual SPIE International Symposium on Smart Structures and Materials*, 2005.

[13] Y. Zhang, B. Fang, Y. Ding, and L. Wang, "Dynamic Parameter Schematic Analysis of the Whole-Rocket Vibration Isolation System," *J. Appl. Sci.*, vol. 13, no. 8, pp. 1318–1324, 2013.

[14] L. K. Liu, L. Liang, G. T. Zheng, and W. H. Huang, "Dynamic Design of Octostrut Platform for Launch Stage Whole-Spacecraft Vibration Isolation," *J. Spacecr. Rockets*, vol. 42, no. 4, 2005.

[15] Y. W. Zhang, B. Fang, and J. Zang, "Dynamic features of passive whole-spacecraft vibration isolation platform based on non-probabilistic reliability," *JVC/Journal Vib. Control*, vol. 21, no. 1, pp. 60–67, 2015.

[16] D. L. Edberg, B. Bartos, J. Goodding, P. Wilke, and T. Davis, “Passive and active launch vibration studies in the LVIS program,” in *5TH ANNUAL INTERNATIONAL SYMPOSIUM ON SMART STRUCTURES AND MATERIALS*, 1998, vol. 3327, pp. 411–422.

[17] B. Fang, S. Li, and W. Huang, “Performance analysis for a new whole-spacecraft isolation using viscoelastic damping material,” in *Active and Passive Smart Structures and Integrated Systems*, 2011, vol. 7977.

[18] Y. Zhang, B. Fang, Y. Chen, and L. Wang, “Performance Analysis of Discrete Whole-Spacecraft Vibration Isolation Platforms for Flexible Spacecrafts,” in *Active and Passive Smart Structures and Integrated Systems*, 2010.

[19] X. Liu, W. Witarto, X. Nie, Z. Shi, and Y. L. Mo, “Periodic material-based vibration isolation for satellites,” *Int. J. Eng. Res. Appl.*, vol. 6, no. 1, pp. 83–90, 2016.

[20] C. Yang, F. Bo, Y. Tianzhi, and H. Wenhu, “Study of Whole-spacecraft Vibration Isolators Based on Reliability Method,” *Chinese J. Aeronaut.*, vol. 22, no. 2, pp. 153–159, 2009.

[21] F. Khorrami, J. Rastegar, and R. S. Erwin, “A Three Degrees-of-Freedom Adaptive-Passive Isolator for Launch Vehicle Payloads,” in *Smart Structures and Materials 2000: Industrial and Commercial Applications of Smart Structures Technologies*, 2000, vol. 3991, pp. 164–175.

[22] G. Lee-Glauser and G. Ahmadi, “Vibration isolation of launch vehicle payload and its subsystem,” *J. Aerosp. Eng.*, vol. 8, no. 1, pp. 1–8, 1995.

[23] D. L. Edberg and B. W. Wilson, “PASSIVE AXIAL VIBRATION ISOLATION SYSTEM FOR A SPACECRAFT LAUNCH VEHICLE,” 5,961,078, 1999.

[24] D. L. Edberg, J. D. Fukushima, and J. P. Grady, “PASSIVE LATERAL VIBRATION ISOLATION SYSTEM FOR A SPACECRAFT LAUNCH VEHICLE,” 6,012,680, 2000.

[25] P. S. Wilke and C. D. Johnson, “WHOLE-SPACECRAFT PASSIVE ISOLATION DEVICES,” US 6,199,801 B1, 2001.

[26] C. D. Johnson, P. S. Wilke, and S. C. Pendleton, “THREE-AXIS, SIX DEGREE-OF-FREEDOM, WHOLE-SPACECRAFT PASSIVE VIBRATION ISOLATION SYSTEM,” US 6,290,183 B1, 2001.

[27] P. S. Wilke and C. D. Johnson, “LOW-PROFILE, MULTI-AXIS, HIGHLY PASSIVELY DAMPED, VIBRATION ISOLATION MOUNT,” US 7,249,756 B1, 2007.

[28] R. S. Johal, P. S. Wilke, and C. D. Johnson, “Rapid Coupled Loads Analysis

and Spacecraft Load Reduction using SoftRide," in *23rd Annual AIAA/USU Conference on Small Satellites*, 2009, pp. 1–6.

[29] C. D. Johnson and P. S. Wilke, "PROTECTING SATELLITES FROM THE DYNAMICS OF THE LAUNCH ENVIRONMENT," in *AIAA*, pp. 1–10.

[30] W. Gibbs, J. Francis, R. Spicer, K. Schaeffer, and M. R. O'Connell, "Vibration Testing of the Orbiting Carbon Observatory (OCO) Spacecraft on a Passive Vibration Isolation System," in *50th AIAA/ASME/ASCE/AHS/ASC Structures, Structural Dynamics, and Materials Conference*, 2009.

[31] C. D. Johnson and P. S. Wilke, "Recent launches using the SoftRide whole-spacecraft vibration isolation system," in *AIAA Space 2001 Conference and Exposition*, 2001, pp. 1–10.

[32] "MOOG CSA Engineering Catalog." . Retrieved October 1, 2018, from https://www.csaengineering.com/content/dam/moog/literature/Space_Defense/spaceliterature/Vibration_Control/MoogCSA_SoftRide_brochure.pdf

[33] D. Sciulli and S. F. Griffin, "WHOLE-SPACECRAFT HYBRID ISOLATION SYSTEM FOR LAUNCH VEHICLES," 6,135,390, 2000.

[34] M. E. Evert, P. C. Janzen, E. H. Anderson, C. Gerhart, and B. K. Henderson, "Active Vibration Isolation System for Launch Load Alleviation," in *Smart Structures and Materials 2004: Industrial and Commercial Applications of Smart Structures Technologies*, 2004.

[35] J. R. Jarosh, G. S. Agnes, and G. G. Karahalis, "Adaptive Control for Payload Launch Vibration Isolation," in *Smart Structures and Materials 2001: Damping and Isolation*, 2001, vol. 4331, pp. 162–174.

[36] R. Jha, A. Bailey, and G. Ahmadi, "Combined active and passive control of space structure vibrations during launch," in *44th AIAA/ASME/ASCE/AHS Structures, Structural Dynamics and Materials Conference*, 2003.

[37] W. Chi, D. Cao, and W. Huang, "Design of active whole-spacecraft vibration isolation based on voice-coil motor," in *Sensors and Smart Structures Technologies for Civil, Mechanical, and Aerospace Systems*, 2014, vol. 9061.

[38] C. Collette, A. Souleille, T. Lampert, and G. Rodrigues, "Active Vibration Isolation of Launcher Vibration Environment," in *14th European Conference on Spacecraft Structures, Materials and Environmental Testing*, 2016.

[39] H. Fei, E. Song, X. Ma, and D. Jiang, "Research on whole-spacecraft vibration isolation based on predictive control," *Procedia Eng.*, vol. 16, pp. 467–476, 2011.

[40] P. Jean, R. Ohayon, and D. Le Bihan, "Semi-active control using magneto-rheological dampers for payload launch vibration isolation," *Smart Struct.*

Mater. 2006 Damping Isol., vol. 6169, 2006.

[41] O. Sigmund, "On the design of compliant mechanisms using topology optimization," *Mech. Struct. Mach.*, vol. 25, no. 4, pp. 493–524, 1997.

[42] L. L. Howell, S. P. Magleby, and B. M. Olsen, *Handbook of Compliant Mechanisms*. Wiley, 2013.

[43] V. Vijayan and T. Karthikeyan, "Passive Vibration Isolation by Compliant Mechanism Using Topology Optimization with Building Blocks," *Res. J. Appl. Sci. Eng. Technol.*, vol. 8, no. 13, pp. 1522–1530, 2014.

[44] N. B. Hubbard, J. W. Wittwer, J. A. Kennedy, D. L. Wilcox, and L. L. Howell, "A Novel Fully Compliant Planar Linear-Motion Mechanism," in *ASME Design Engineering Technical Conferences*, 2004.

[45] S. A. Zirbel, K. A. Tolman, B. P. Trease, and L. L. Howell, "Bistable mechanisms for space applications," *PLoS One*, vol. 11, no. 12, pp. 1–18, 2016.

[46] T. M. Allred, "Compliant Mechanism Suspensions," Brigham Young University, 2003.

[47] M. Ling, J. Cao, M. Zeng, J. Lin, and D. Inman, "Enhanced mathematical modeling of the displacement amplification ratio for piezoelectric compliant mechanisms," *Smart Mater. Struct.*, vol. 25, 2016.

[48] A. E. Albanesi, V. D. Fachinotti, and M. A. Pucheta, "A Review on Design Methods for Compliant Mechanisms," in *Mecanica Computacional*, 2010, vol. XXIX, pp. 59–72.

[49] V. Vijayan and T. Karthikeyan, "Design of Compliant Mechanism for Vibration Isolation using Topology Optimization and Flexible Building Blocks," *J. Eng. Technol.*, vol. 3, no. 1, pp. 46–51, 2013.

[50] V. Vijayan and T. Karthikeyan, "Material Selection of Compliant Mechanism for Vibration Isolation," *Mech. Mech. Eng.*, vol. 18, no. 2, pp. 121–134, 2014.

[51] V. Vijayan, T. Karthikeyan, M. Udayakumar, and K. Chellamuthu, "Passive Vibration Isolation by Compliant Mechanism Using Topology Optimization," *Int. J. Acoust. Vib.*, vol. 19, no. 4, pp. 269–275, 2014.

[52] R. Rajesh, V. Vijayan, and T. Karthikeyan, "Topology Optimization and Flexible Building Block Design and Analysis of Compliant Mechanism for Vibration Isolation," *Int. J. Sci. Eng. Res.*, vol. 4, no. 8, p. 46, 2013.

[53] V. Vijayan and T. Karthikeyan, "Design and Analysis of Compliant Mechanism for Active Vibration Isolation Using FEA Technique," *Int. J. Recent Trends Eng.*, vol. 1, no. 5, pp. 77–81, 2009.

[54] S. M. Lyon, P. A. Erickson, M. S. Evans, and L. L. Howell, "Prediction of the

First Modal Frequency of Compliant Mechanisms Using the Pseudo-Rigid-Body Model," *J. Mech. Des.*, vol. 121, no. 2, pp. 309–313, 1999.

[55] Y.-Q. Yu, L. L. Howell, C. Lusk, Y. Yue, and M.-G. He, "Dynamic Modeling of Compliant Mechanisms Based on the Pseudo-Rigid-Body Model," *J. Mech. Des.*, vol. 127, no. 4, pp. 760–765, 2005.

[56] W. Wang and Y. Yu, "Analysis of frequency characteristics of compliant mechanisms," *Front. Mech. Eng. China*, vol. 2, no. 3, pp. 267–271, 2007.

[57] M. Ling, J. Cao, Z. Jiang, and J. Lin, "Theoretical modeling of attenuated displacement amplification for multistage compliant mechanism and its application," *Sensors Actuators, A Phys.*, vol. 249, no. September, pp. 15–22, 2016.

[58] European Space Agency, "Sentinel-2." p. 2, 2013.

[59] *Vega User's Manual Issue 4*. 2014.

[60] E. I. Rivin, *Passive Vibration Isolation*. ASME Press, 2003.

[61] C. W. de Silva, *Vibration and Shock Handbook*. CRC Press, 2005.

[62] J. S. Arora, *Introduction to Optimum Design*, 2nd Ed. Elsevier, 2004.

[63] Altair, *Practical Aspects of Structural Optimization - A Study Guide*, 2nd Ed. 2015.

[64] P. W. Christensen and A. Klarbring, *An Introduction to Structural Optimization*. Springer, 2009.

[65] M. P. Bendsøe and O. Sigmund, *Topology Optimization: Theory, Methods, and Applications*, 2nd Ed. Springer, 2003.

[66] "ISO 10846-2 Acoustics and vibration - Laboratory measurement of vibro-acoustic transfer properties of resilient elements - Part 2: Direct method for determination of the dynamic stiffness of resilient supports for translatory motion." 2008.

[67] *NASA Systems Engineering Handbook*. 2007.

APPENDICES

A. 3M ISD 112 – SHEAR MODULUS AND LOSS FACTOR NOMOGRAPH

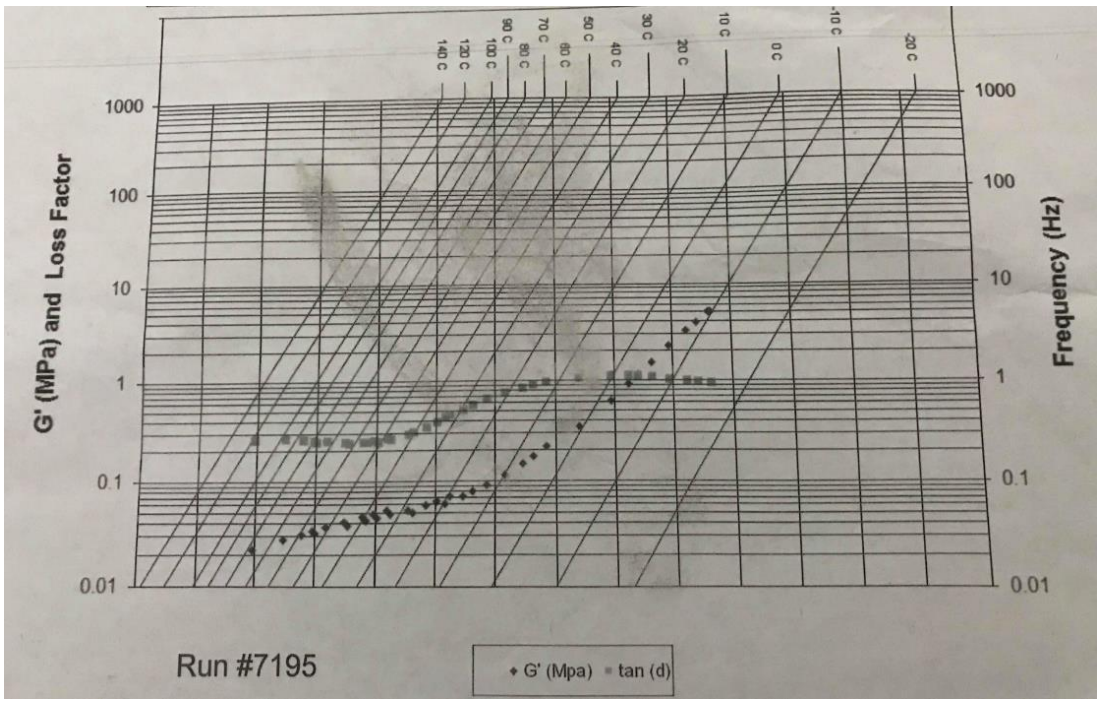

B. TEST MATRIX

Test #	Test Item	Test Type	Frequency [Hz]	Vibration Axis	Vibration Input	Sweep Rate [oct/min]	Test Duration [s]
1	T1	Sine Sweep	5-2000	x	0.1 g	4	130
2	T1	Harmonic	2-20	x	Harmonic - lateral	2	100
3	T1	Random	20 -2000	x	3.6 gRMS	-	60
4	T1	Random	20 -2000	x	6.5 gRMS	-	60
5	T1	Random	20 -2000	x	3.14 gRMS	-	60
6	T1	Sine Sweep	5-2000	x	0.1 g	4	130
7	T1	Sine Sweep	5-2000	y	0.1 g	4	130
8	T1	Harmonic	5-20	y	Harmonic - longitudinal	2	60
9	T1	Random	20 -2000	y	3.6 gRMS	-	60
10	T1	Random	20 -2000	y	6.5 gRMS	-	60
11	T1	Random	20 -2000	y	3.14 gRMS	-	60
12	T1	Sine Sweep	5-2000	y	0.1 g	4	130
13	T2	Sine Sweep	5-2000	x	0.2 g	4	130
14	T2	Harmonic	2-20	x	Harmonic - lateral	2	100
15	T2	Random	20 -2000	x	3.6 gRMS	-	60
16	T2	Random	20 -2000	x	6.5 gRMS	-	60
17	T2	Random	20 -2000	x	3.14 gRMS	-	60
18	T2	Sine Sweep	5-2000	x	0.2 g	4	130
19	T2	Sine Sweep	5-2000	y	0.2 g	4	130
20	T2	Harmonic	5-20	y	Harmonic - longitudinal	2	60
21	T2	Random	20 -2000	y	3.6 gRMS	-	60
22	T2	Random	20 -2000	y	6.5 gRMS	-	60
23	T2	Random	20 -2000	y	3.14 gRMS	-	60
24	T2	Sine Sweep	5-2000	y	0.2 g	4	130
25	S1	Sine Sweep	5-2000	x	0.1 g	4	130
26	S1	Harmonic	2-20	x	Harmonic - lateral	2	100
27	S1	Random	20 -2000	x	3.6 gRMS	-	60
28	S1	Random	20 -2000	x	6.5 gRMS	-	60
29	S1	Random	20 -2000	x	3.14 gRMS	-	60
30	S1	Sine Sweep	5-2000	x	0.1 g	4	130

Test #	Test Item	Test Type	Frequency [Hz]	Vibration Axis	Vibration Input	Sweep Rate [oct/min]	Test Duration [s]
31	S1	Sine Sweep	5-2000	y	0.1 g	4	130
32	S1	Harmonic	5-20	y	Harmonic - longitudinal	2	60
33	S1	Random	20 -2000	y	3.6 gRMS	-	60
34	S1	Random	20 -2000	y	6.5 gRMS	-	60
35	S1	Random	20 -2000	y	3.14 gRMS	-	60
36	S1	Sine Sweep	5-2000	y	0.1 g	4	130

C. SPECIFICATIONS OF TRIAXIAL ICP ACCELEROMETER

PERFORMANCE	**English**	**SI**
Sensitivity (±10 %)	10 mV/g	1.02 mV/(m/s²)
Measurement Range	±500 g pk	±4905 m/s² pk
Frequency Range (+/-5 %)	0.7 to 7000 Hz	0.7 to 7000 Hz
Frequency Range (+/-10 %)	0.4 to 10000 Hz	0.4 to 10000 Hz
Resonant Frequency	≥30 kHz	≥30 kHz
Broadband Resolution (1 to 10000 Hz)	0.0008 g rms	.008 m/s² rms
Non-Linearity	1 %	1 %
Transverse Sensitivity	≤6 %	≤6 %
TEDS Compliant (Per IEEE 1451.4)	Yes	Yes
ENVIRONMENTAL		
Overload Limit (Shock)	±5000 g pk	±49050 m/s² pk
Temperature Range (Operating)	-65 to 250 °F	-54 to 121 °C
Temperature Response	See Graph	See Graph
Base Strain Sensitivity	.001 g/με	.01 (m/s²)/με
ELECTRICAL		
Excitation Voltage	20 to 30 VDC	20 to 30 VDC
Constant Current Excitation	2 to 20 mA	2 to 20 mA
Output Impedance	≤200 Ohm	≤200 Ohm
Output Bias Voltage	8 to 12 VDC	8 to 12 VDC
Discharge Time Constant	0.8 to 2.4 sec	0.8 to 2.4 sec
Settling Time (within 10% of bias)	≤5 sec	≤5 sec
Spectral Noise (1 Hz)	300 μg/√Hz	2943 (μm/sec2)/√Hz
Spectral Noise (10 Hz)	50 μg/√Hz	491 (μm/sec2)/√Hz
Spectral Noise (100 Hz)	35 μg/√Hz	343 (μm/sec2)/√Hz
Spectral Noise (1 kHz)	8 μg/√Hz	79 (μm/sec2)/√Hz
PHYSICAL		
Sensing Element	Ceramic	Ceramic
Sensing Geometry	Shear	Shear
Housing Material	Titanium	Titanium

Sealing	Hermetic	Hermetic
Size - Height	0.40 in	10.2 mm
Size - Length	0.75 in	19.1 mm
Size - Width	0.40 in	10.2 mm
Weight	0.15 oz	4.2 gm
Electrical Connector	1/4-28 4-Pin	1/4-28 4-Pin
Electrical Connection Position	Side	Side
Mounting	Adhesive	Adhesive